Climate4you update April 2024

Climate4you.com

Summary of observations until April 2024:

1: Observed average global air temperature change last 40 years is about +0.18°C per decade.
If unchanged, additional average global air temperature increase by year 2100 will be about +1.3°C.
However, part of the apparent temperature increase reported is due to administrative changes, and
the real future increase may therefore be smaller.

2: Tide gauges along coasts indicate a typical global sea level increase of about 1-2 mm/yr.
Coastal sea level change rate last 100 year has essential been stable, but with periodic variations.
If unchanged, global sea level at coasts will typically increase 8-16 cm by year 2100, although many
locations in regions affected by glaciation 20,000 years ago, will experience a relative sea level drop.

3: Since 2004 the global oceans above 1900 m depth on average have warmed about 0.07°C.
The maximum warming (about 0.2°C, 0-100 m depth) mainly affects oceans near Equator,
where the incoming solar radiation is at maximum.

4: Sources and sinks for CO_2 are many. However, changes in atmospheric CO_2 follow changes in global
air temperature, and changes in global air temperature follow changes in ocean surface temperature.

5: There was no perceptible effect on atmospheric CO_2 due to the 2020-21 COVID-related drop in
GHG emissions, underlining the fact that natural sinks and sources for atmospheric CO_2 far outweigh
human contributions. Therefore, any future reductions in the use of fossil fuels are unlikely
to have any significant effect on the amount of atmospheric CO_2.

Contents:

2

April 2024 global surface air temperature overview

General: This newsletter contains graphs and diagrams showing a selection of key meteorological variables, updated to the most recent past month, if possible. All temperatures are given in degrees Celsius.

Traditionally, a 30 -year reference period is often used by various meteorological institutions for comparison purposes and are supposed to be updated through the end of each decade ending in zero (e.g., 1951-1980, 1961-1990, 1971-2000, etc.). The concept of a normal climate goes back to the first part of the 20th century. At that time, lasting to about 1960, it was generally believed that for all practical purpose's climate could be considered constant, no matter how obvious year-to-year fluctuations might have been. On this basis meteorologist decided to operate with an average or normal climate, defined by a 30-year period, called the normal period, assuming that it was of sufficient length to iron out all intervening variations. In fact, using a 30-yr 'normal' period is truly unfortunate, as observations clearly demonstrate that various global climate parameters (see, e.g., page 20) are influenced by periodic changes of 50-70 years duration. The frequently used 30-yr reference period is roughly half this time interval and is therefore highly unsuited as reference period. In the maps on page 4, showing the geographical pattern of surface air temperature anomalies, the last previous 10 years are therefore used as reference period. This decadal approach corresponds well to the typical memory horizon for many people and is also adopted as reference period by other institutions, e.g., the Danish Meteorological Institute (DMI).

 In many diagrams shown in this newsletter the thin line represents the monthly global average value, and the thick line indicate a simple running 37-month average, nearly corresponding to a three-year average. The year 1979 has been chosen as starting point in many diagrams, as this approximately corresponds to both the beginning of satellite observations and the onset of the late 20th century warming period. However, most of the data series have a longer record length, which may be inspected in greater detail on www.climate4you.com.

3

April 2024 surface air temperature

General: For April 2024, the GISS data portal provided AIRS interpolated surface air data, based on satellite observations. According to the GISS and NCDC records, the April global temperature was still very high, but lower than in the previous month. The UAH lower troposphere satellite series also show the March temperature anomaly to be very high (RSS satellite series is not yet published beyond February 2024). The AIRS v6 April global average temperature anomaly compared to the last 10 years confirms the above impression (see, diagrams p.4-5). Positive anomalies in April were especially pronounced for Canada, eastern Europe, and western Russia. The main reason, however, for the overall positive global temperature anomaly in April 2024 are the vast regions around Equator with temperatures above the average for the last 10 years, a derived effect of the now declining El Niño episode in the Pacific Ocean.

The Northern Hemisphere surface temperature anomality pattern (p.4) was characterised by strong regional contrasts, mainly controlled by the dominant jet stream position. Especially Canada, eastern Europe and western Russia were warm relative to the average for the last 10 years. In contrast, western and northern Europe and northern Russia were relatively cold. Ocean wise, The Greenland Sea and the Norwegian Sea were cold, while other parts of the North Atlantic region were a mixture of relatively warm and cold regions. The eastern Pacific Ocean was relatively cold, while the western part was warm. PDO (p.20) remains negative. Arctic Ocean surface air temperatures were below the 10-yr average.

Near the Equator temperatures were generally above the 10-year average. Ocean heat released during the ongoing warm El Niño episode is affecting most Equatorial regions.

Southern Hemisphere temperatures were near the 10-yr average. Most of Australia and southern South America were relatively cold. Most of the Antarctic continent had temperatures below the 10-yr average.

April 2024 global surface air temperature overview versus average April last 10 years

Surface air temperature April 2024 versus April last 10yr

Surface air temperature April 2024 versus April last 10 yr

Surface air temperature April 2024 versus April last 10 yr
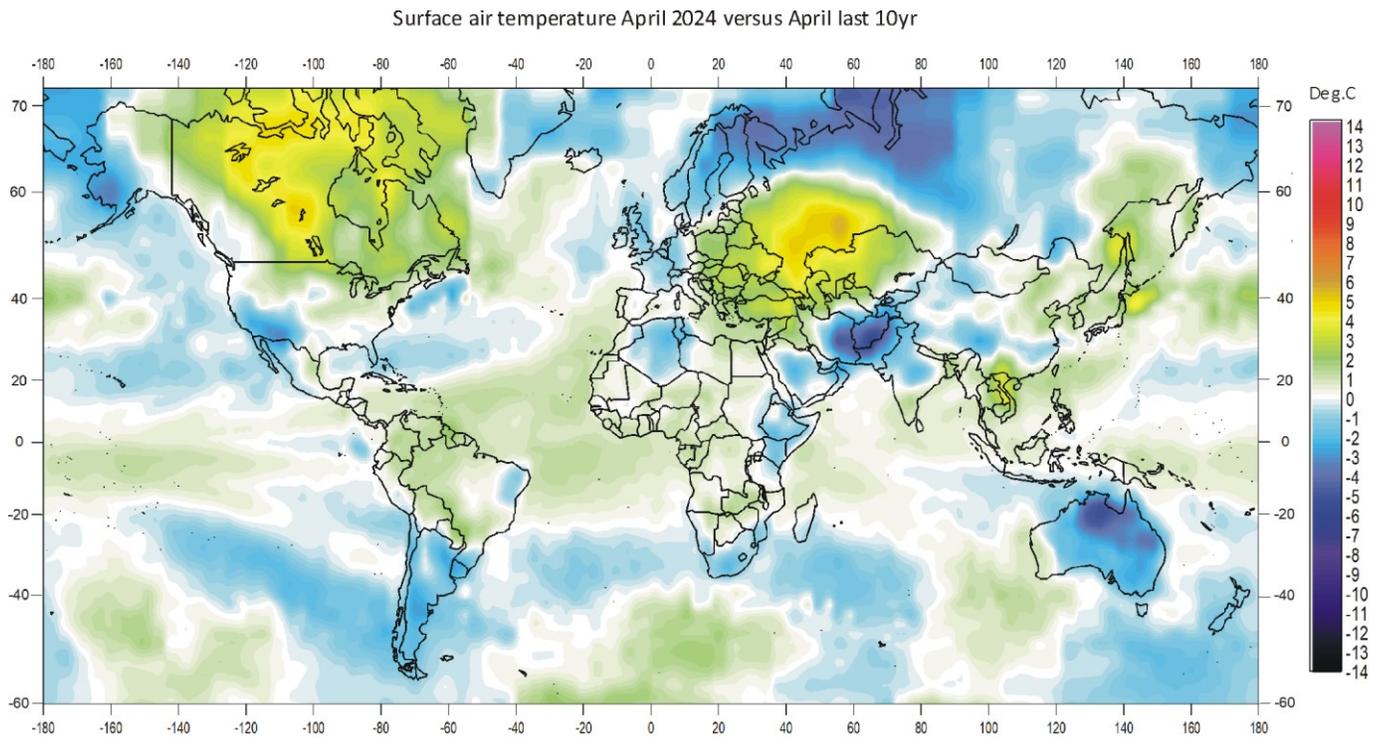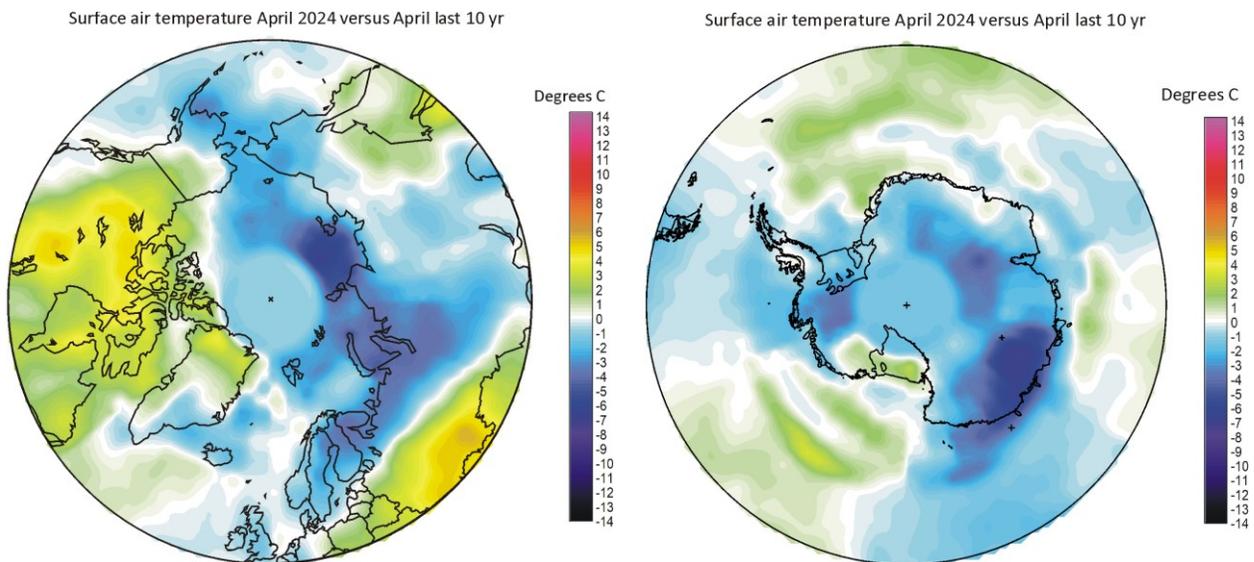
April 2024 surface air temperature compared to the average of April over the last 10 years. Green-yellow-red colours indicate areas with higher temperature than the 10-year average, while blue colours indicate lower than average temperatures. Data source: Remote Sensed Surface Temperature Anomaly, AIRS/Aqua L3 Monthly Standard Physical Retrieval 1-degree x 1-degree V006 (https://airs.jpl.nasa.gov/), obtained from the GISS data portal (https://data.giss.nasa.gov/gistemp/maps/index_v4.html).

April 2024 global surface air temperature compared to April 2023
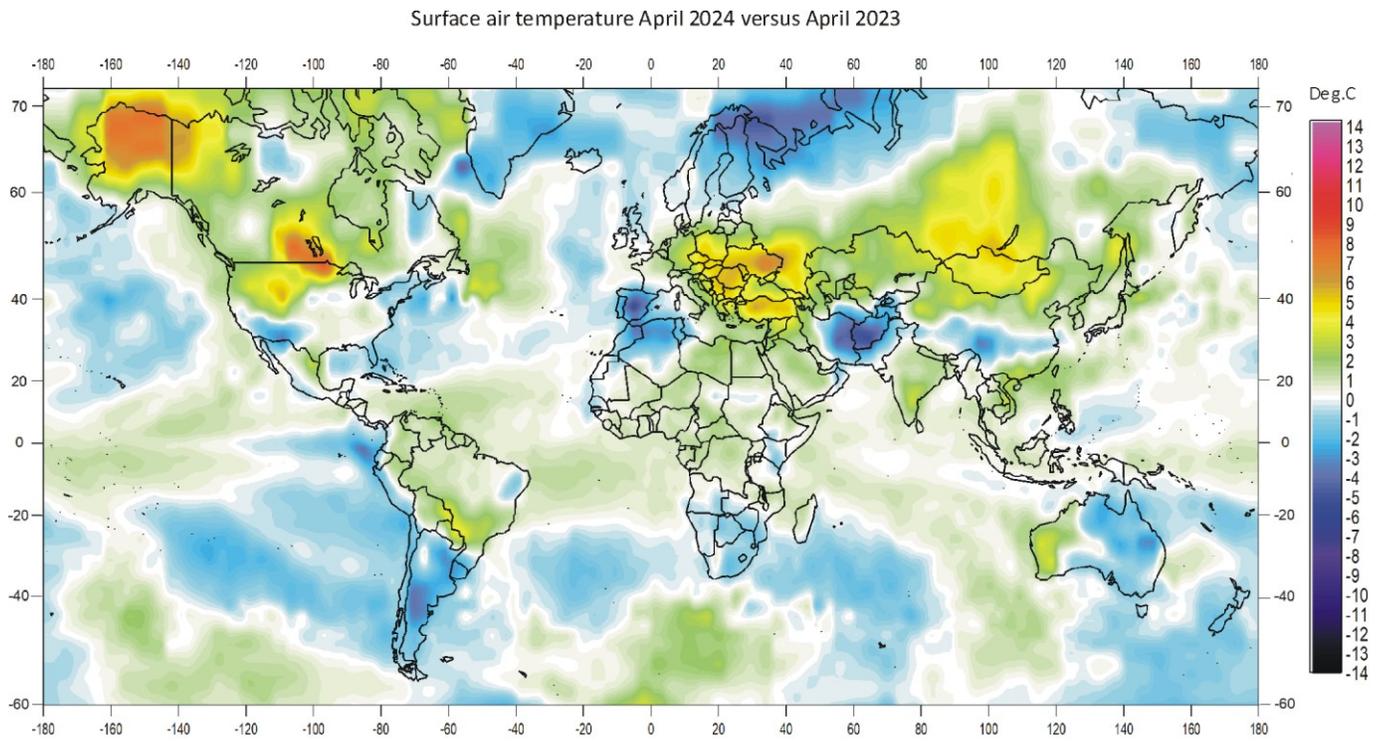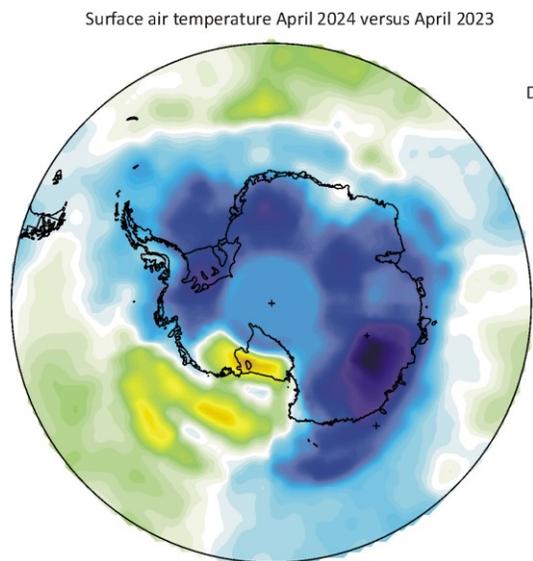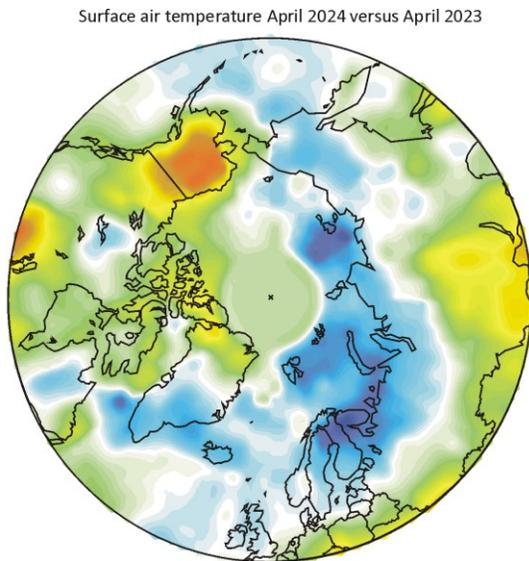
April 2024 surface air temperature compared to April 2023. Green-yellow-red colours indicate regions where the present month was warmer than last year, while blue colours indicate regions where the present month was cooler than last year. Variations in monthly temperature from one year to the next has no tangible climatic importance but may nevertheless be interesting to study. Data source: Remote Sensed Surface Temperature Anomaly, AIRS/Aqua L3 Monthly Standard Physical Retrieval 1-degree x 1-degree V006 (https://airs.jpl.nasa.gov/), obtained from the GISS data portal (https://data.giss.nasa.gov/gistemp/maps/index_v4.html).
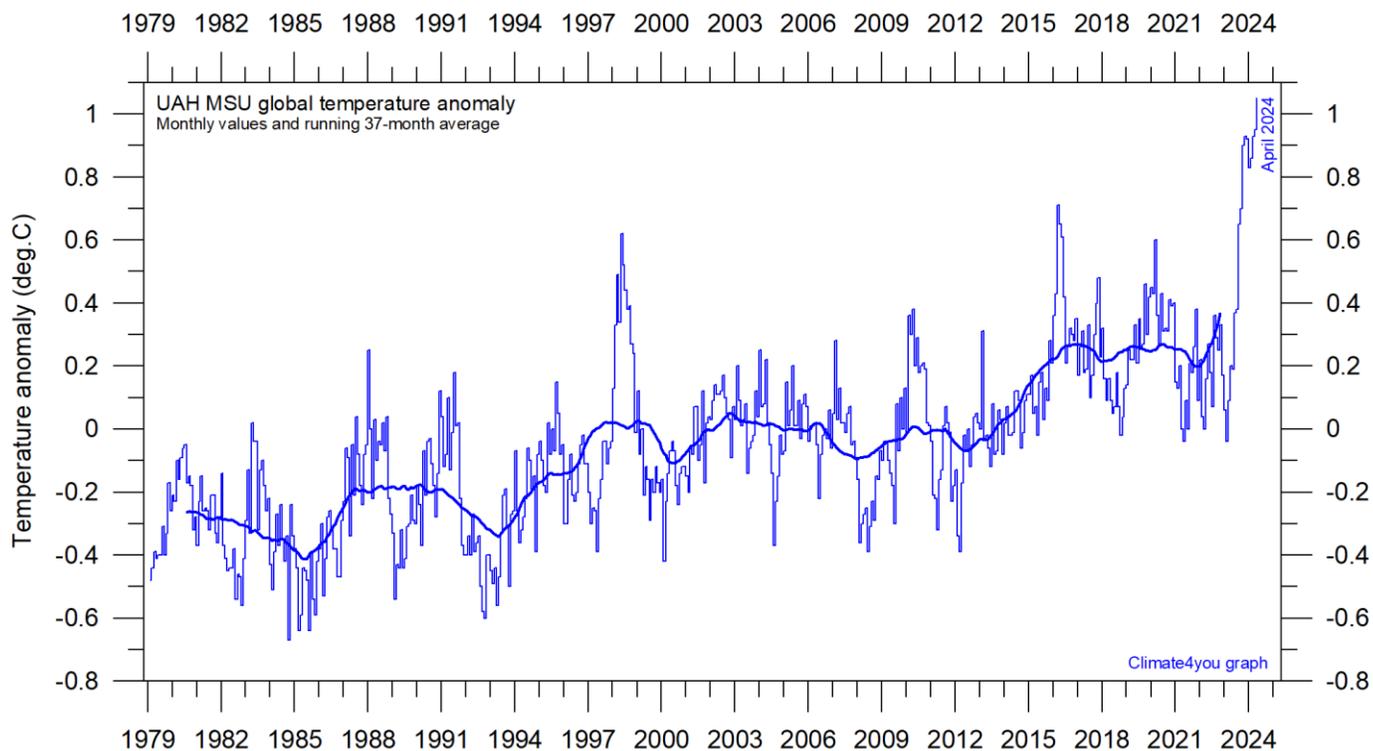
Global monthly average lower troposphere temperature (thin line) since 1979 according to University of Alabama at Huntsville, USA. The thick line is the simple running 37-month average. Reference period 1991-2020.

Global monthly average lower troposphere temperature (thin line) since 1979 according to according to Remote Sensing Systems (RSS), USA. The thick line is the simple running 37-month average.

Temperature quality class 2: HadCRUT global surface air temperature, updated to March 2024

HadCRUT5 non-infilled global temperature anomaly
Monthly values and running 37-month average

March 2024

Climate4you graph
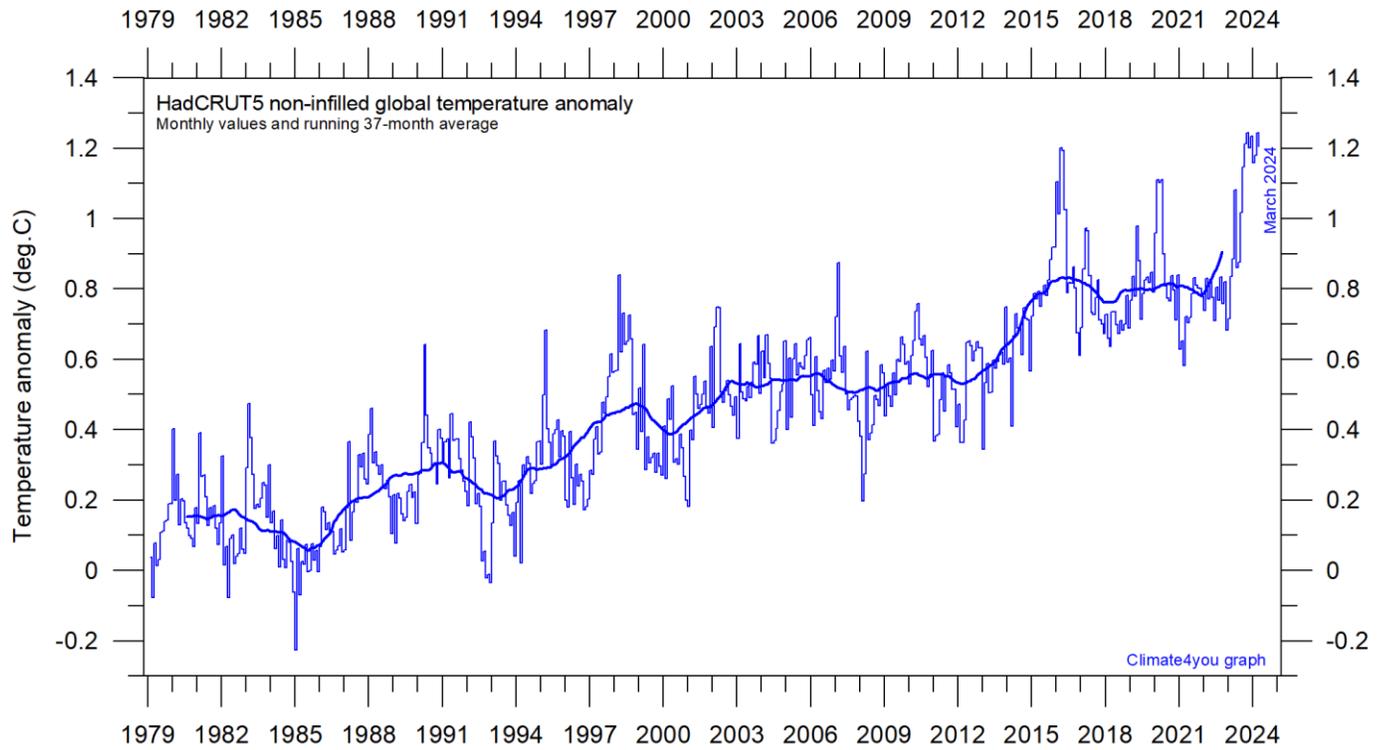
7   *Global monthly average surface air temperature (thin line) since 1979 according to the Hadley Centre for Climate Prediction and Research and the University of East Anglia's Climatic Research Unit (CRU), UK. The thick line is the simple running 37-month average.*

Temperature quality class 3: GISS and NCDC global surface air temperature, updated to April 2024
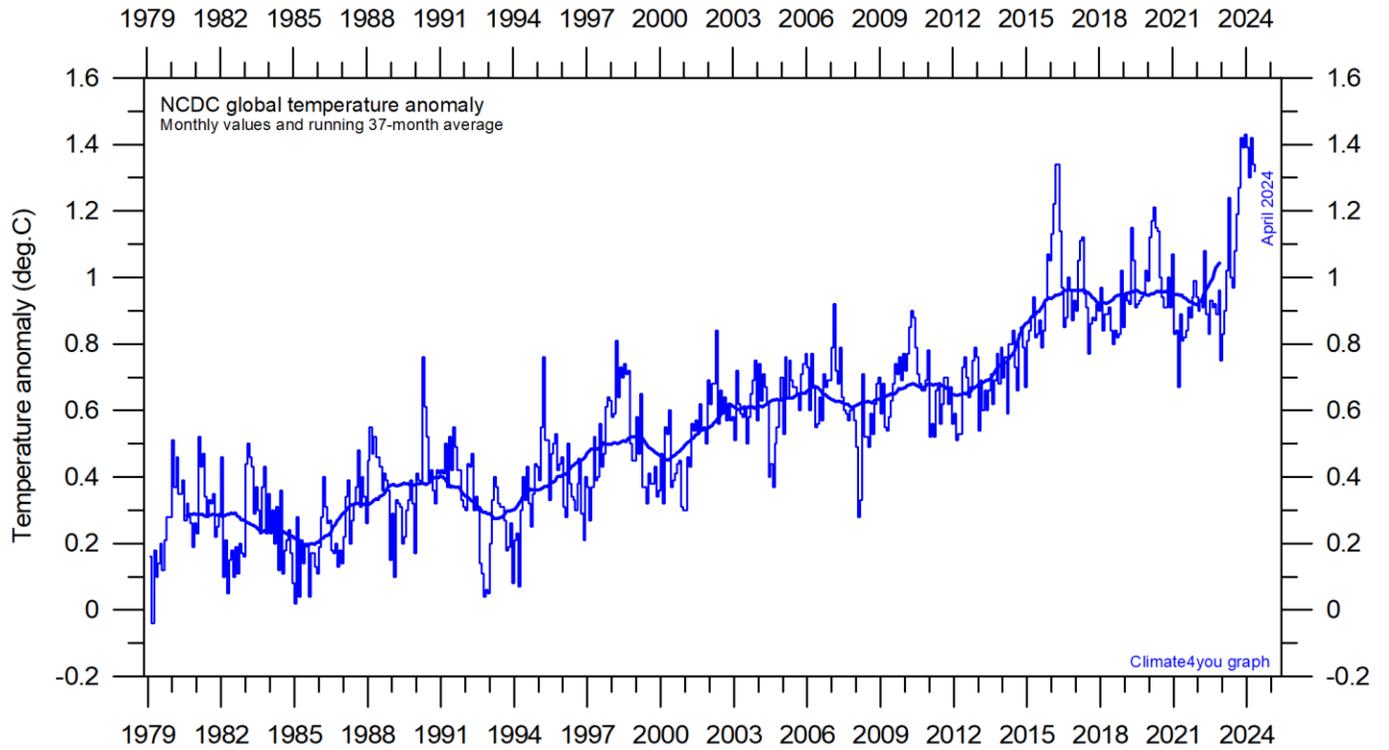
Global monthly average surface air temperature since 1979 according to according to the *National Climatic Data Center* (NCDC), USA. The thick line is the simple running 37-month average.
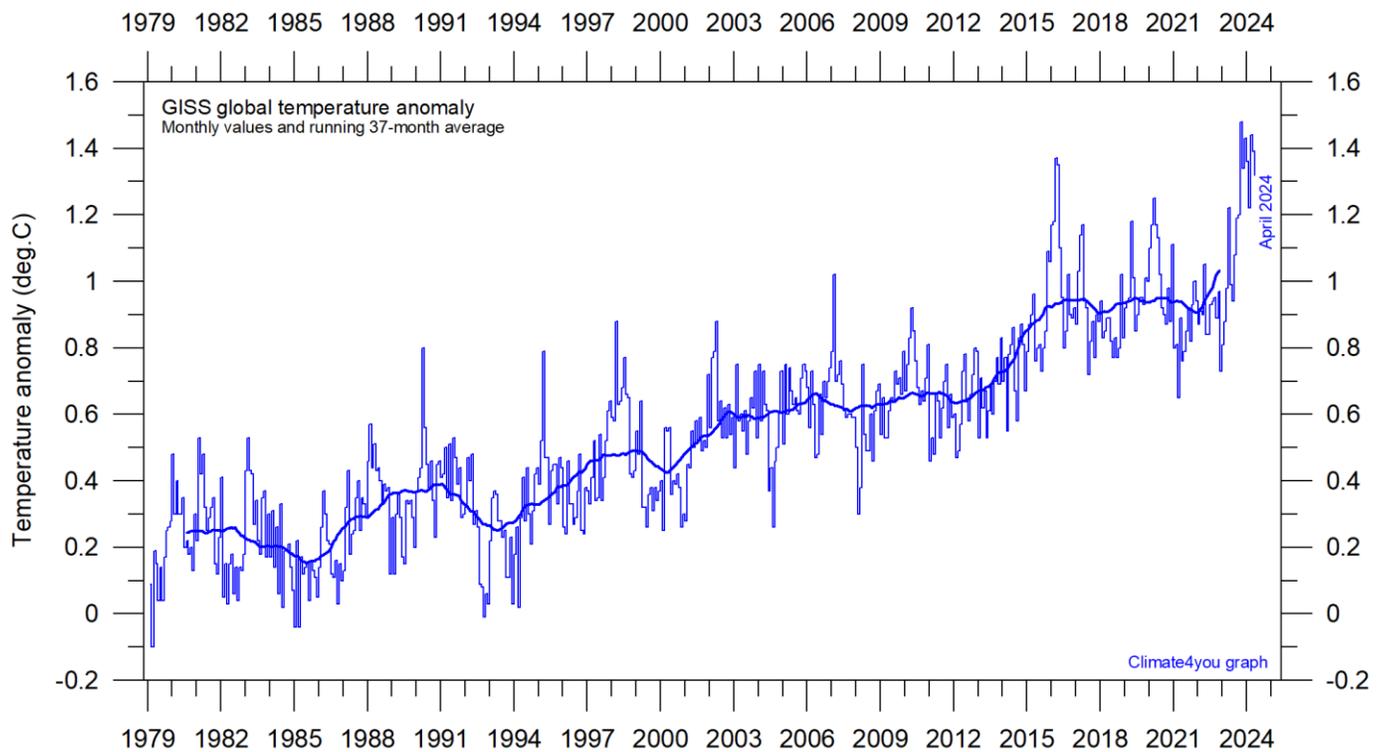
Global monthly average surface air temperature (thin line) since 1979 according to according to the *Goddard Institute for Space Studies* (GISS), at Columbia University, New York City, USA, using ERSST_v4 ocean surface temperatures. The thick line is the simple running 37-month average.

A note on data record stability and -quality:

The temperature diagrams shown above all have 1979 as starting year. This roughly marks the beginning of the recent episode of global warming, after termination of the previous episode of global cooling from about 1940. In addition, the year 1979 also represents the starting date for the satellite-based global temperature estimates (UAH and RSS). For the three surface air temperature records (HadCRUT, NCDC and GISS), they begin much earlier (in 1850 and 1880, respectively), as can be inspected on www.climate4you.com.

For all three surface air temperature records, but especially NCDC and GISS, administrative changes to anomaly values are quite often introduced, even affecting observations many years back in time. Some changes from the recent past may be due to the delayed addition of new station data or change of station location, while others probably have their origin in changes of the technique implemented to calculate average values from the raw data. It is clearly impossible to evaluate the validity of such administrative changes for the outside user of these records; it is only possible to note that such changes quite often are introduced (se example diagram next page).

In addition, the three surface records represent a blend of sea surface data collected by moving ships or by other means, plus data from land stations of partly unknown quality and unknown degree of representativeness for their region. Many of the land stations also has been moved geographically during their period of operation, instrumentation have been changed, and they are influenced by changes in their near surroundings (vegetation, buildings, etc.). The surface network is inherently heterogeneous (dense over continents but sparse over oceans) and probably contaminated by urbanization surrounding many measurement sites.

The satellite temperature records also have their problems, but these are generally of a more technical nature and probably therefore better correctable. In addition, the temperature sampling by satellites is more regular and complete on a global basis than that represented by the surface records. It is also important that the sensors on satellites measure temperature directly by microwave radiance (thereby unobstructed by clouds), while most modern surface temperature measurements are indirect, using electronic resistance.

Everybody interested in climate science should gratefully acknowledge the big efforts put into maintaining the different temperature databases referred to in the present newsletter. At the same time, however, it is also important to realise that all temperature records cannot be of equal scientific quality. The simple fact that they to some degree differ shows that they cannot all be correct.

On this background, and for practical reasons, Climate4you therefore operates with three quality classes (1-3) for global temperature records, with 1 representing the highest quality level:

Quality class 1: The satellite records (UAH and RSS).
Quality class 2: The HadCRUT surface record.
Quality class 3: The NCDC and GISS surface records.

The main reason for discriminating between the three surface records is the following:

While both NCDC and GISS often experience quite large administrative changes (see example on p.10), and therefore essentially must be considered as unstable records, the changes introduced to HadCRUT are fewer and smaller. For obvious reasons, as the past does not change, any record undergoing continuing changes cannot describe the past correctly all the time. Frequent and large corrections in a database unavoidably signal a fundamental uncertainty about what is likely to represent the correct values.

You can find more on the issue of lack of temporal stability on www.climate4you.com (go to: *Global Temperature*, and then proceed to *Temporal Stability*).
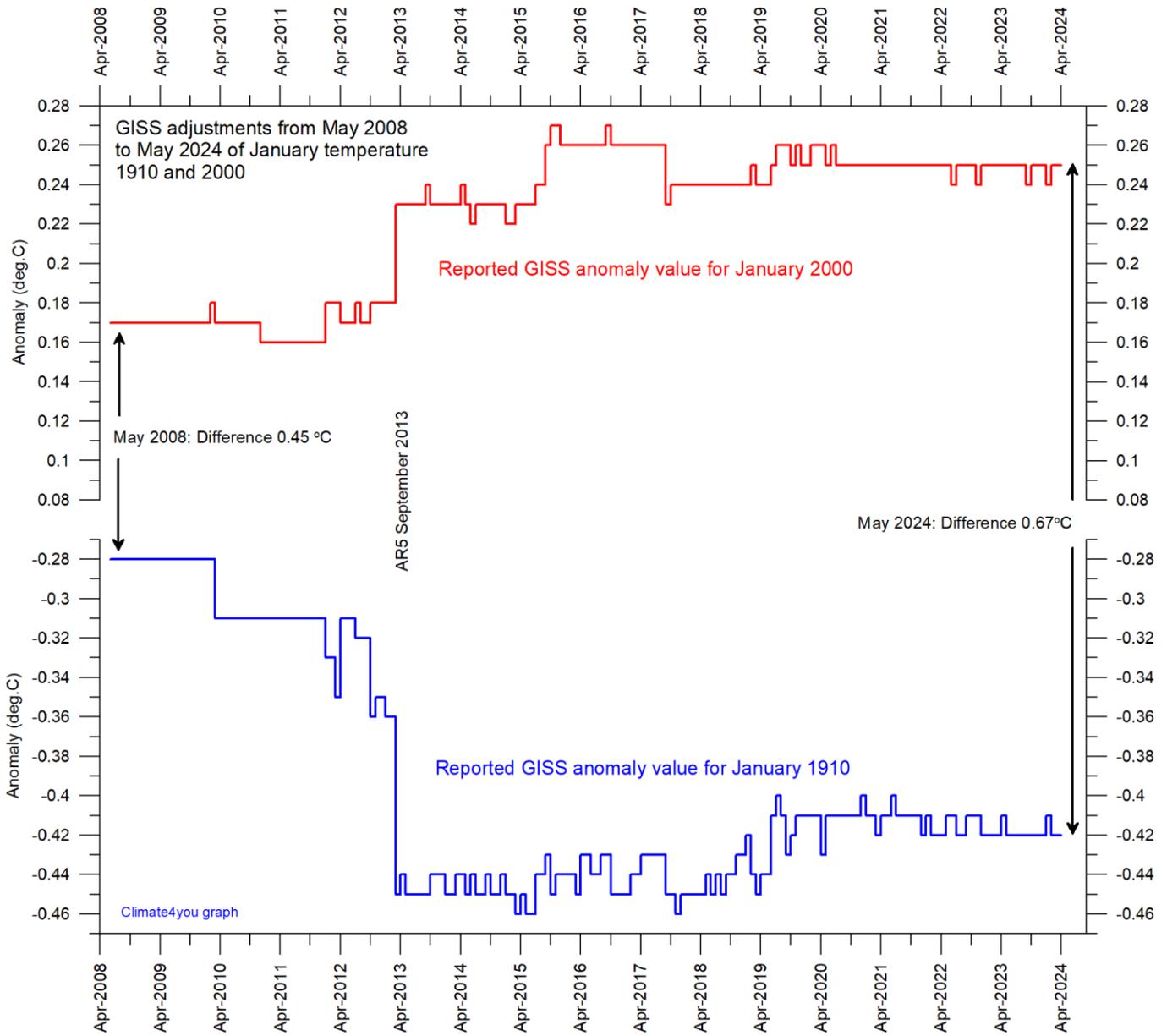
Diagram showing the monthly adjustments made since May 2008 by the [Goddard Institute for Space Studies](#) (GISS), USA, as recorded by published anomaly values for the two months January 1910 and January 2000. AR5 indicates timing of publication of IPCC report AR5 Climate Change 2013: The Physical Science Basis.

The administrative upsurge of the temperature increase from January 1915 to January 2000 has grown from 0.45 (reported May 2008) to 0.67°C (reported May 2024). This represents an about 49% administrative temperature increase over this period, meaning that a significant (about half) part of the apparent global temperature increase from January 1910 to January 2000 (as reported by GISS) is caused by administrative changes of the original data since May 2008.

Comparing global surface air temperature and lower troposphere satellite temperatures; updated to February 2024
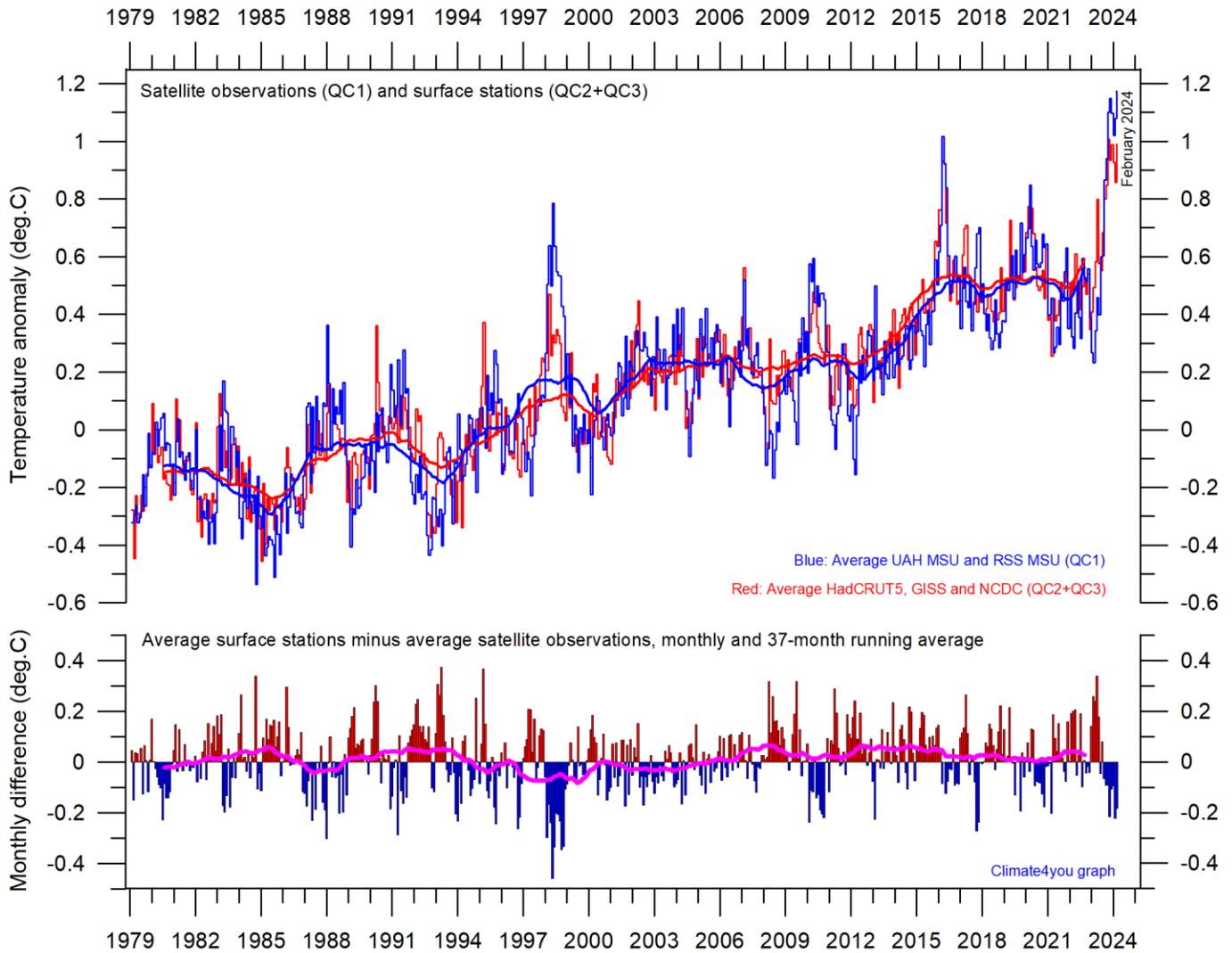
Plot showing the average of monthly global surface air temperature estimates (HadCRUT5, GISS and NCDC) and satellite-based temperature estimates (RSS MSU and UAH MSU). The thin lines indicate the monthly value, while the thick lines represent the simple running 37-month average, nearly corresponding to a running 3-yr average. The lower panel shows the monthly difference between average surface air temperature and satellite temperatures. As the base period differs for the different temperature estimates, they have all been normalised by comparing to the average value of 30 years from January 1979 to December 2008.

Global air temperature linear trends updated to February 2024
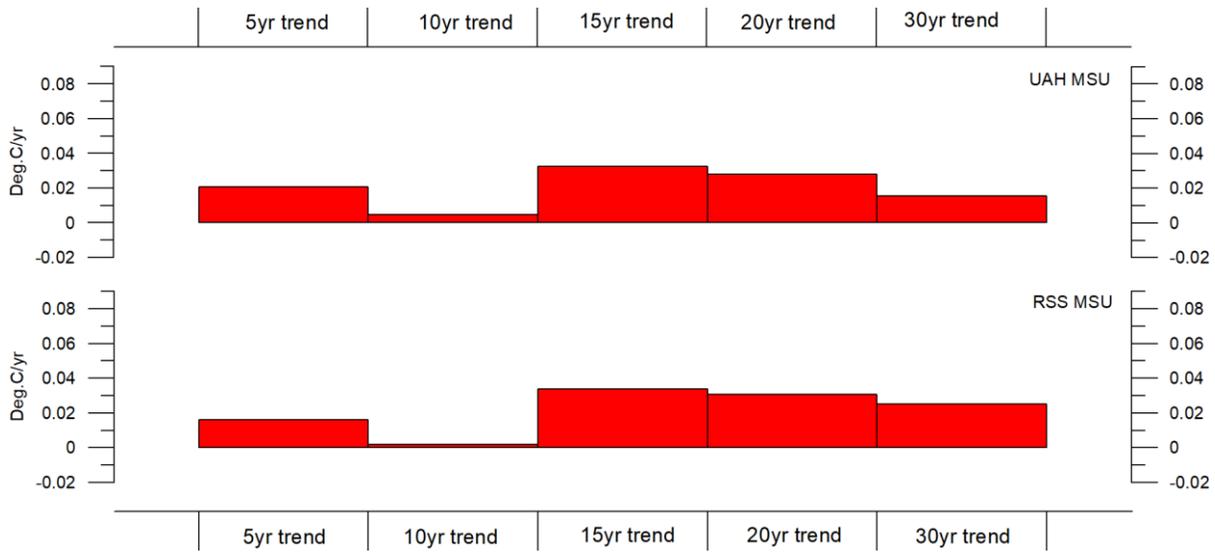
Diagram showing the latest 5, 10, 20 and 30-yr linear annual global temperature trend, calculated as the slope of the linear regression line through the data points, for two satellite-based temperature estimates (UAH MSU and RSS MSU).
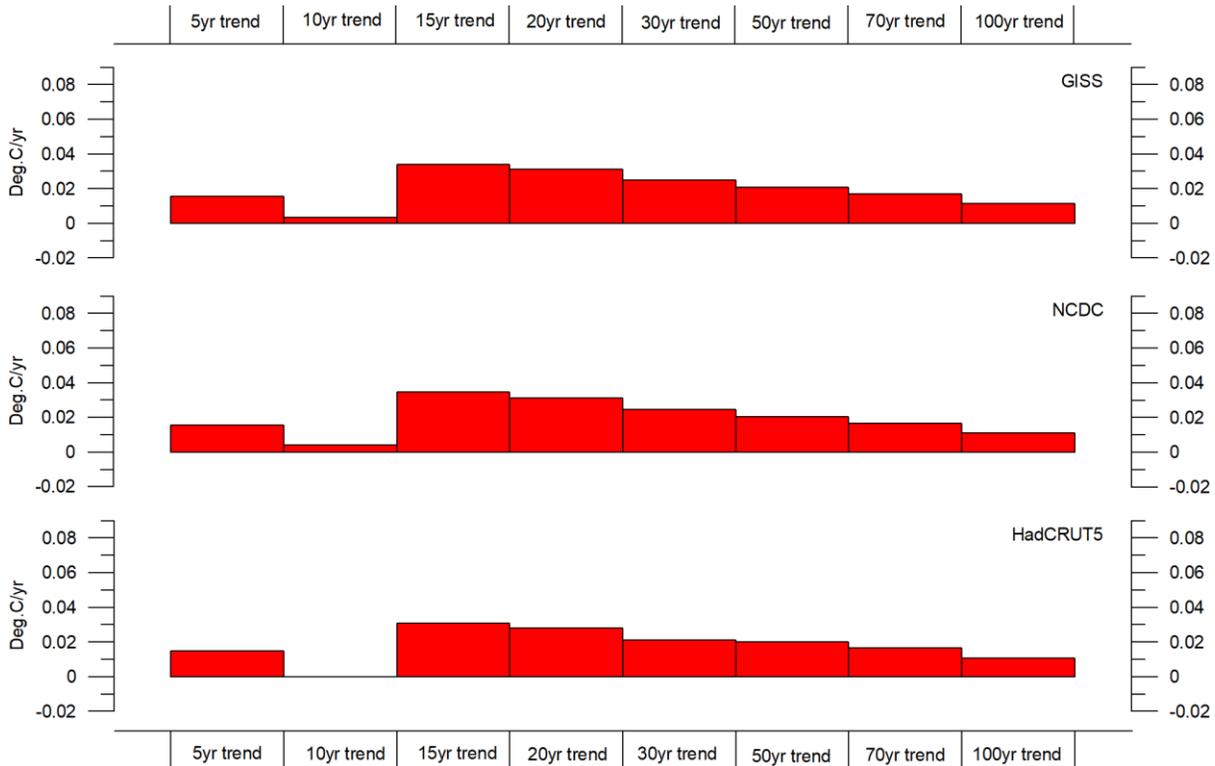
Diagram showing the latest 5, 10, 20, 30, 50, 70 and 100-year linear annual global temperature trend, calculated as the slope of the linear regression line through the data points, for three surface-based temperature estimates (GISS, NCDC and HadCRUT5).

All in one, Quality Class 1, 2 and 3; updated to February 2024
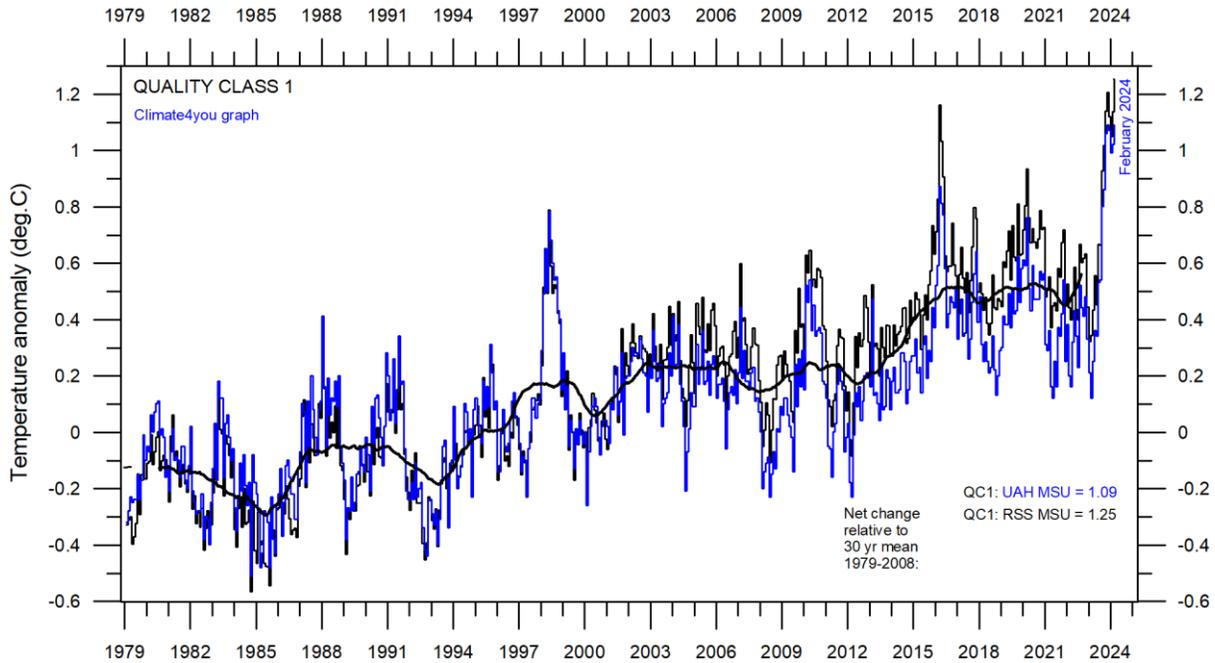
Superimposed plot of Quality Class 1 (UAH and RSS) global monthly temperature estimates. As the base period differs for the individual temperature estimates, they have all been normalised by comparing with the average value of the initial 120 months (30 years) from January 1979 to December 2008. The heavy black line represents the simple running 37 month (c. 3 year) mean of the average of both temperature records. The numbers shown in the lower right corner represent the temperature anomaly relative to the individual 1979-2008 averages.

13
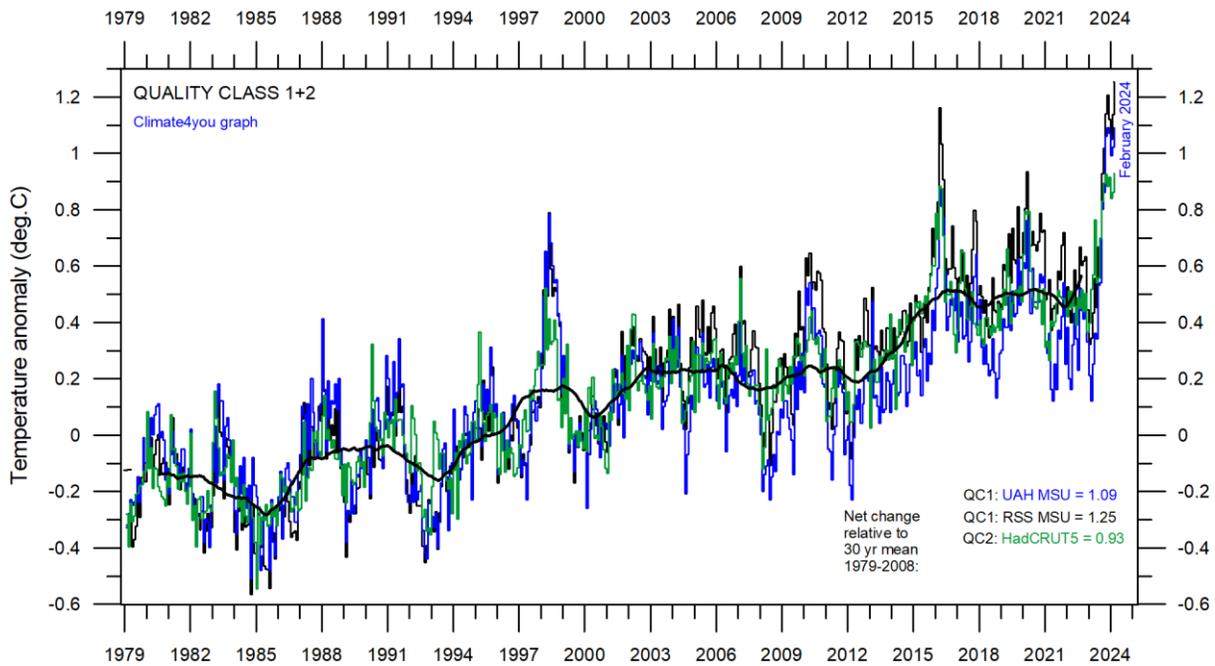
Superimposed plot of Quality Class 1 and 2 (UAH, RSS and HadCRUT) global monthly temperature estimates. As the base period differs for the individual temperature estimates, they have all been normalised by comparing with the average value of the initial 120 months (30 years) from January 1979 to December 2008. The heavy black line represents the simple running 37 month (c. 3 year) mean of the average of all three temperature records. The numbers shown in the lower right corner represent the temperature anomaly relative to the individual 1979-2008 averages.
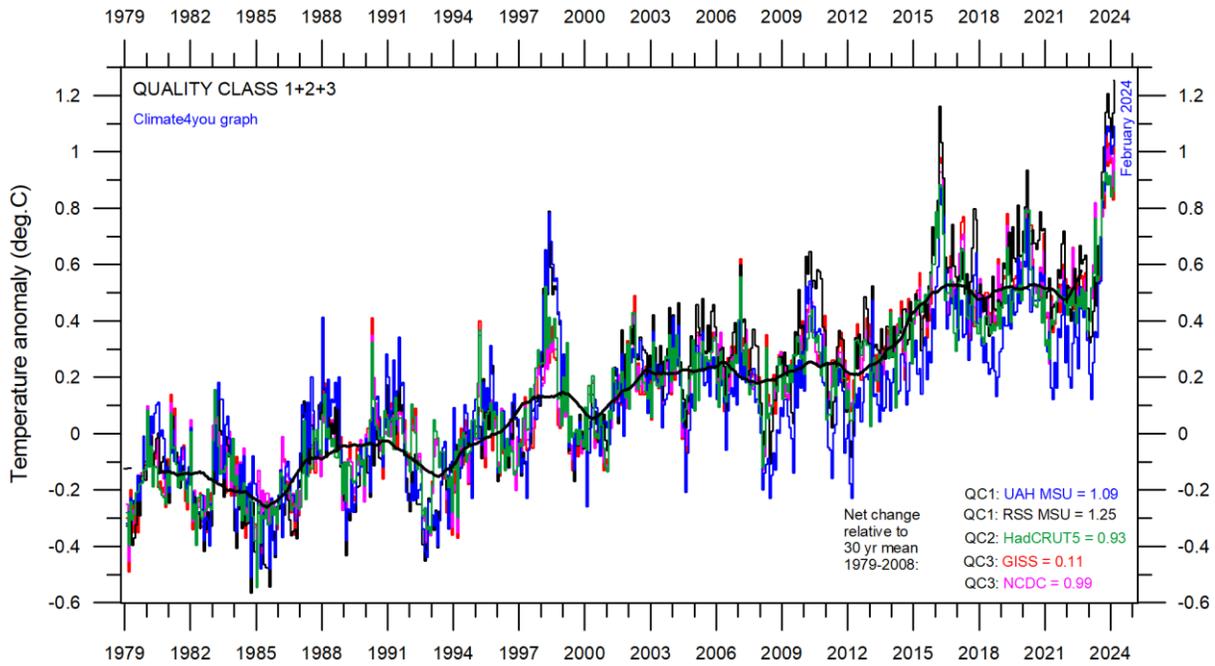
Superimposed plot of Quality Class 1, 2 and 3 global monthly temperature estimates (UAH, RSS, HadCRUT, GISS and NCDC). As the base period differs for the individual temperature estimates, they have all been normalised by comparing with the average value of the initial 120 months (30 years) from January 1979 to December 2008. The heavy black line represents the simple running 37 month (c. 3 year) mean of the average of all five temperature records. The numbers shown in the lower right corner represent the temperature anomaly relative to the individual 1979-2008 averages.

Please see reflections on page 9 relating to the above three quality classes.

Satellite- and surface-based temperature estimates are derived from different types of measurements and comparing them directly as in the above diagrams therefore may be somewhat ambiguous.

However, as both types of estimates often are discussed together in various news media, the above composite diagrams may nevertheless be of some interest.

In fact, the different types of temperature estimates appear to agree as to the overall temperature variations on a 2-3-year scale, although on a shorter time scale there are often considerable differences between the individual records. However, since about 2003 the surface records used to be drifting towards higher temperatures than the combined satellite record, but this overall tendency was much removed by the major adjustment of the RSS satellite series in 2015 (see lower diagram on page 6).

The combined records (diagram above) suggest a modest global air temperature increase over the last 40 years, about 0.18°C per decade. It should be noted that the apparent temperature increases since about 2003 at least partly is the result of ongoing administrative adjustments (page 9-10). At the same time, none of the temperature records considered here indicates any overall temperature decrease during the last 20 years.

The present temperature development does not exclude the possibility that global temperatures may begin to increase significantly later. On the other hand, it also remains a possibility that Earth just now is passing an overall temperature peak, and that global temperatures may begin to decrease during the coming 5-10 years.

As always, time will show which of these possibilities is correct.

Global sea surface temperature, updated to April 2024
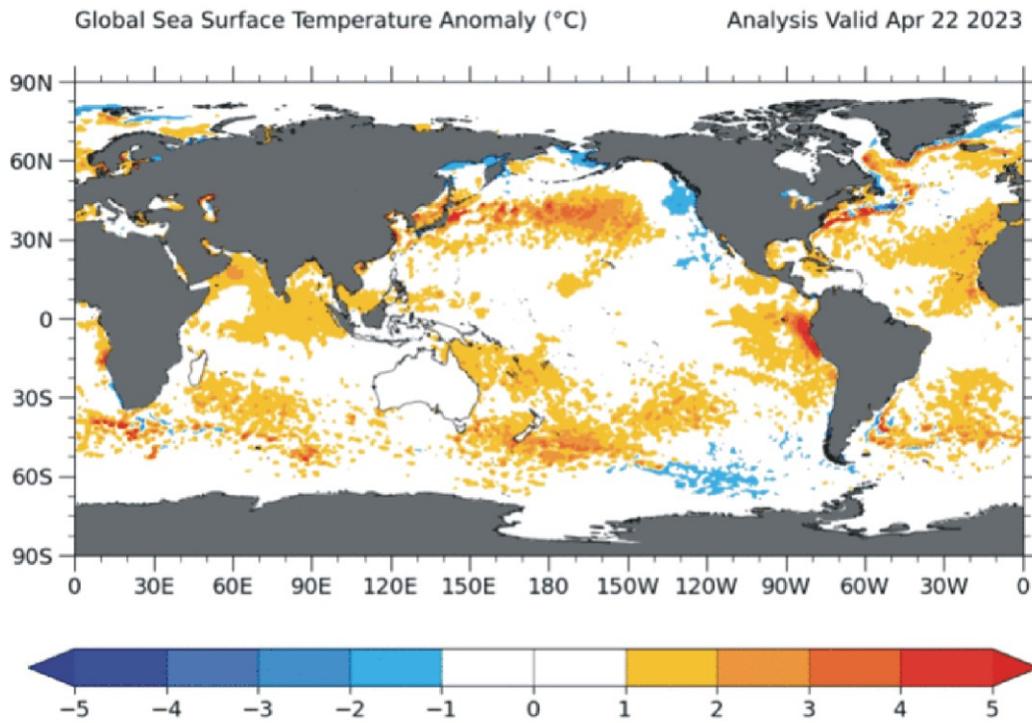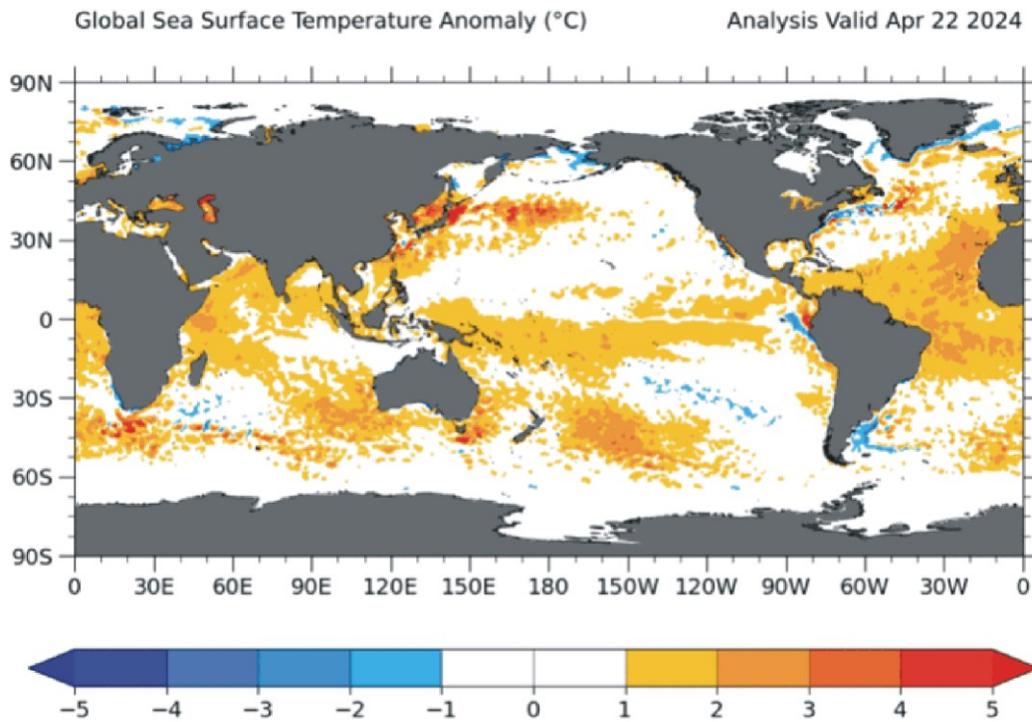
*Sea surface temperature anomaly on 22 April 2024 (upper map) and 2023 (lower map). Map source: Plymouth State Weather Center. Reference period: 1977-1991.*

Because of the large surface areas near Equator, the temperature of the surface water in these regions is especially important for the global atmospheric temperature (p. 6-8). In fact, 50% of planet Earth's surface area is located within 30ºN and 30ºS.

A mixture of relatively warm and cold water presently dominates much of the global ocean surface, but with notable variations from month to month. All such ocean surface temperature changes will be influencing global air temperatures in the months to come. A cold La Niña episode (Pacific Ocean) has recently ended and is now followed by a warm El Niño episode (maps p.15 and diagram p.25).

The significance of short-term cooling or warming reflected in air temperatures should never be overstated. Whenever Earth experiences cold La Niña or warm El Niño episodes major heat exchanges take place between the Pacific Ocean and the atmosphere above, sooner or later showing up in estimates of the global air temperature.

However, this does not necessarily reflect similar changes in the total heat content of the atmosphere-ocean system. In fact, global net changes can be small and such heat exchanges may mainly reflect redistribution of energy between ocean and atmosphere. What matters is the overall temperature development when seen over several years.
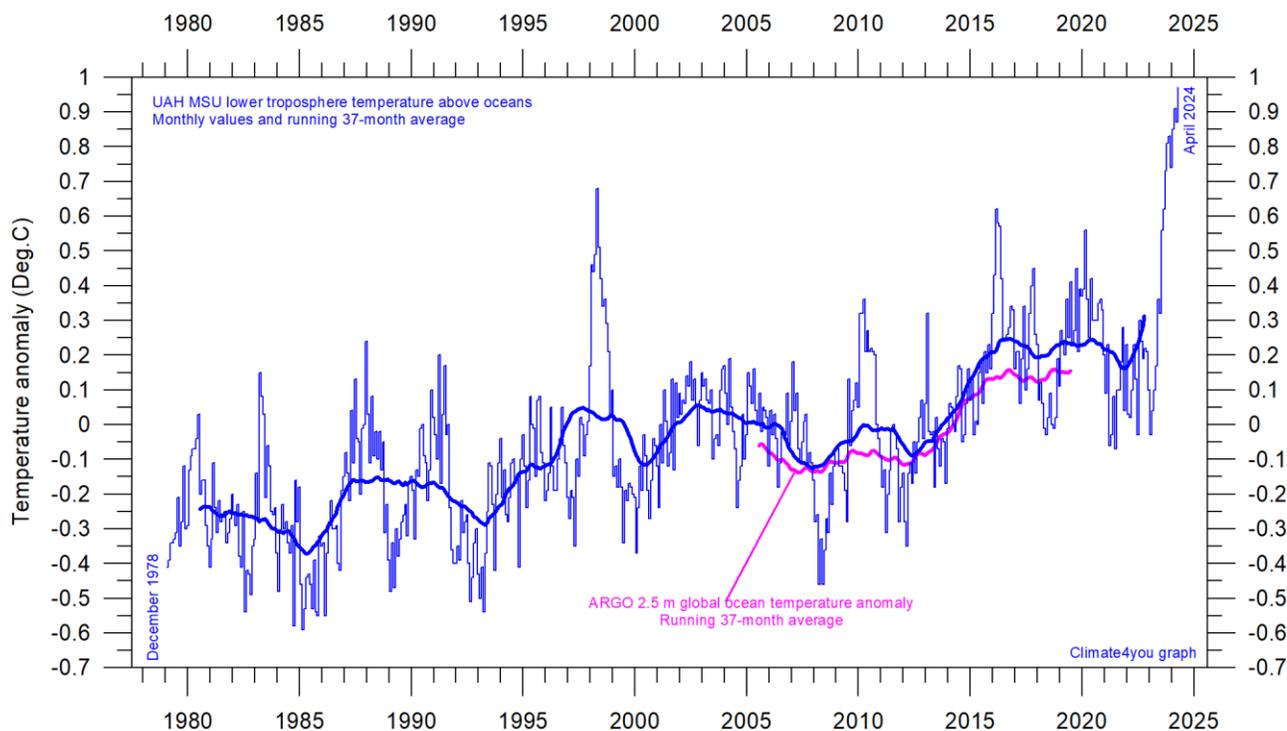
Global monthly average lower troposphere temperature over oceans (thin line) since 1979 according to University of Alabama at Huntsville, USA. The thick line is the simple running 37-month average. Insert: Argo global ocean temperature anomaly from floats, displaced vertically to make visual comparison easier. UAH reference period: 1991-2020.
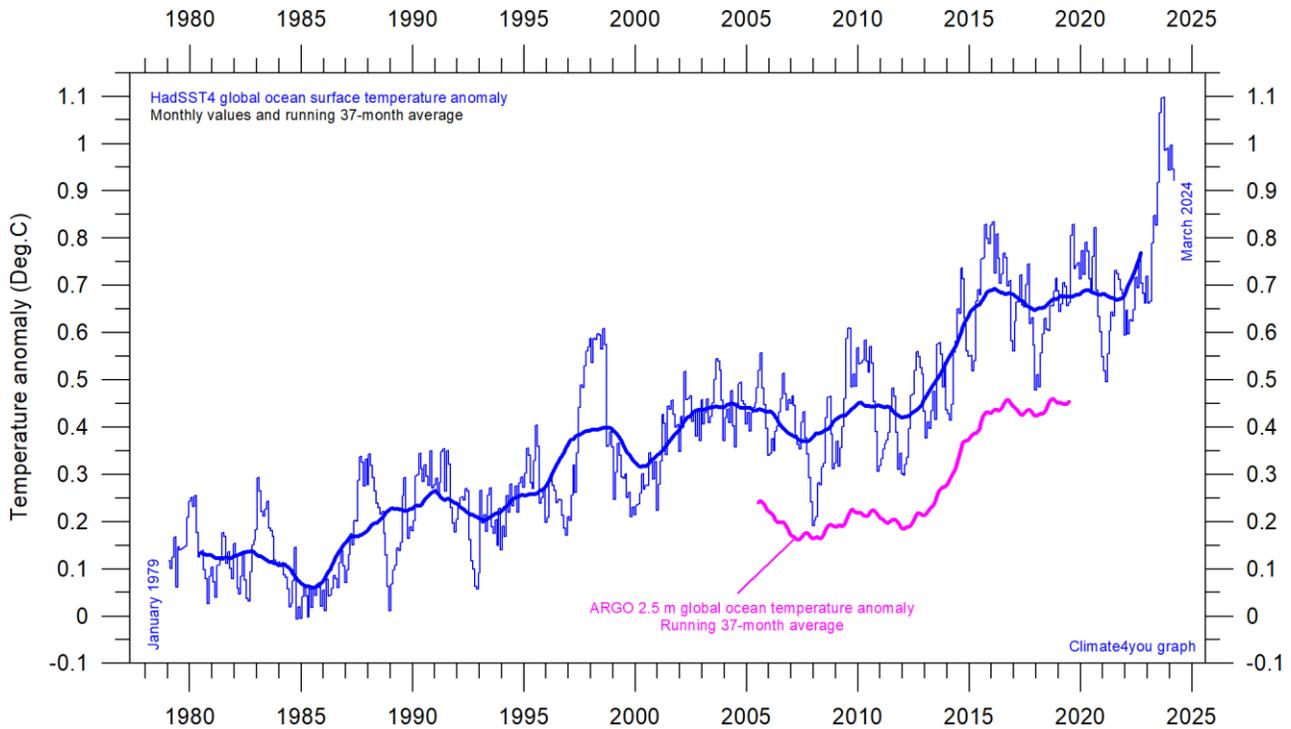
Global monthly average sea surface temperature since 1979 according to University of East Anglia's [Climatic Research Unit](CRU) (CRU), UK. Base period: 1961-1990. The thick line is the simple running 37-month average. Insert: Argo global ocean temperature anomaly from floats, displaced vertically to make visual comparison easier.
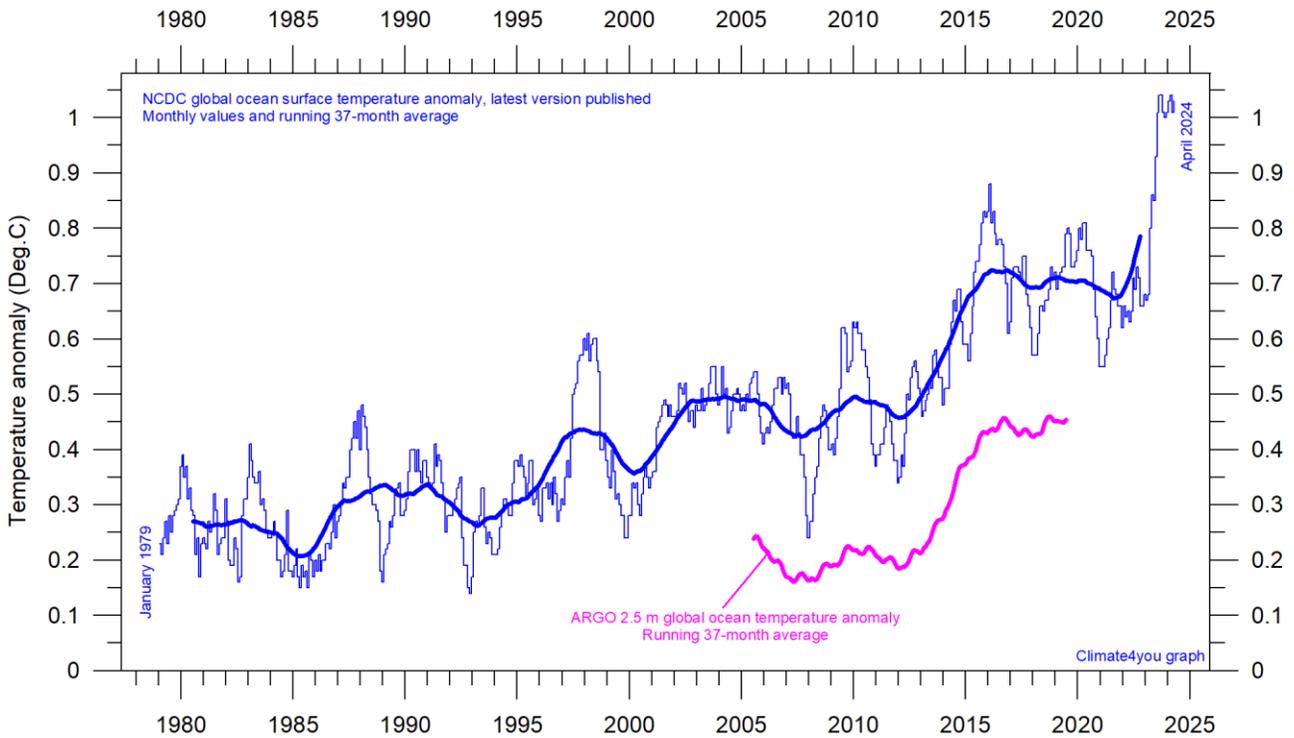
Global monthly average sea surface temperature since 1979 according to the [National Climatic Data Center](NCDC) (NCDC), USA. Base period: 1901-2000. The thick line is the simple running 37-month average. Insert: Argo global ocean temperature anomaly from floats, displaced vertically to make visual comparison easier.

Ocean temperature in uppermost 100 m, updated to March 2024
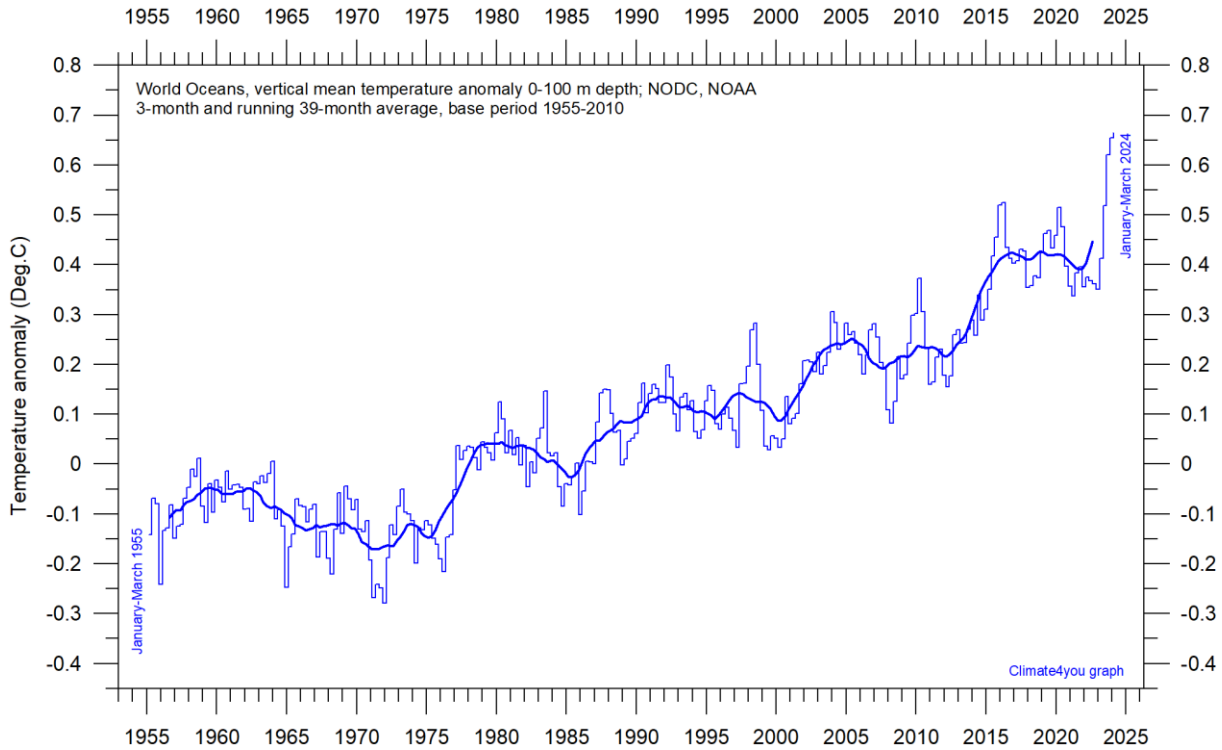
World Oceans vertical average temperature 0-100 m depth since 1955. The thin line indicates 3-month values, and the thick line represents the simple running 39-month (c. 3 year) average. Data source: NOAA National Oceanographic Data Center (NODC). Base period 1955-2010.

18
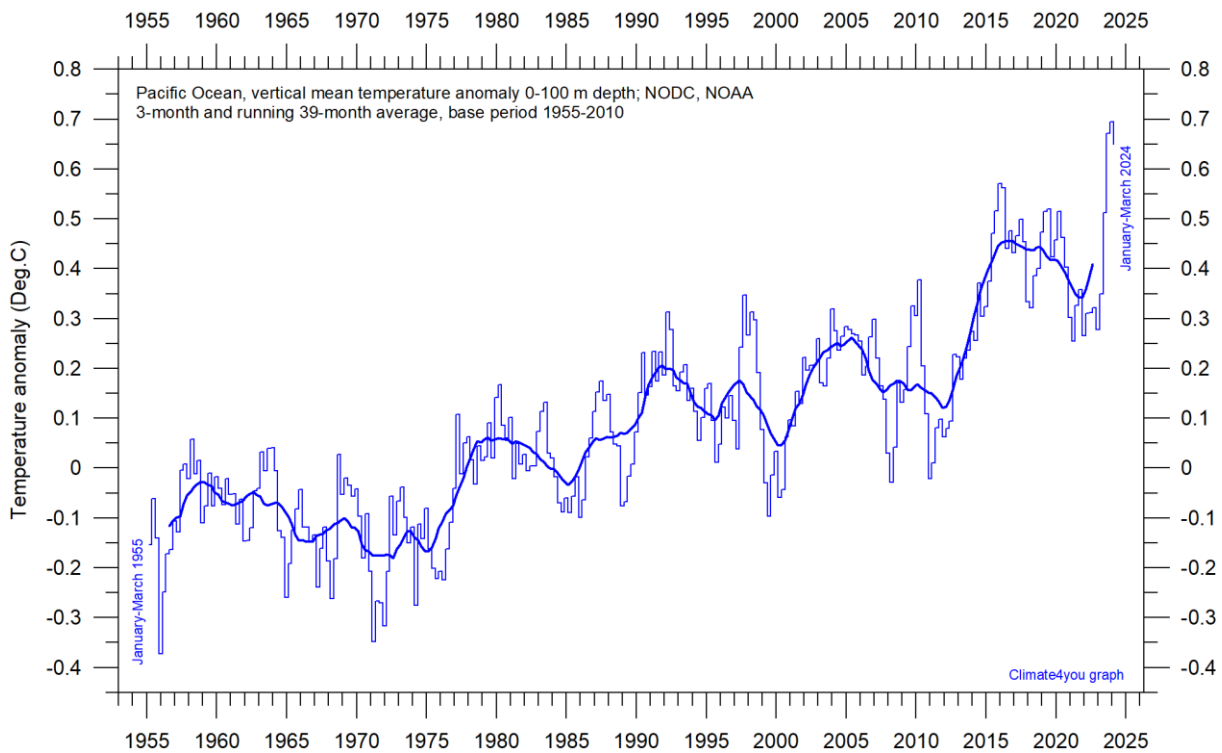
Pacific Ocean vertical average temperature 0-100 m depth since 1955. The thin line indicates 3-month values, and the thick line represents the simple running 39-month (c. 3 year) average. Data source: NOAA National Oceanographic Data Center (NODC). Base period 1955-2010.
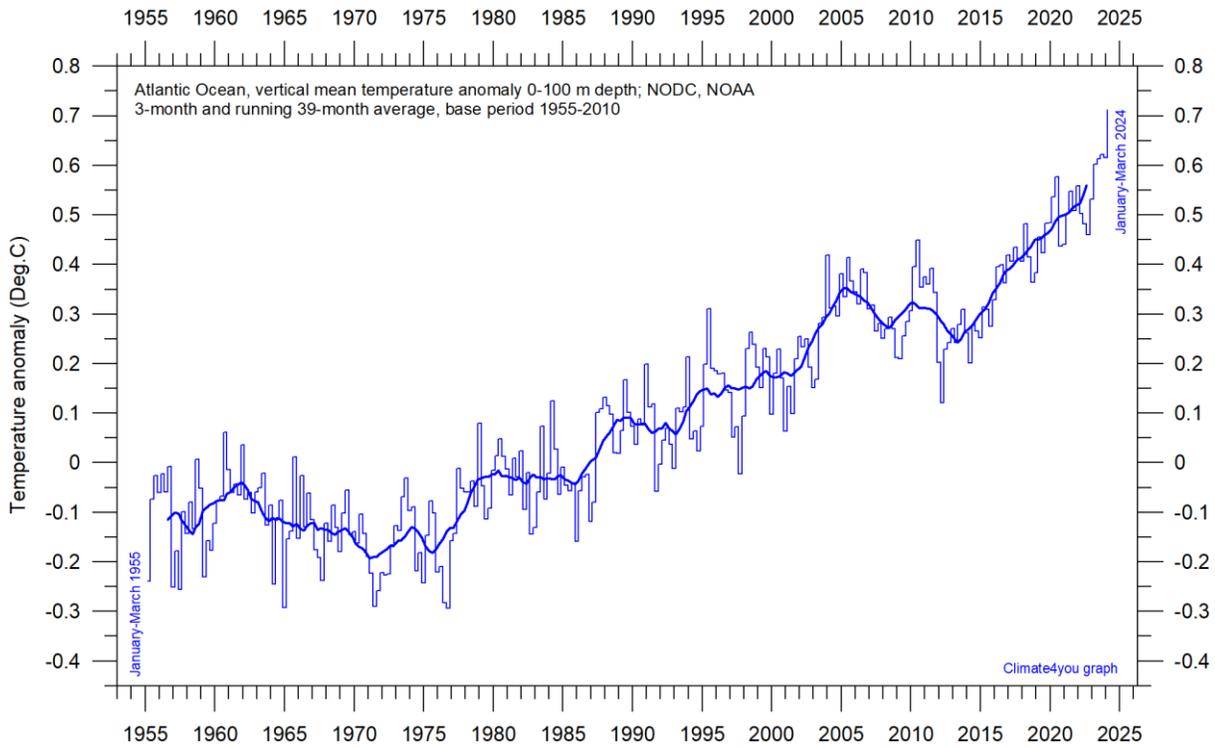
Atlantic Ocean vertical average temperature 0-100 m depth since 1955. The thin line indicates 3-month values, and the thick line represents the simple running 39-month (c. 3 year) average. Data source: [NOAA National Oceanographic Data Center](#) (NODC). Base period 1955-2010.
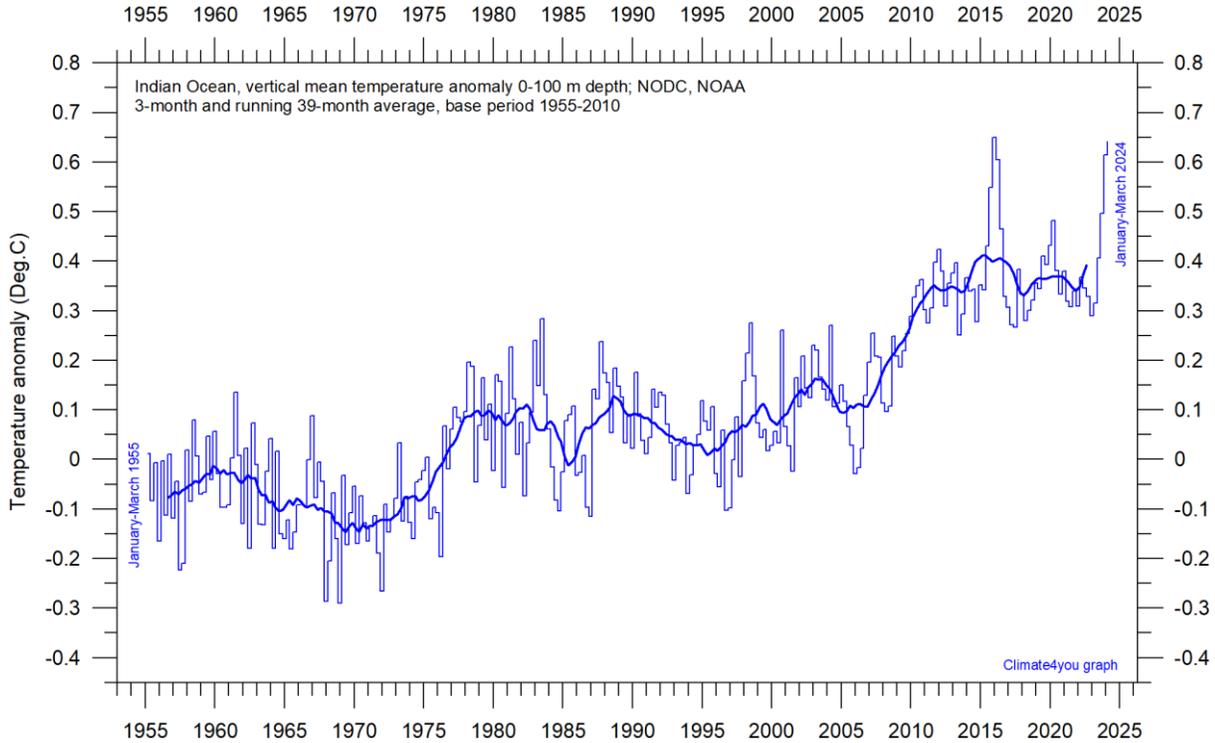
Indian Ocean vertical average temperature 0-100 m depth since 1955. The thin line indicates 3-month values, and the thick line represents the simple running 39-month (c. 3 year) average. Data source: [NOAA National Oceanographic Data Center](#) (NODC). Base period 1955-2010.

# Pacific Decadal Oscillation (PDO), updated to April 2024
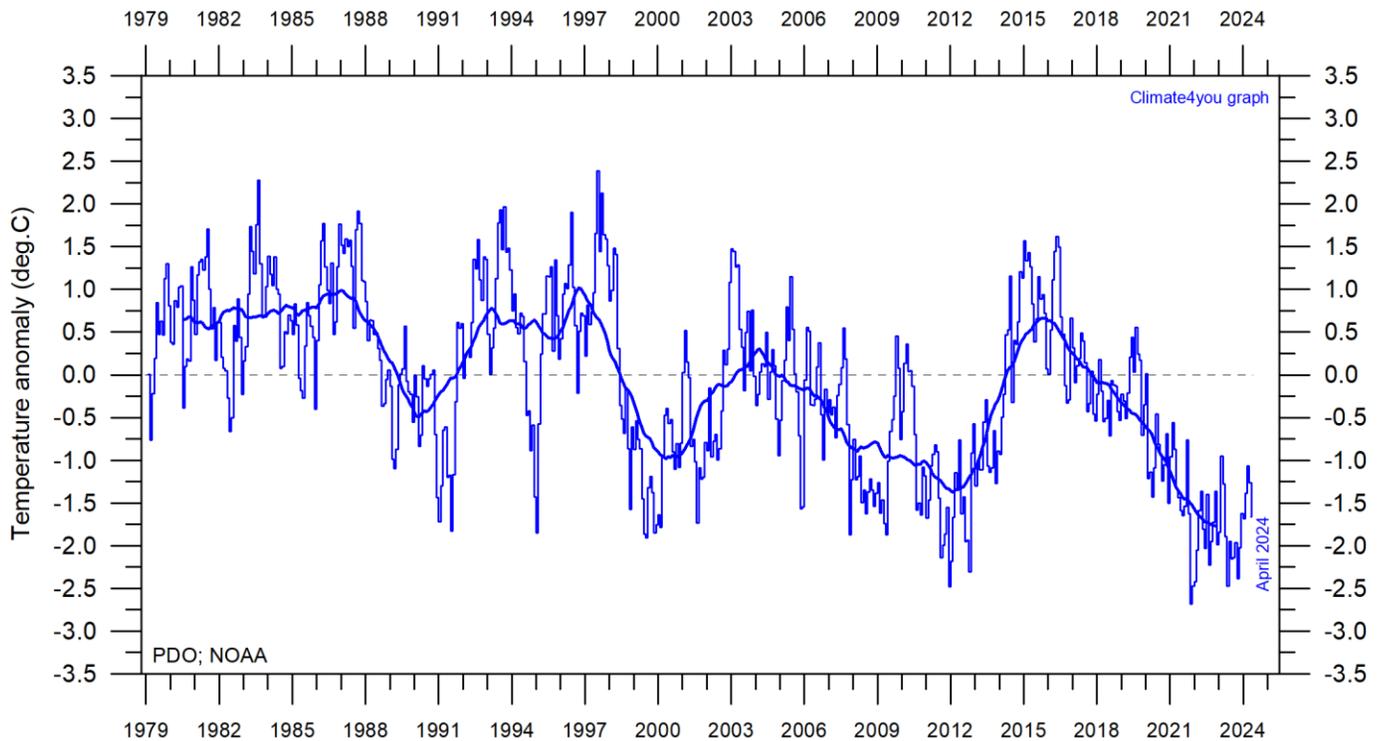
Monthly values of the Pacific Decadal Oscillation *(PDO) since January 1979. The PDO is a long-lived El Niño-like pattern of Pacific climate variability, and the data series goes back to January 1854. Base period: 1982-2002. The thin line indicates monthly PDO values, and the thick line is the simple running 37-month average. Data source: NOAA Physical Science Laboratory (version PDO ERSST V5 plotted above).*

The PDO is a long-lived El Niño-like pattern of Pacific climate variability, with data extending back to January 1854. Causes for PDO are not currently known, but even in the absence of a theoretical understanding, PDO climate information improves season-to-season and year-to-year climate forecasts for North America because of its strong tendency for multi-season and multi-year persistence. The PDO also appears to be roughly in phase with global temperature changes. Thus, from a societal impact's perspective, recognition of PDO is important because it shows that "normal" climate conditions can vary over time periods comparable to the length of a human's lifetime.

The PDO illustrates how global temperatures are tied to sea surface temperatures in the Pacific Ocean, the largest ocean on Earth. When sea surface temperatures are relatively low (negative phase PDO), as it was from 1945 to 1977, global air temperature often decreases. When Pacific Ocean surface temperatures are high (positive phase PDO), as from 1977 to 1998, global surface air temperature often increases.

A Fourier frequency analysis (not shown here) shows the PDO record to be influenced by a significant 5.6-year cycle, and feasibly also by a longer 18.6-year long period, corresponding to the length of the lunar nodal tide.
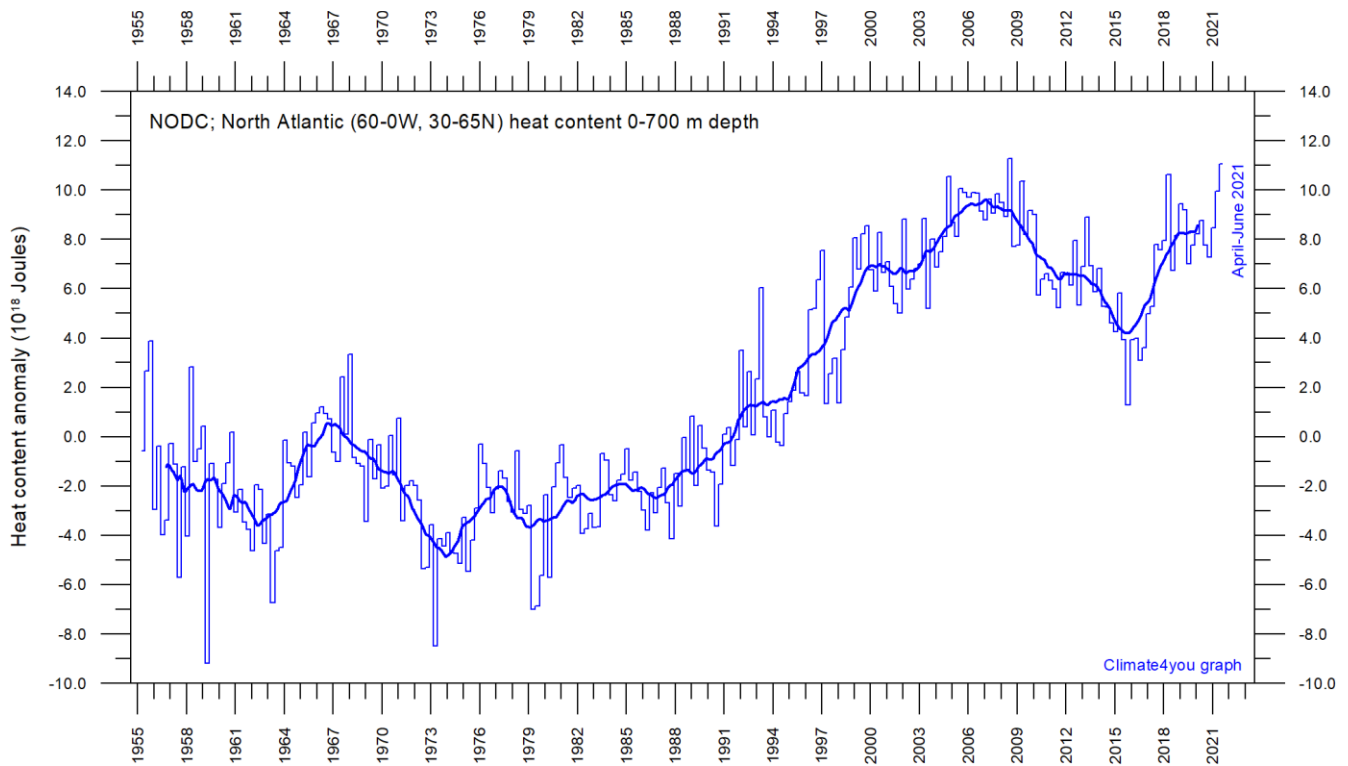
Global monthly heat content anomaly (10^{18} Joules) in the uppermost 700 m of the North Atlantic (60-0W, 30-65N; see map above) *ocean since January 1955. The thin line indicates monthly values, and the thick line represents the simple running 37-month (c. 3 year) average. Data source: National Oceanographic Data Center (NODC).*

North Atlantic temperatures 0-800 m depth along 59°N, 30-0W, updated to December 2021
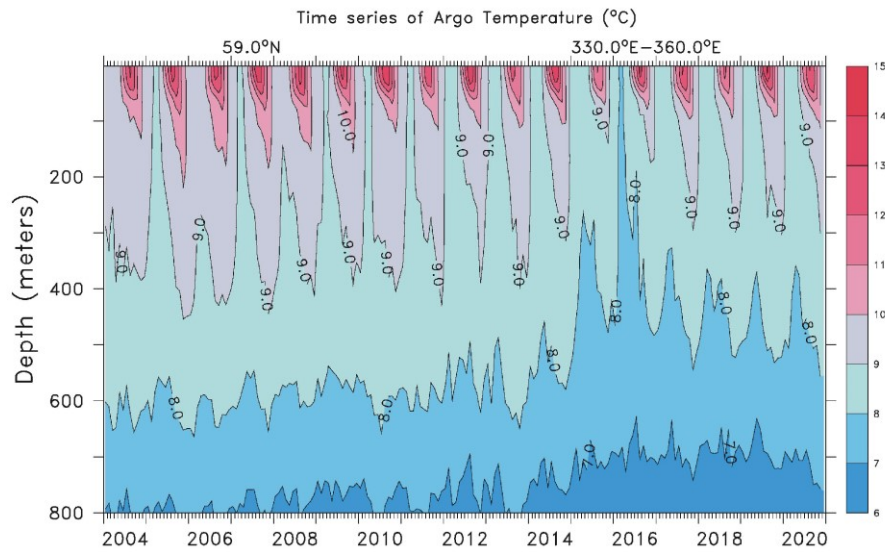
Time series depth-temperature diagram along 59 N across the North Atlantic Current from 30°W to 0°W, from surface to 800 m depth. Source: Global Marine Argo Atlas. See also the diagram below.
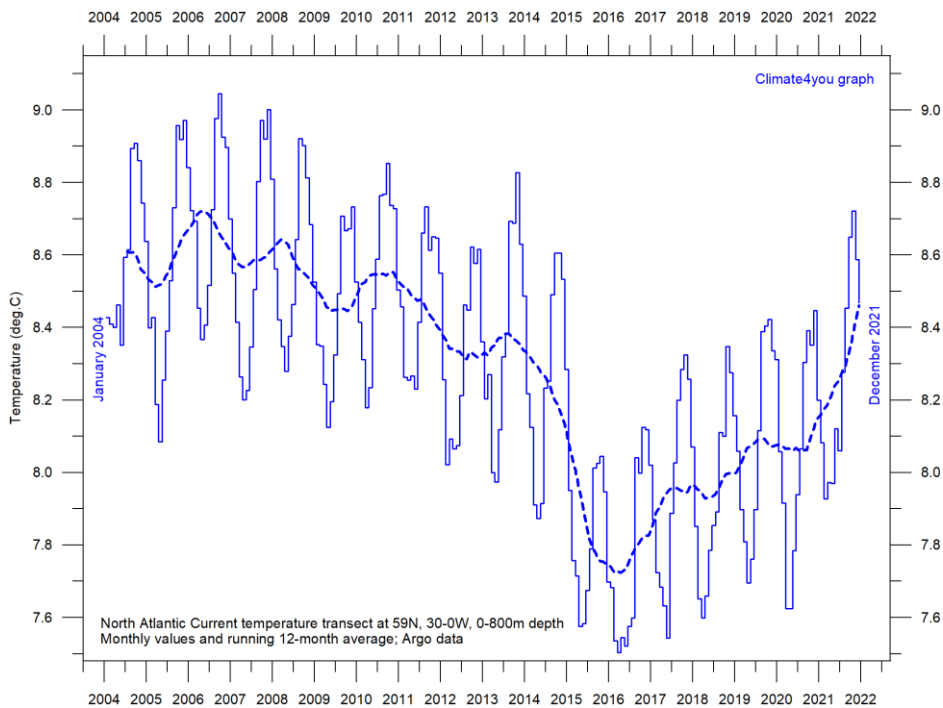
Average temperature along 59 N, 30-0W, 0-800m depth, corresponding to the main part of the North Atlantic Current, using Argo-data. Source: Global Marine Argo Atlas. Additional information can be found in: Roemmich, D. and J. Gilson, 2009. The 2004-2008 mean and annual cycle of temperature, salinity, and steric height in the global ocean from the Argo Program. Progress in Oceanography, 82, 81-100.

Global ocean temperature 0-1900 m depth summary, updated to December 2021
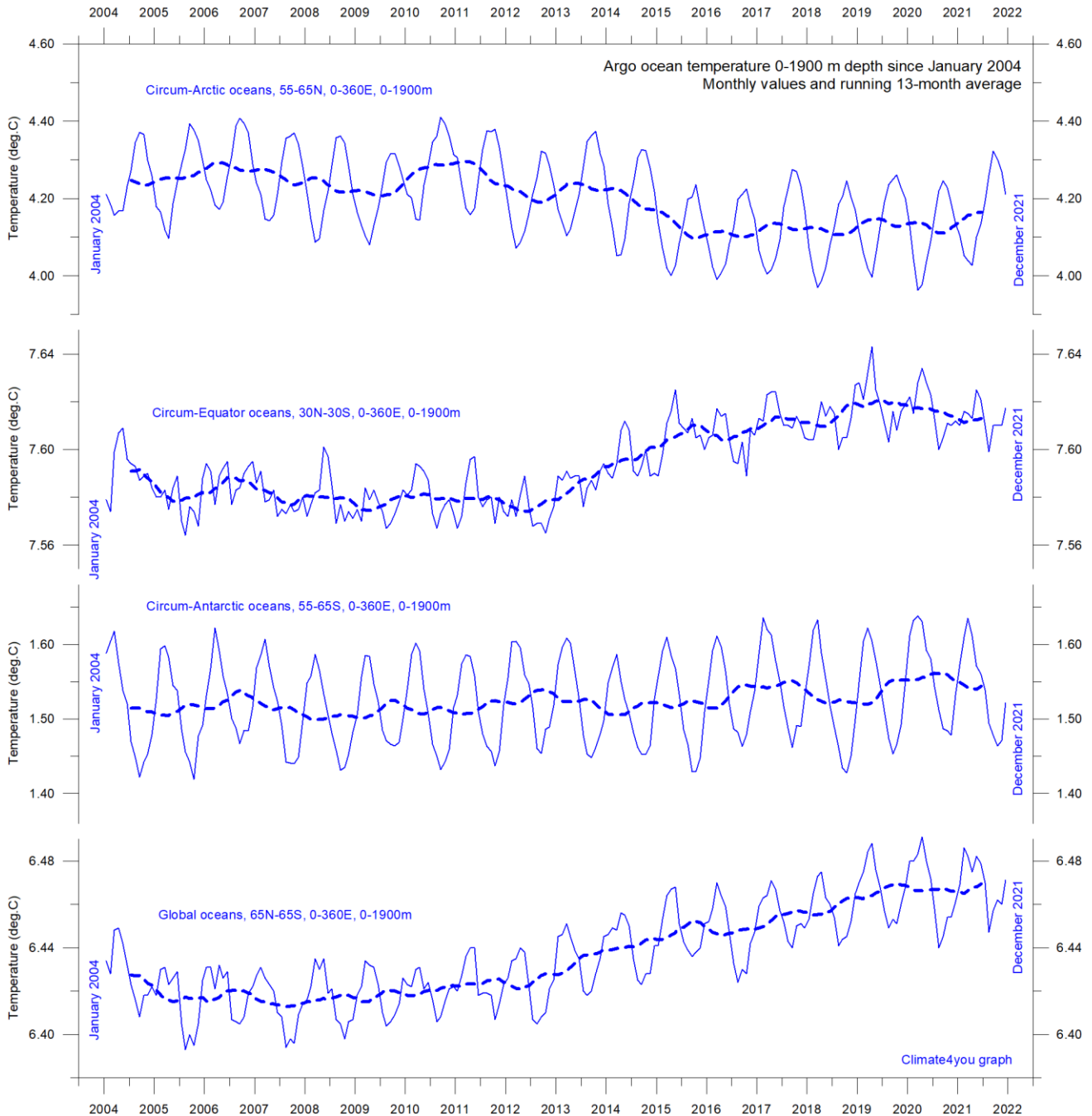
Summary of average temperature in uppermost 1900 m in different parts of the global oceans, using Argo-data. Source: Global Marine Argo Atlas. Additional information can be found in: Roemmich, D. and J. Gilson, 2009. The 2004-2008 mean and annual cycle of temperature, salinity, and steric height in the global ocean from the Argo Program. Progress in Oceanography, 82, 81-100.

The temperature of the global oceans down to 1900 m depth has been increasing since about 2011, but with a possible peak around 2020. The global increase since 2013 is mainly due to changes occurring near the Equator, between 30ºN and 30ºS. In contrast, for the circum-Arctic oceans north of 55ºN, depth-integrated ocean temperatures have been decreasing since 2011, but with a possible low around 2019. Near the Antarctic, south of 55ºS, temperatures have essentially been stable. At most latitudes, a clear annual rhythm is evident.

Global ocean net temperature change since 2004 at different depths, updated to December 2020
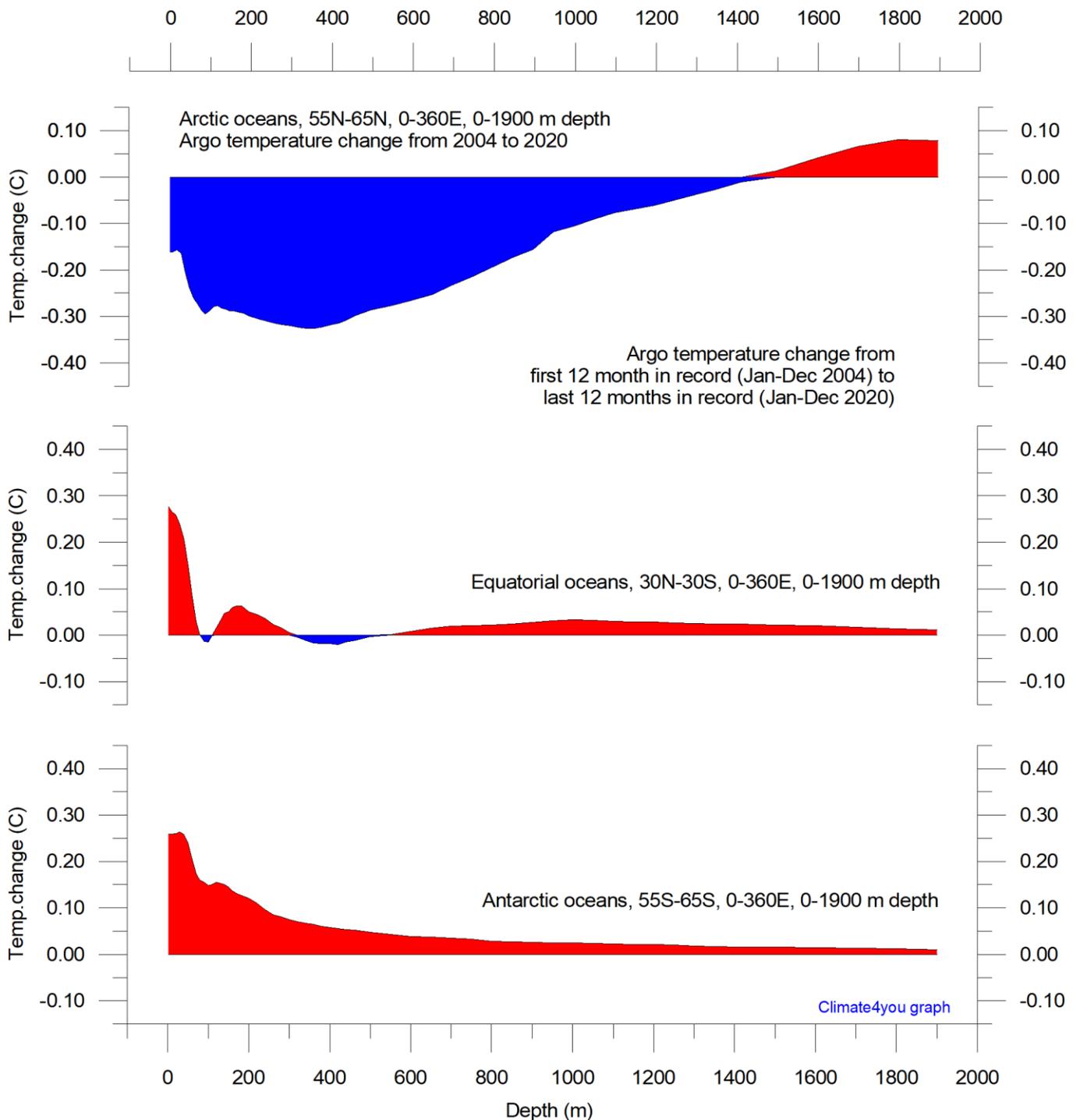
Net temperature change since 2004 from surface to 1900 m depth in different parts of the global oceans, using *Argo*-data. Source: *Global Marine Argo Atlas*. Additional information can be found in: Roemmich, D. and J. Gilson, 2009. The 2004-2008 mean and annual cycle of temperature, salinity, and steric height in the global ocean from the Argo Program. *Progress in Oceanography*, 82, 81-100. Please note that due to the spherical form of Earth, northern and southern latitudes represent only small ocean volumes, compared to latitudes near the Equator.

La Niña and El Niño episodes, Oceanic Niño Index (ONI), updated to April 2024
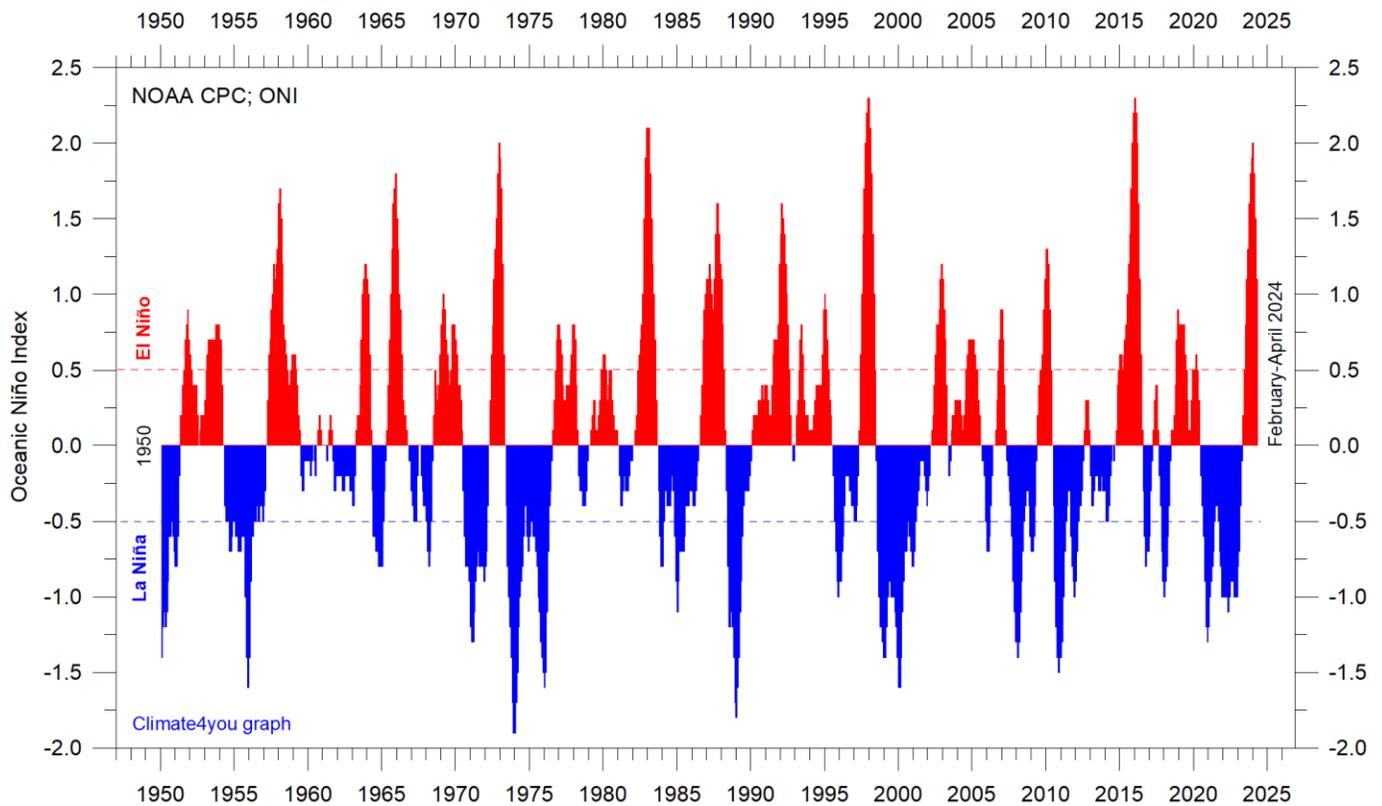
Warm (>+0.5ºC) and cold (<0.5ºC) episodes for the Oceanic Niño Index (ONI), defined as 3 month running mean of ERSSTv4 SST anomalies in the Niño 3.4 region (5ºN-5ºS, 120º-170ºW)]. For historical purposes cold and warm episodes are defined when the threshold is met for a minimum of 5 consecutive over-lapping seasons. Anomalies are centred on 30-yr base periods updated every 5 years.

In the Pacific Ocean, trade winds usually blow west along the equator, pushing warm water from South America towards Asia. To replace that warm water, cold water rises from the depths near South America. During El Niño episodes, trade winds weaken, and warm water is spreading back east, toward South America. In contrast, during La Niña episodes, trade winds are stronger than usual, pushing more warm water than usual toward Asia, and upwelling of cold water near South America therefore increases.

The 2015-16 El Niño episode is among the strongest since the beginning of the record in 1950. Considering the entire record, however, recent variations between El Niño and La Niña episodes do not appear abnormal in any way.

A Fourier frequency analysis (not shown here) shows the ONI record to be influenced by a significant 3.6-year cycle, and feasibly also by a longer 5.6-year cycle.
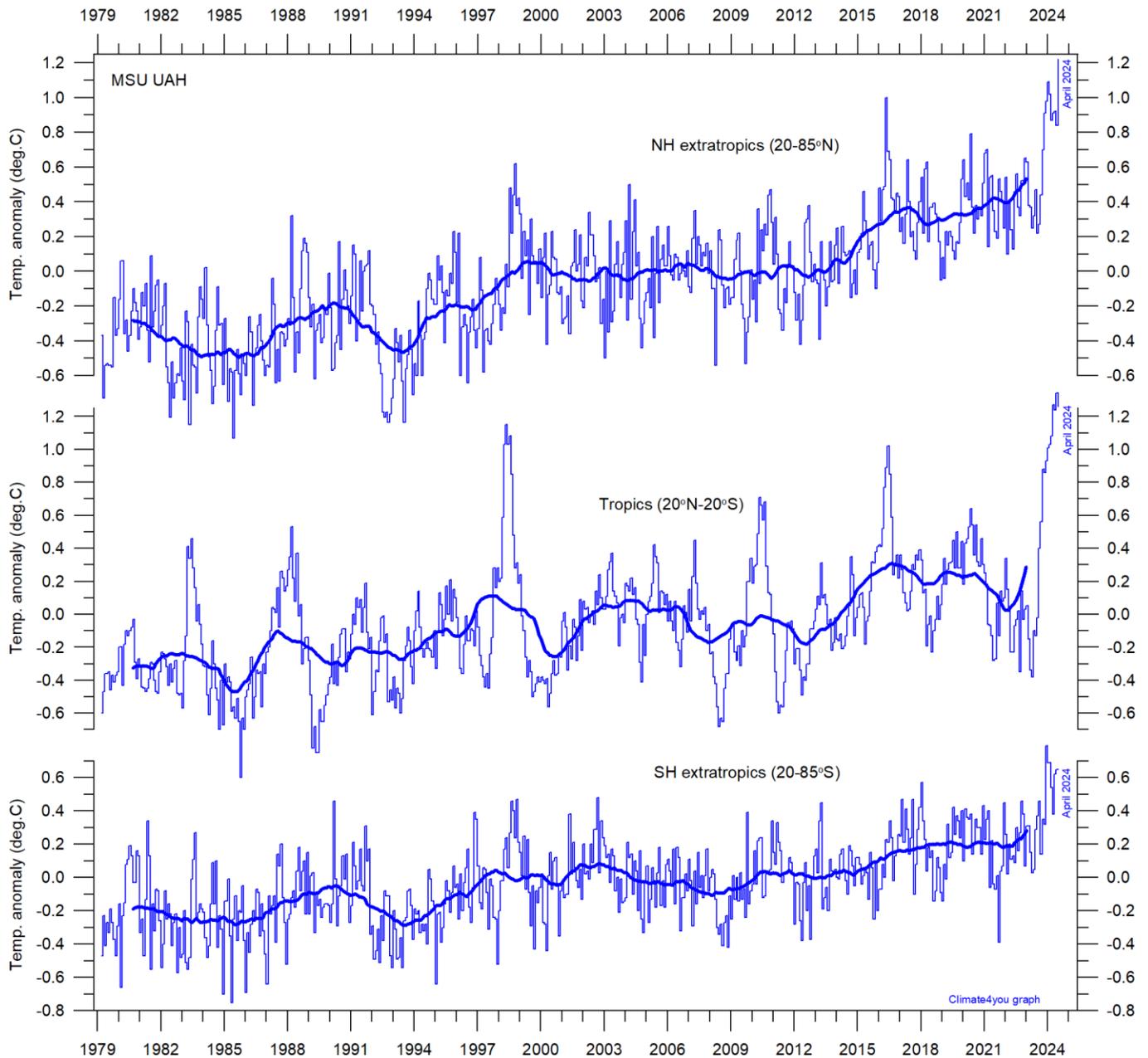
Global monthly average lower troposphere temperature since 1979 for the tropics and the northern and southern extratropics, according to University of Alabama at Huntsville, USA. Thin lines show the monthly temperature. Thick lines represent the simple running 37-month average, nearly corresponding to a running 3-year average. Reference period 1981-2010.

The overall warming since 1980 has dominantly been a northern hemisphere phenomenon, and mainly played out as a marked change between 1994 and 1999. However, this rather rapid temperature change is probably influenced by the Mt. Pinatubo eruption 1992-93 and the subsequent 1997 El Niño episode. The diagram also shows the temperature effects of the strong Equatorial El Niño's in 1997 and 2015-16, as well as the moderate El Niño in 2019. Apparently, these effects were spreading to higher latitudes in both hemispheres with some delay. Just now a new El Niño is playing out in the Pacific Ocean (p.25), as clearly shown by tropics surface air temperatures.

Arctic and Antarctic lower troposphere temperature, updated to April 2024
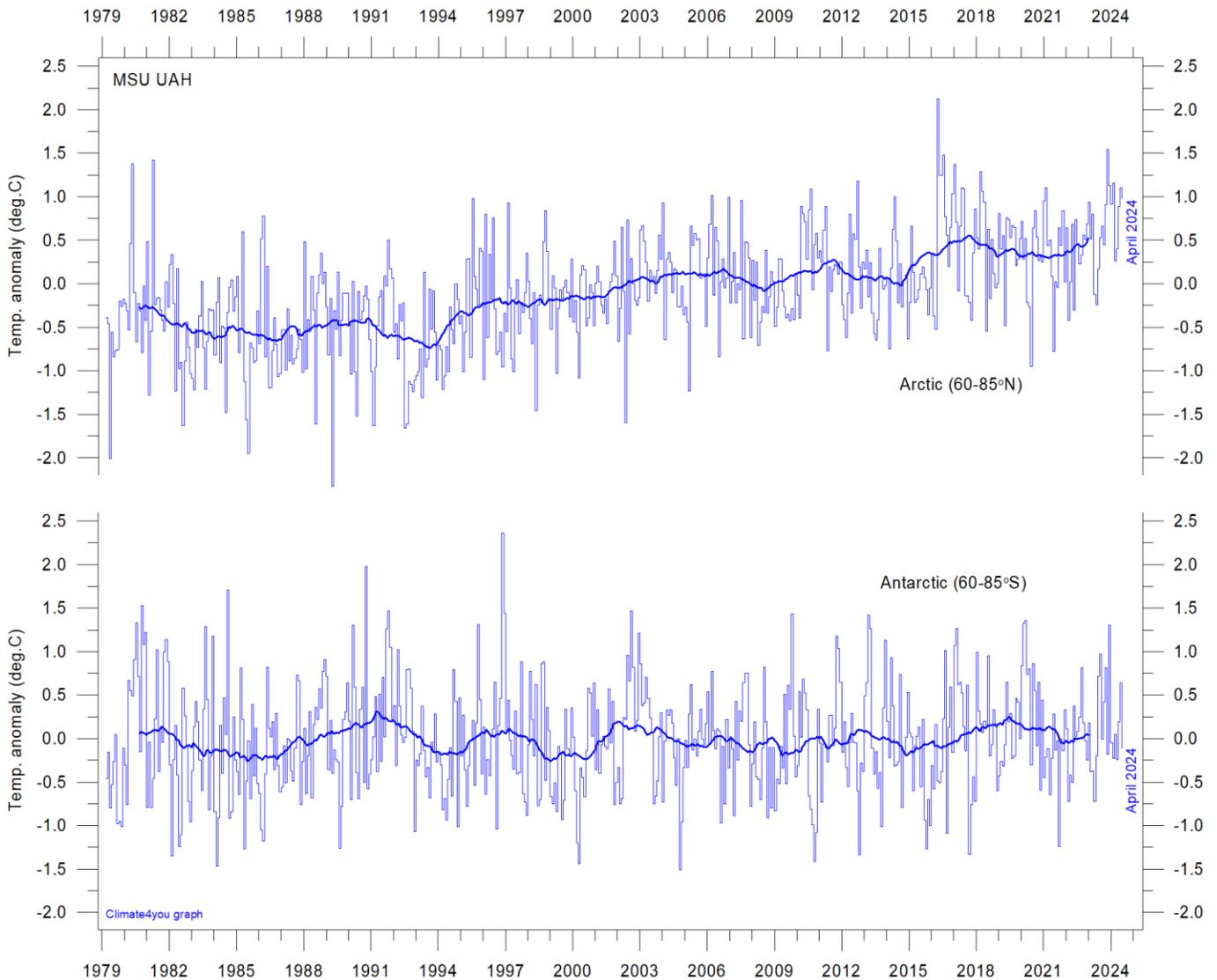
Global monthly average lower troposphere temperature since 1979 for the North Pole and South Pole regions, based on satellite observations (University of Alabama at Huntsville, USA). Thin lines show the monthly temperature. The thick line is the simple running 37-month average, nearly corresponding to a running 3-year average. Reference period 1991-2020.

In the Arctic region, warming mainly took place 1994-96, and less so subsequently. In 2016, however, temperatures peaked for several months, presumably because of oceanic heat given off to the atmosphere during the 2015-15 El Niño (see also diagram on page 25) and subsequently advected to higher latitudes.

This underscores how Arctic air temperatures may be affected not only by variations in local conditions but also by variations playing out in geographically remote regions.

A slight temperature decrease has characterised the Arctic since the marked 2016 El Niño peak. In contrast, the present (2023-24) El Niño episode is recorded by Arctic temperatures in a less pronounced way.

In the Antarctic region, temperatures have basically remained stable since the onset of the satellite record in 1979. In 2016-17 a small temperature peak visible in the monthly record may be interpreted as the subdued effect of the recent El Niño episode.

Arctic and Antarctic surface air temperature, updated to December 2021

Diagram showing area weighted Arctic (70-90ºN) monthly surface air temperature anomalies (HadCRUT4) since January 2000, in relation to the WMO normal period 1961-1990. The thin line shows the monthly temperature anomaly, while the thicker line shows the running 37-month (c. 3 year) average.

Diagram showing area weighted Antarctic (70-90ºS) monthly surface air temperature anomalies (HadCRUT4) since January 2000, in relation to the WMO normal period 1961-1990. The thin line shows the monthly temperature anomaly, while the thicker line shows the running 37-month (c. 3 year) average.

Diagram showing area weighted Arctic (70-90ºN) monthly surface air temperature anomalies (HadCRUT4) since January 1957, in relation to the WMO normal period 1961-1990. The thin line shows the monthly temperature anomaly, while the thicker line shows the running 37-month (c. 3 year) average.

Diagram showing area weighted Antarctic (70-90ºS) monthly surface air temperature anomalies (HadCRUT4) since January 1957, in relation to the WMO normal period 1961-1990. The thin line shows the monthly temperature anomaly, while the thicker line shows the running 37-month (c. 3 year) average.

Diagram showing area-weighted Arctic (70-90ºN) monthly surface air temperature anomalies ([HadCRUT4](#)) since January 1920, in relation to the WMO [normal period](#) 1961-1990. The thin line shows the monthly temperature anomaly, while the thicker line shows the running 37-month (c. 3 year) average.

Because of the relatively small number of Arctic stations before 1930, month-to-month variations in the early part of the Arctic temperature record 1920-2018 are higher than later (diagram above).

The period from about 1930 saw the establishment of many new Arctic meteorological stations, first in Russia and Siberia, and following the 2nd World War, also in North America, explaining the above difference.

The period since 2005 is warm, about as warm as the period 1930-1940.

As the HadCRUT4 data series has improved high latitude coverage data coverage (compared to the HadCRUT3 series), the individual 5ºx5º grid cells have been weighted according to their surface area. This area correction is especially important for polar regions, where longitudes converge rapidly. This approach differs from the approach used by Gillet et al. 2008, which calculated a simple average, with no correction for the substantial latitudinal surface area effect in polar regions.

The area weighted Arctic HadCRUT4 surface air temperature anomalies (p.28-30) correspond rather well to the lower troposphere temperature anomalies recorded by satellites (p.27).

Literature:

Gillett, N.P., Stone, D.A., Stott, P.A., Nozawa, T., Karpechko, A.Y.U., Hegerl, G.C., Wehner, M.F. and Jones, P.D. 2008. Attribution of polar warming to human influence. *Nature Geoscience* 1, 750-754.

Long Arctic annual surface air temperature series, updated to year 2023
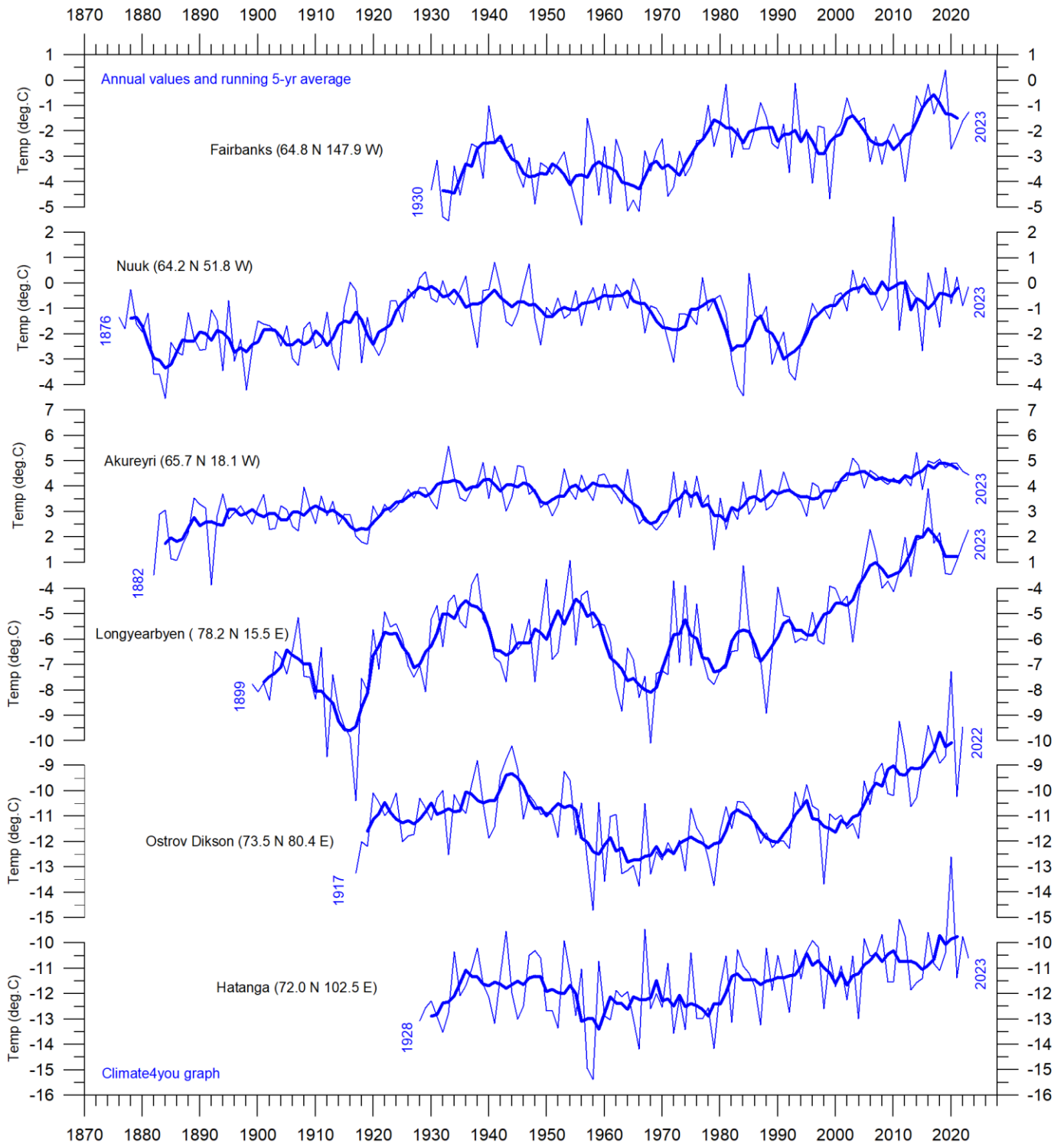
Arctic annual surface air temperature series, selected because of their length of observation time. The thin blue line represents the mean annual air temperature, and the thick blue line is the running 5-year average. Annual values were calculated from monthly average temperatures. More info on Climate4you.

Long Antarctic annual surface air temperature series, updated to year 2023
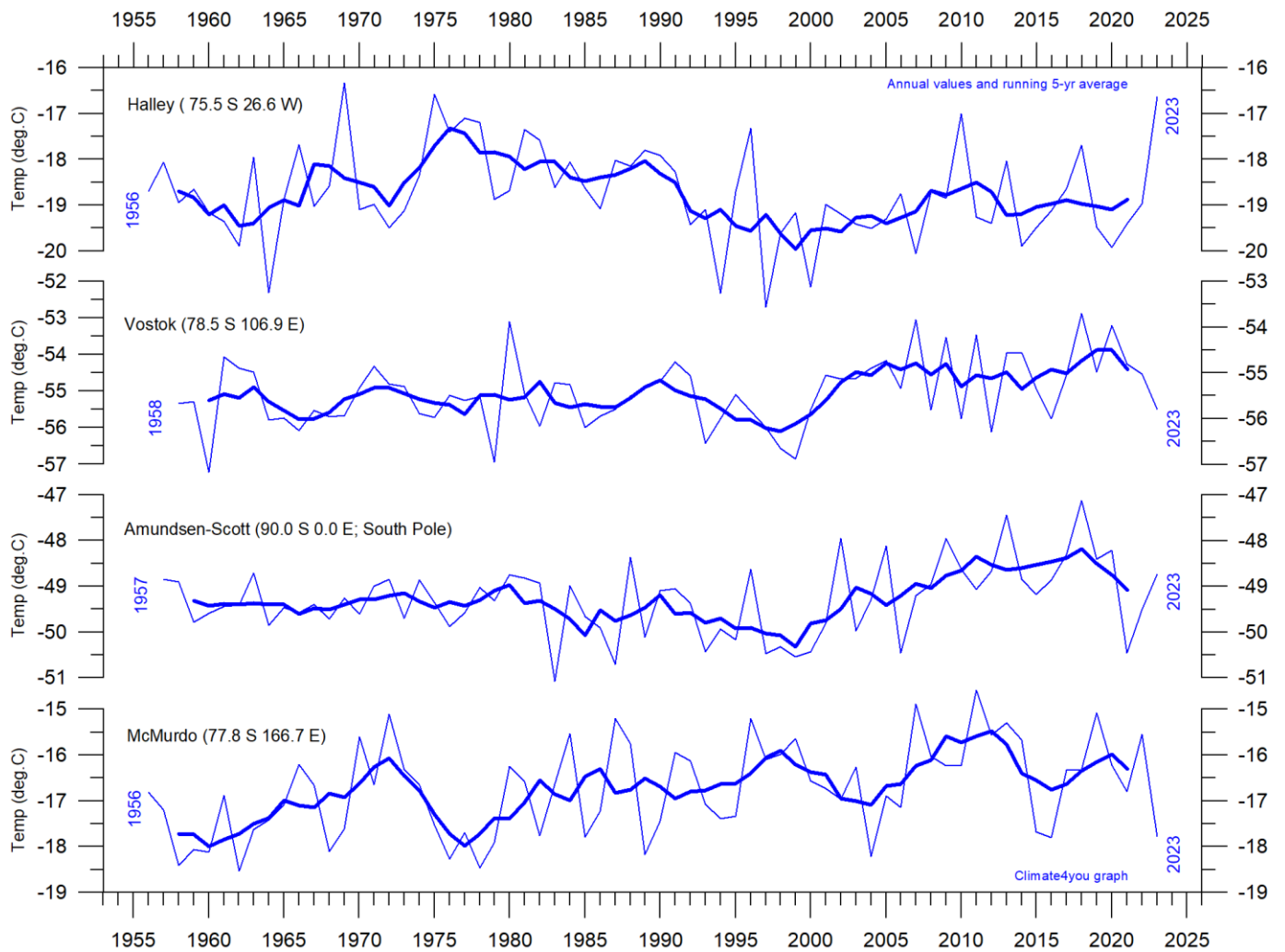
Antarctic annual surface air temperature series, selected because of their length of observation time. The thin blue line represents the mean annual air temperature, and the thick blue line is the running 5-year average. Annual values were calculated from monthly average temperatures. More info on Climate4you.

Temperature over land versus over oceans, updated to April 2024
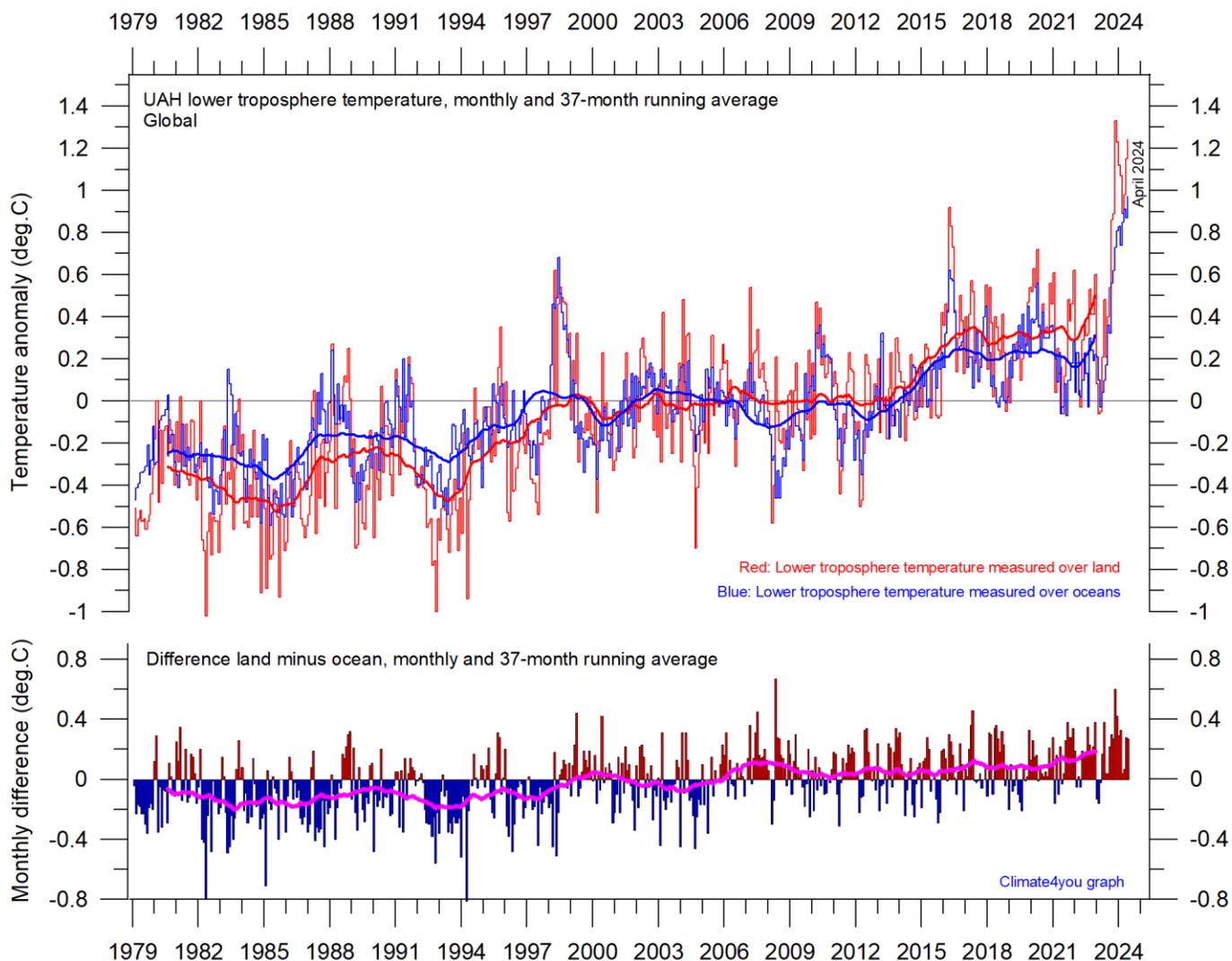
Global monthly average lower troposphere temperature since 1979 measured over land and oceans, respectively, according to [University of Alabama](#) at Huntsville, USA. Thick lines are the simple running 37-month average, nearly corresponding to a running 3-year average. Reference period 1991-2020.

Since 1979, the lower troposphere over land has warmed much more than over oceans, suggesting that the overall warming is derived mainly from incoming solar radiation. In addition, there may be supplementary reasons for this divergence, such as, e.g., variations in cloud cover and changes in land use.

The present (2023) El Niño episode is recorded more pronounced over land regions, compared to ocean regions.

Troposphere and stratosphere temperatures from satellites, updated to April 2024
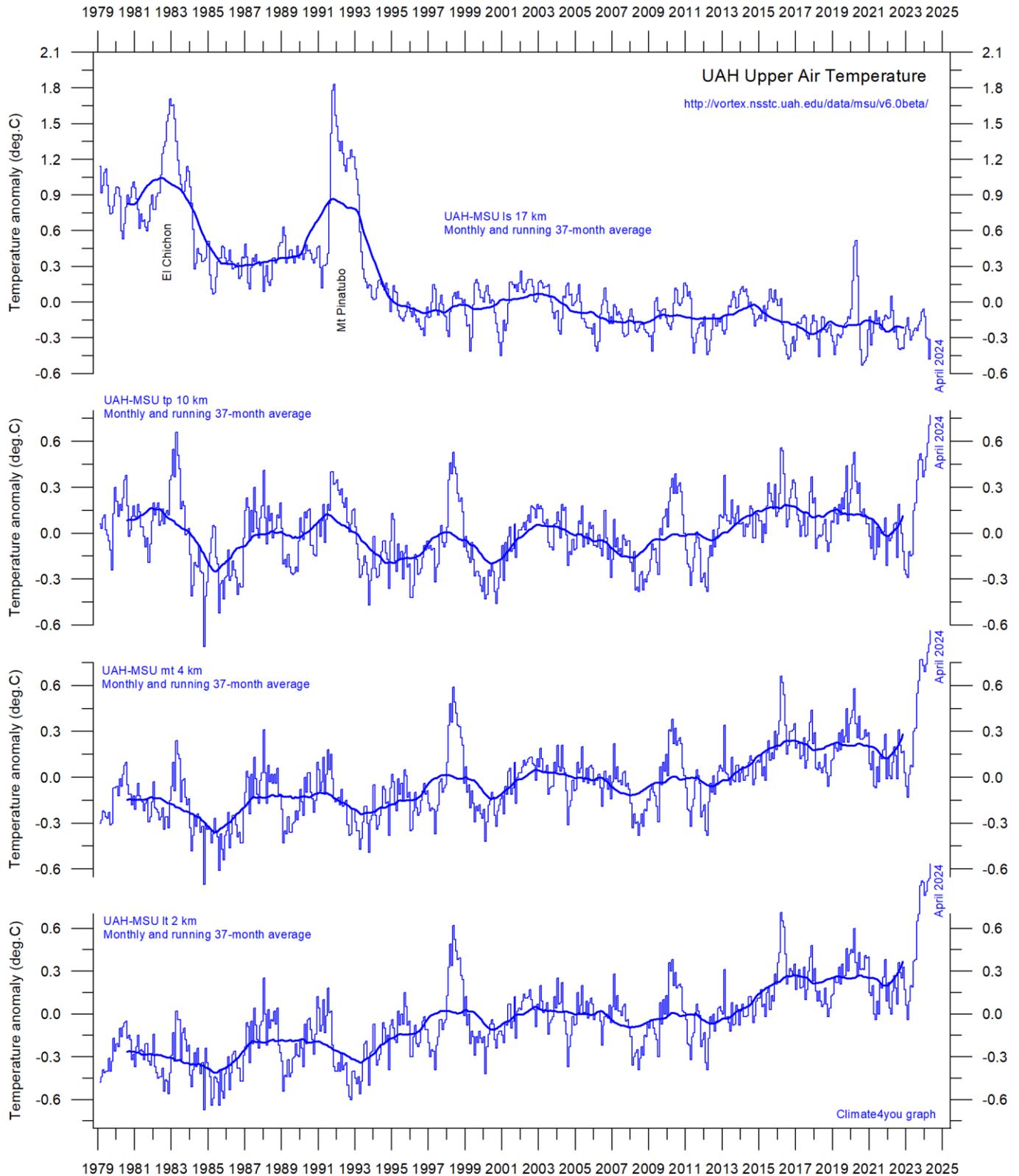
Global monthly average temperature in different according to University of Alabama at Huntsville, USA. The thin lines represent the monthly average, and the thick line the simple running 37-month average, nearly corresponding to a running 3-year average. Reference period 1991-2020.

Arctic and Antarctic sea ice, updated to April 2024
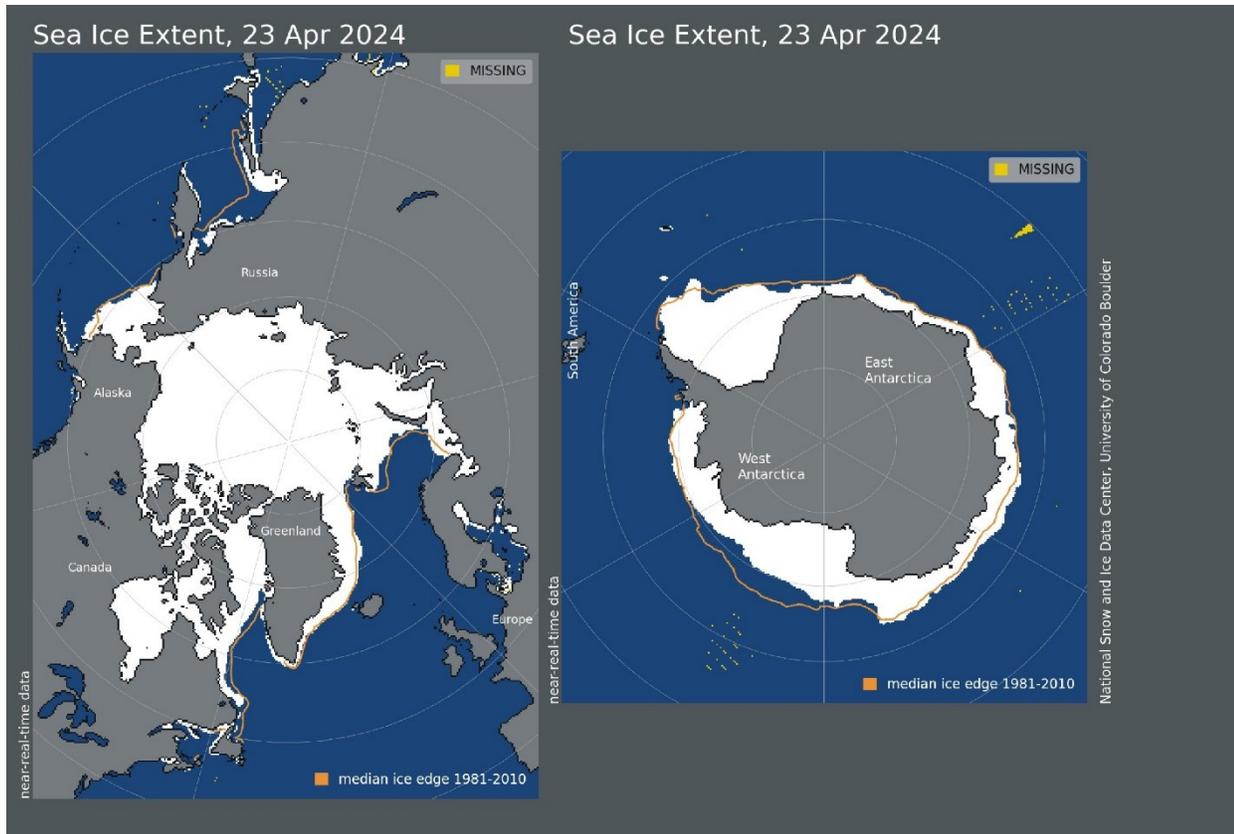
Sea ice extent 23 April 2024. The median limit of sea ice (orange line) is defined as 15% sea ice cover, according to the average of satellite observations 1981-2010 (both years included). Sea ice may therefore well be encountered outside and open water areas inside the limit shown in the diagrams above. Map source: National Snow and Ice Data Center (NSIDC).
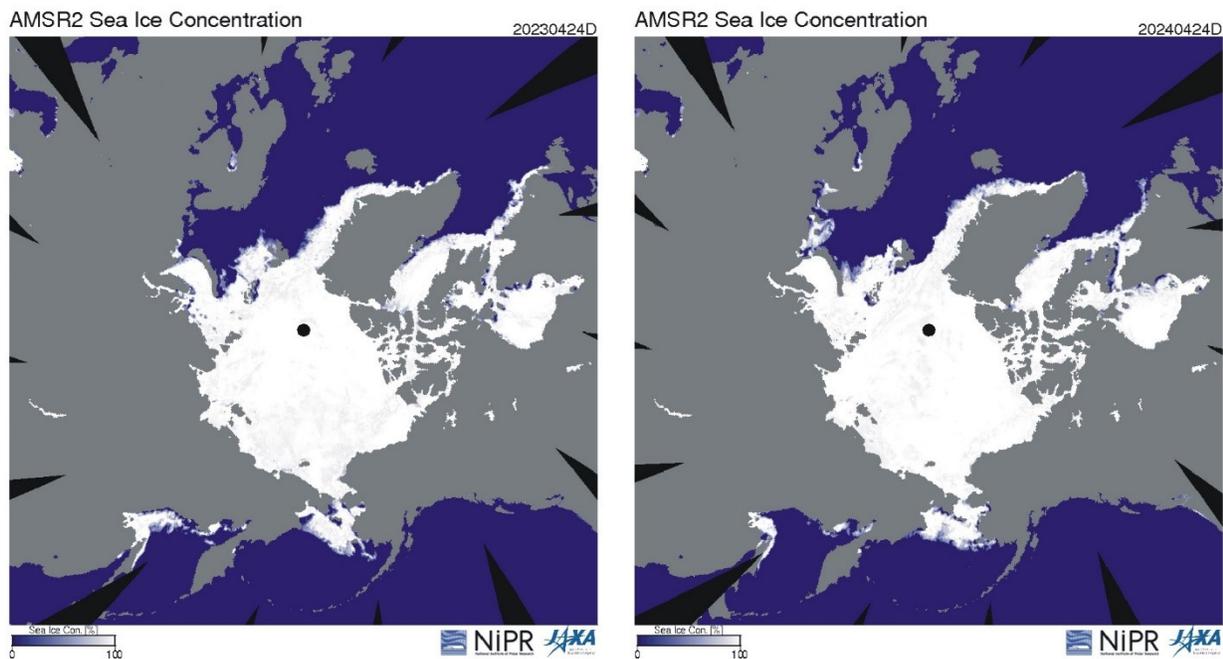
Diagrams showing Arctic sea ice extent and concentration 24 April 2023 (left) and 2024 (right), according to the Japan Aerospace Exploration Agency (JAXA).
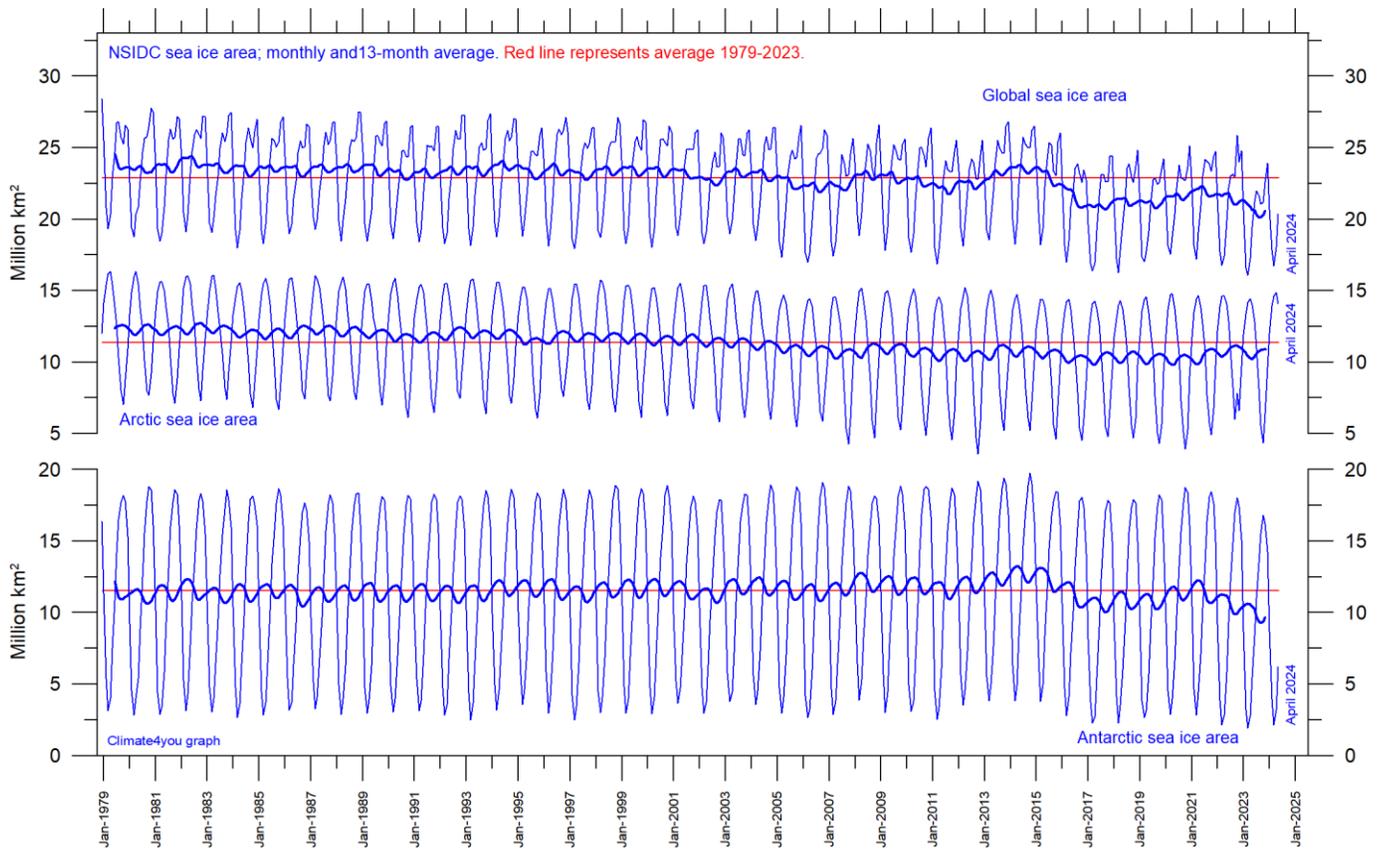
Graphs showing monthly Antarctic, Arctic, and global sea ice extent since November 1978, according to the [National Snow and Ice data Center](#) (NSIDC).

36
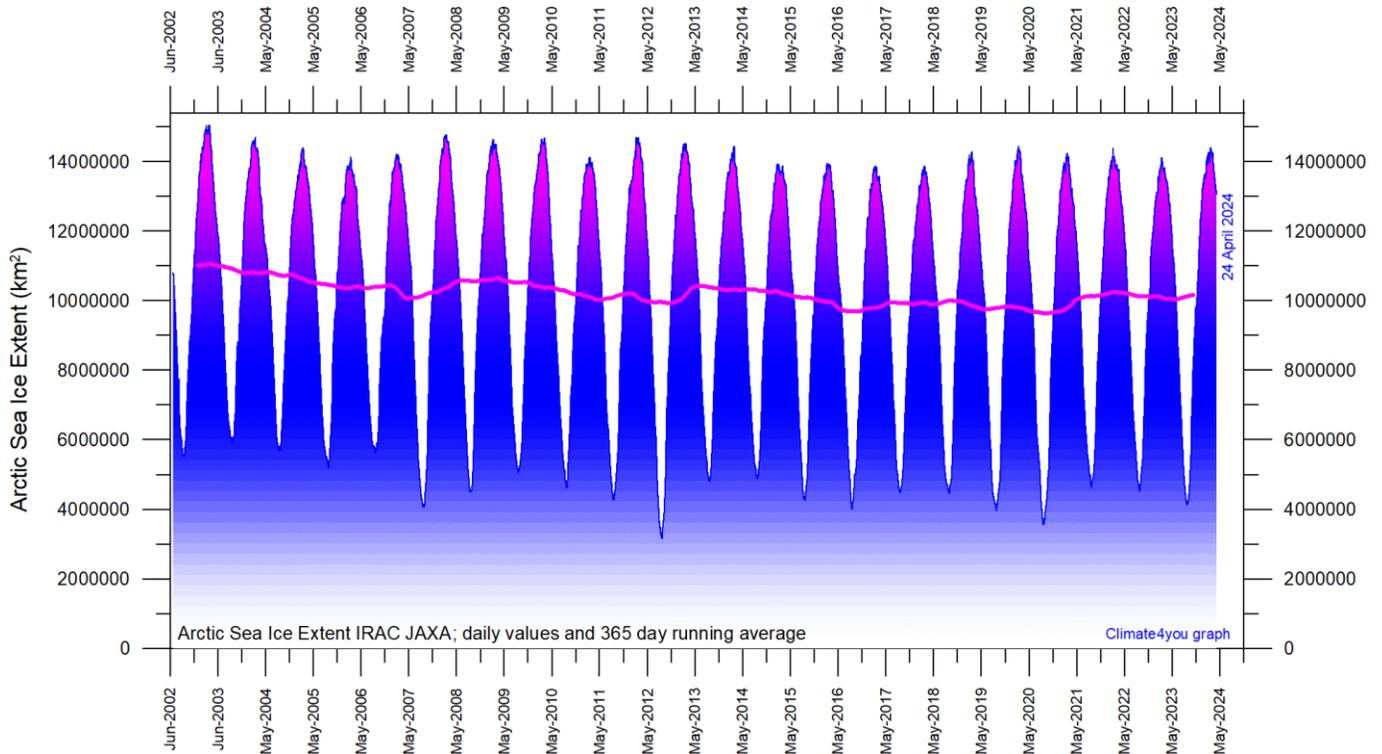
Diagram showing daily Arctic sea ice extent since June 2002, to 24 April 2024, data courtesy of [Japan Aerospace Exploration Agency](#) (JAXA).

Sea Ice Thickness, 21-Apr-2024
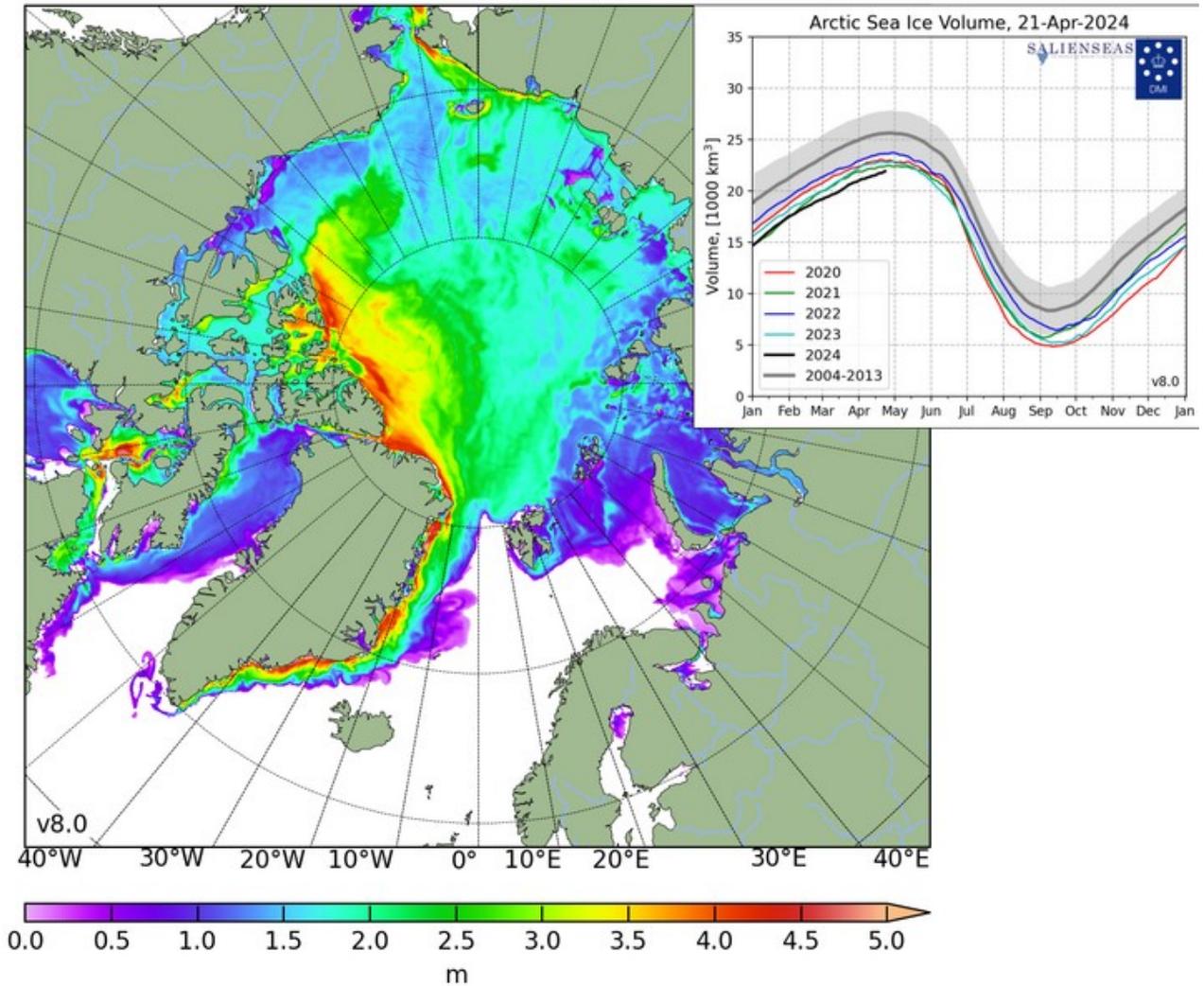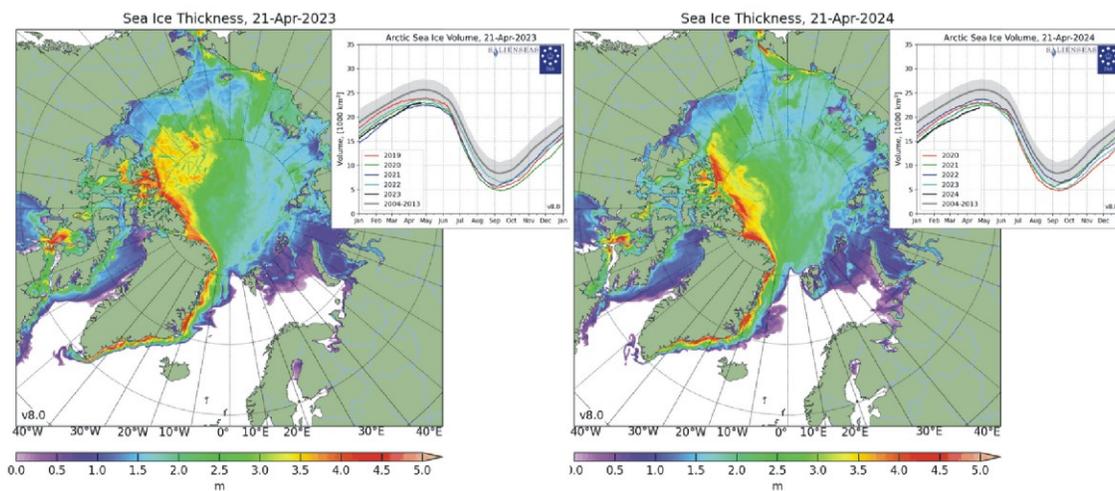
Diagrams showing Arctic sea ice extent and thickness 21 April 2023 (left) and 2024 (right and above) and the seasonal cycles of the calculated total arctic sea ice volume, according to [The Danish Meteorological Institute (DMI)](). The mean sea ice volume and standard deviation for the period 2004-2013 are shown by grey shading. Please note that DMI on 7 December 2021 changed their sea ice calculation model. DMI's description of the model version change can be read here: http://polarportal.dk/en/sea-ice-and-icebergs/sea-ice-thickness-and-volume/

12 month average sea ice extent (Mill. km^2); NSIDC

Southern Hemisphere

October 1979

October 1979

Million km^2

April 2024

April 2024

Northern Hemisphere

Global 12 month average sea ice extent (Mill. km^2); NSIDC

October 1979

Global average 1979-2023

Million km^2

April 2024

Climate4you graph
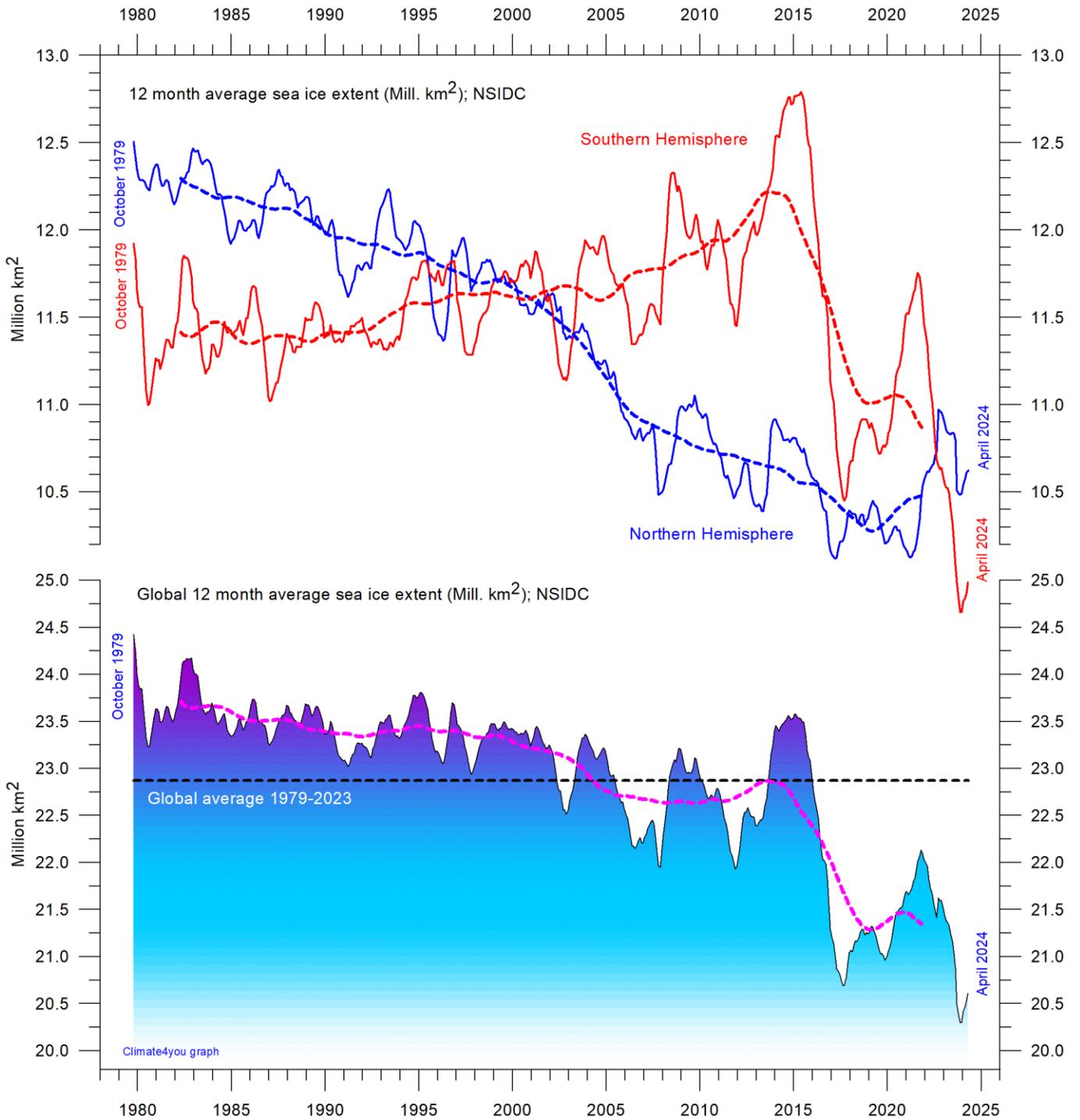
12 month running average sea ice extension, global and in both hemispheres since 1979, the satellite-era. The October 1979 value represents the monthly 12-month average of November 1978 - October 1979, the November 1979 value represents the average of December 1978 - November 1979, etc. The stippled lines represent a 61-month (ca. 5 years) average. Data source: National Snow and Ice Data Center (NSIDC).

Sea level in general

Global (or eustatic) sea-level change is measured relative to an idealised reference level, the geoid, which is a mathematical model of planet Earth's surface (Carter et al. 2014). Global sea-level is a function of the volume of the ocean basins and the volume of water they contain. Changes in global sea-level are caused by – but not limited to - four main mechanisms:

1. Changes in local and regional air pressure and wind, and tidal changes introduced by the Moon.
2. Changes in ocean basin volume by tectonic (geological) forces.
3. Changes in ocean water density caused by variations in currents, water temperature and salinity.
4. Changes in the volume of water caused by changes in the mass balance of terrestrial glaciers.

In addition to these there are other mechanisms influencing sea-level, such as storage of ground water, storage in lakes and rivers, evaporation, etc.

Mechanism 1 is controlling sea-level at many sites on a time scale from months to several years. As an example, many coastal stations show a pronounced annual variation reflecting seasonal changes in air pressures and wind speed. Longer-term climatic changes playing out over decades or centuries will also affect measurements of sea-level changes. Hansen et al. (2011, 2015) provide excellent analyses of sea-level changes caused by recurrent changes of the orbit of the Moon and other phenomena.

Mechanism 2 – with the important exception of earthquakes and tsunamis - typically operates over long (geological) time scales and is not significant on human time scales. It may relate to variations in the seafloor spreading rate, causing volume changes in mid-ocean mountain ridges, and to the slowly changing configuration of land and oceans. Another effect may be the slow rise of basins due to isostatic offloading by deglaciation after an ice age. The floor of the Baltic Sea and the Hudson Bay are presently rising, causing a slow net transfer of water from these basins into the adjoining oceans. Slow changes of excessively big glaciers (ice sheets) and movements in the mantle will affect the gravity field and thereby the vertical position of the ocean surface. Any increase of the total water mass as well as sediment deposition into oceans increase the load on their bottom, generating sinking by viscoelastic flow in the mantle below. The mantle flow is directed towards the surrounding land areas, which will rise, thereby partly compensating for the initial sea level increase induced by the increased water mass in the ocean.

Mechanism 3 (temperature-driven expansion) only affects the uppermost part of the oceans on human time scales. Usually, temperature-driven changes in density are more important than salinity-driven changes. Seawater is characterised by a relatively small coefficient of expansion, but the effect should however not be overlooked, especially when interpreting satellite altimetry data. Temperature-driven expansion of a column of seawater will not affect the total mass of water within the column considered and will therefore not affect the potential at the top of the water column. Temperature-driven ocean water expansion will therefore not in itself lead to any lateral displacement of water, but only locally lift the ocean surface. Near the coast, where people are living, the depth of water approaches zero, so no measurable temperature-driven expansion will take place here (Mörner 2015). Mechanism 3 is for that reason not important for coastal regions.

Mechanism 4 (changes in glacier mass balance) is an important driver for global sea-level changes along coasts, for human time scales. Volume changes of floating glaciers – ice shelves – has no influence on the global sea-level, just like volume changes of floating sea ice has no influence. Only the mass-balance of grounded or land-based glaciers is important for the global sea-level along coasts.

Summing up: Presumably, mechanism 1 and 4 are the most important for understanding sea-level changes along coasts.

References:

Carter R.M., de Lange W., Hansen, J.M., Humlum O., Idso C., Kear, D., Legates, D., Mörner, N.A., Ollier C., Singer F. & Soon W. 2014. Commentary and Analysis on the Whitehead& Associates 2014 NSW Sea-Level Report. Policy Brief, NIPCC, 24. September 2014, 44 pp. http://climatechangereconsidered.org/wp-content/uploads/2014/09/NIPCC-Report-on-NSW-Coastal-SL-9z-corrected.pdf

Hansen, J.-M., Aagaard, T. and Binderup, M. 2011. Absolute sea levels and isostatic changes of the eastern North Sea to central Baltic region during the last 900 years. Boreas, 10.1111/j.1502-3885.2011.00229.x. ISSN 0300–9483.

Hansen, J.-M., Aagaard, T. and Huijpers, A. 2015. Sea-Level Forcing by Synchronization of 56- and 74-YearOscillations with the Moon's Nodal Tide on the Northwest European Shelf (Eastern North Sea to Central Baltic Sea). Journ. Coastal Research, 16 pp.

Mörner, Nils-Axel 2015. Sea Level Changes as recorded in nature itself. Journal of Engineering Research and Applications, Vol.5, 1, 124-129.

Global sea level from satellite altimetry, updated to September 2023
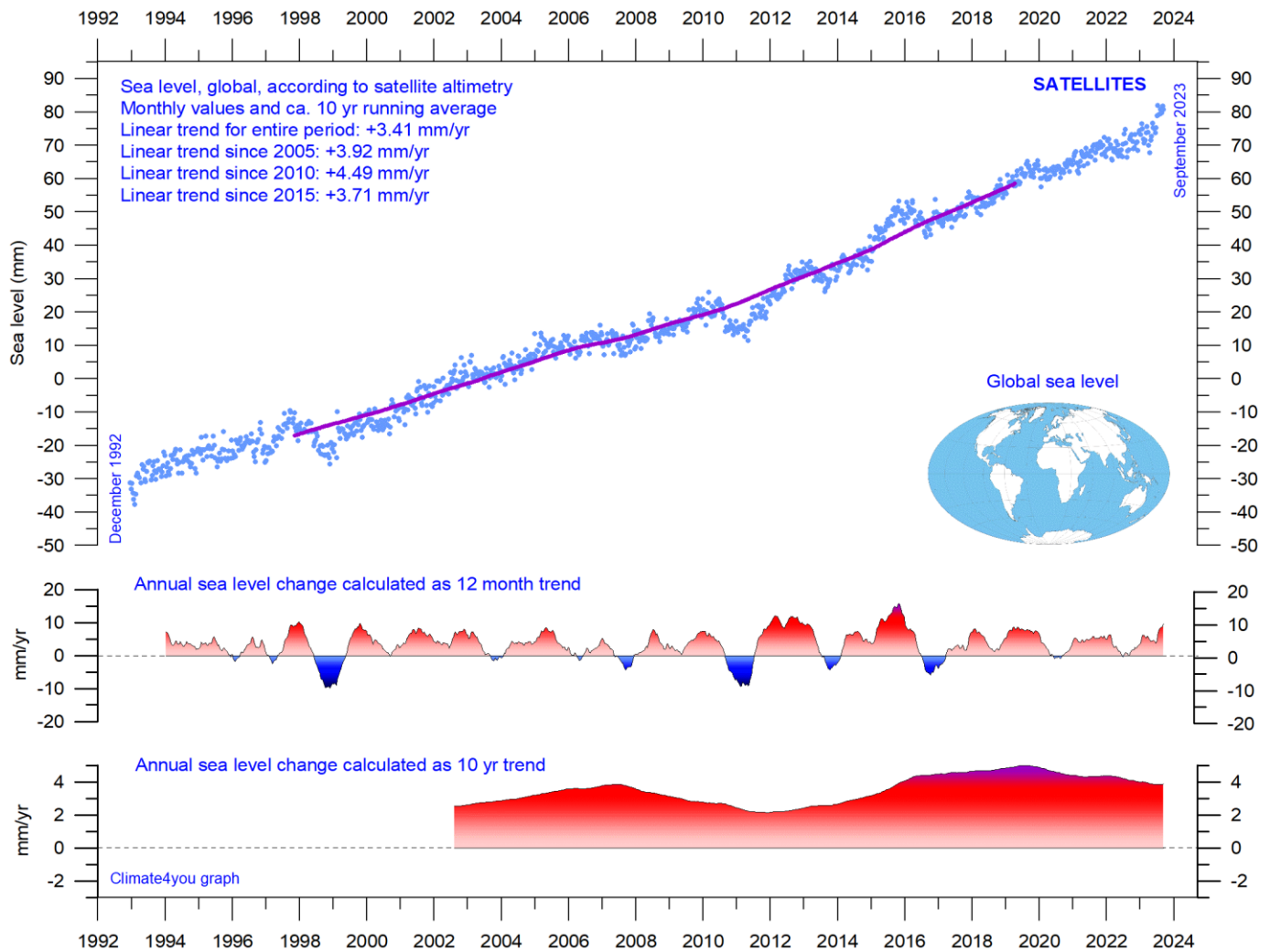
Global sea level since December 1992 according to the Colorado Center for Astrodynamics Research at University of Colorado at Boulder. The blue dots are the individual observations, and the purple line represents the running 121-month (ca. 10 year) average. The two lower panels show the annual sea level change, calculated for 1 and 10-year time windows, respectively. These values are plotted at the end of the interval considered. Compare with tide-gauge diagram on page 41.

Ground truth is a term used in various fields to refer to information provided by direct observation as opposed to information provided by inference, such as, e.g., by satellite observations.

In remote sensing using satellite observations, ground truth data refers to information collected on location. Ground truth allows the satellite data to be related to real features observed on the planet surface. The collection of ground truth data enables calibration of remote-sensing data, and aids in the interpretation and analysis of what is being sensed or recorded by satellites. Ground truth sites allow the remote sensor operator to correct and improve the interpretation of satellite data.

For satellite observations on sea level ground true data are provided by the classical tide gauges (example diagram on next page), that directly measures the local sea level many places distributed along the coastlines on the surface of the planet.

Global sea level from tide-gauges, extended Holgate-9, updated to December 2022
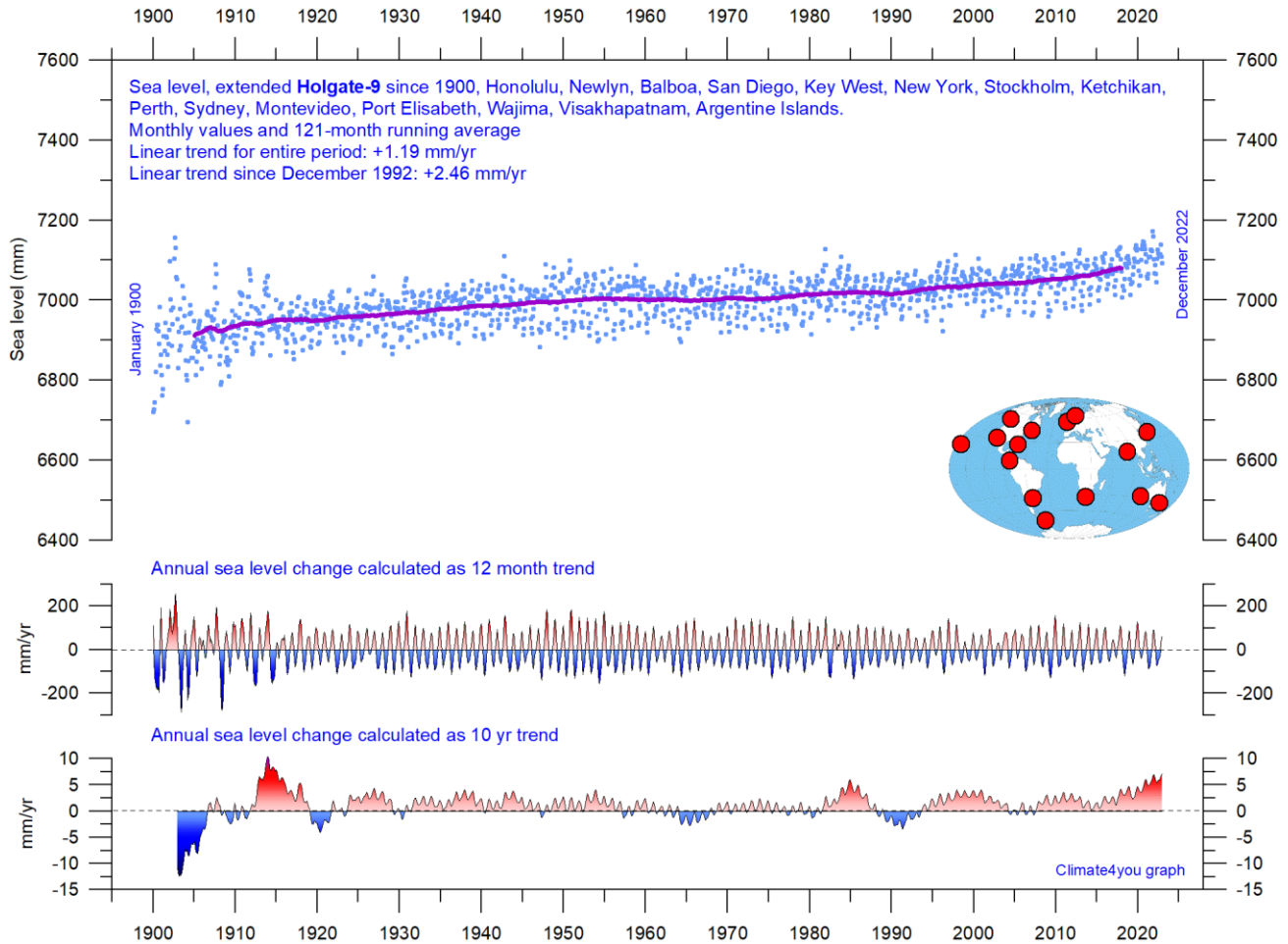
Extended Holgate-9 monthly tide-gauge data from PSMSL Data Explorer. Holgate (2007) suggested 9 stations to capture the global variability found in a larger number of stations over the last half century studied previously. However, some of the stations suggested by Holgate has not reported values for several years, leading to the southern hemisphere now being seriously underrepresented in his original data set. Therefore, in the above diagram several other long tide-gauge series have been included, to provide a more balanced representation of both hemispheres (15 stations in total). The blue dots are the individual average monthly observations, and the purple line represents the running 121-month (ca. 10 year) average. The two lower panels show the average annual sea level change, calculated for moving 1 and 10-year windows, respectively. These values are plotted at the end of the time window considered, month by month.

Data from tide-gauges all over the world suggest an average global sea-level rise of 1-2 mm/year, while the modern satellite-derived record (since 1992, page 40) suggest a rise of about 3.4 mm/year, or more. The difference between the two data sets is remarkable. It is however known that satellite observations are facing several complications in areas near the coast. Vignudelli et al. (2019) provide an updated overview of the current limitations of classical satellite altimetry in coastal regions. Since 2015 a sea level increase rate may be suggested by the above composite record.

References:

Holgate, S.J. 2007. On the decadal rates of sea level change during the twentieth century. Geophys. Res. Letters, 34, L01602, doi:10.1029/2006GL028492

Vignudelli et al. 2019. Satellite Altimetry Measurements of Sea Level in the Coastal Zone. *Surveys in Geophysics, Vol.* 40, p. 1319–1349. https://link.springer.com/article/10.1007/s10712-019-09569-1

41

This month's selected sea level station (tide-gauge): Cocos (Keeling) Island, Indian Ocean
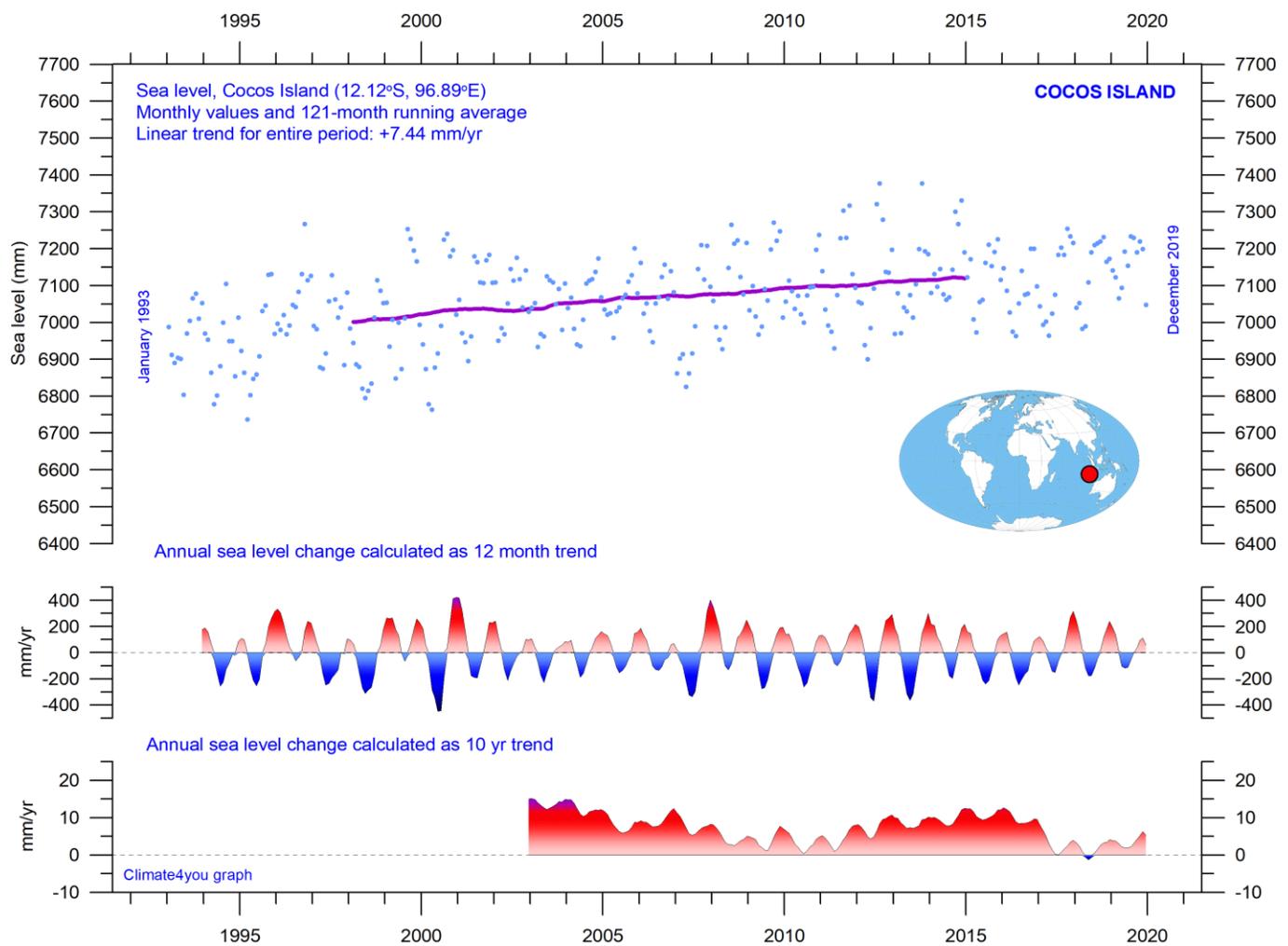
Cocos (Keeling) Island monthly tide gauge data from PSMSL Data Explorer. The blue dots are the individual monthly observations, and the purple line represents the running 121-month (ca. 10 yr) average. The two lower panels show the annual sea level change, calculated for 1 and 10 yr time windows, respectively. These values are plotted at the end of the interval considered.

Cocos (Keeling) Island is an Australian external territory in the eastern part of the Indian Ocean, comprising a small archipelago approximately midway between Australia and Sri Lanka. The territory consists of two atolls made up of 27 coral islands, of which only two are inhabited.

If the observed relative sea level rise at Cocos Island since 1993 continues, relative sea level will have increased about 60 cm by year 2100. Probably, this change will be accommodated by the ongoing growth of coral colonies.

On the morning of 9 November 1914, the islands became the site of the Battle of Cocos, one of the first naval battles of World War I. A landing party from the legendary German light cruiser SMS Emden captured and disabled the wireless and cable communications

station on Direction Island, but not before the station was able to transmit a distress call. The Australian cruiser HMAS Sydney was detached from a nearby convoy to investigate. In the ensuing battle SMS Emden was outranged and outgunned by the larger and faster HMAS Sydney. After a two-hour gallant fight Fregattenkapitän Karl von Müller decided to beach SMS Emden on the nearby North Keeling Island, to prevent further loss of life.

The Indian Ocean is the third-largest of the world's oceanic divisions, covering 70,560,000 km^2 or almost 20% of the water on Earth's surface. In contrast to the Atlantic and Pacific, the Indian Ocean is enclosed by major landmasses and an archipelago on three sides and does not stretch from pole to pole. In fact, it can be likened to an embayed ocean, and several other features make the Indian Ocean unique. It constitutes the core of the large-scale Tropical Warm Pool which, when interacting with the atmosphere, affects the climate both regionally and globally. Asia blocks heat export in the ocean towards north, and the Indian Ocean is the warmest ocean in the world.

The Indian Ocean contains several islands, some of which is known from the ongoing sea-level change debate, mainly because of a claimed rapid relative sea level rise. Many of these islands are volcanic in origin, and due to their high bedrock density, they will inevitably sink slowly because of crustal deformation. Several of these volcanic islands were eroded down to the former 120-130 m long-lasting lower sea level during the Quaternary glaciations. The position and outline of several of these eroded and drowned volcanoes are today indicated at the ocean surface by fringing coral reefs, where colonies of reef building corals have been able to accommodate the about 120 m sea level rise since the maximum of the last glacial period, keeping pace with rising sea level by vertical growth and accretion. In the Indian Ocean, coral reefs are widespread north of 30°S.

Northern Hemisphere weekly and seasonal snow cover, updated to April 2024
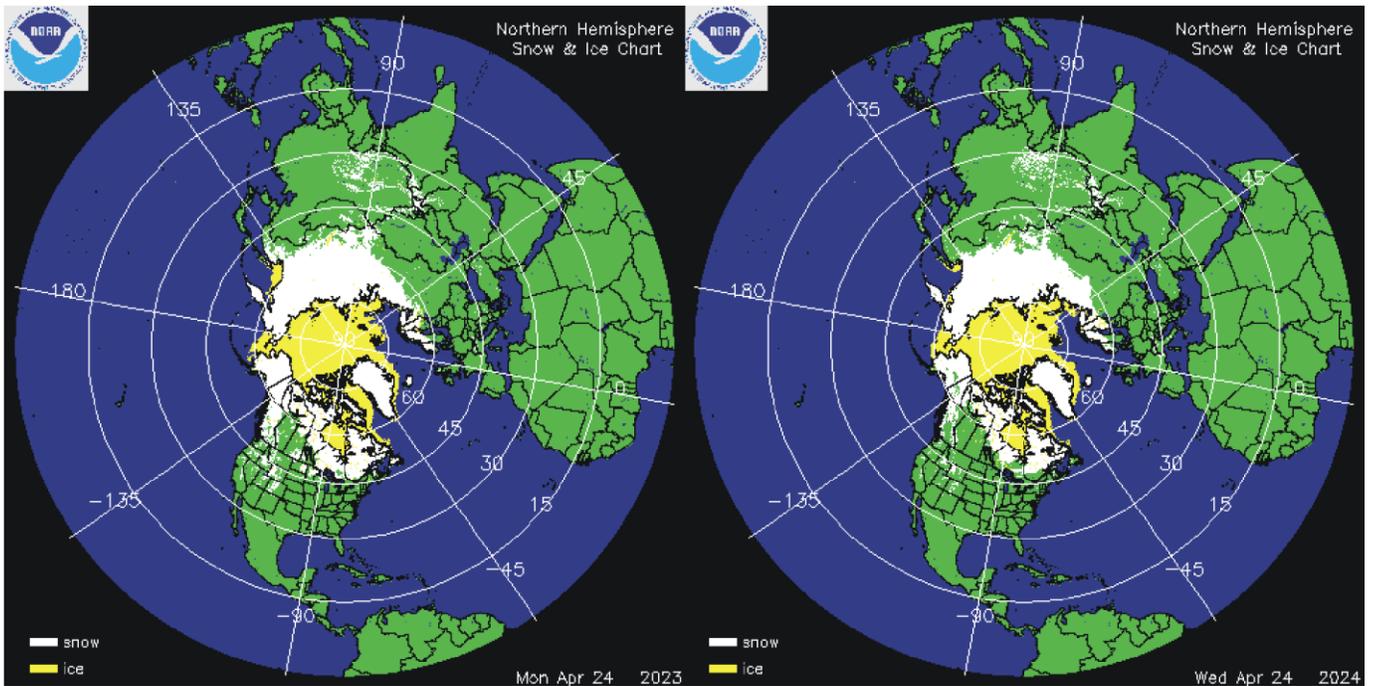
Northern hemisphere snow cover (white) and sea ice (yellow) 24 April 2023 (left) and 2024 (right). Map source: National Ice Center (NIC).
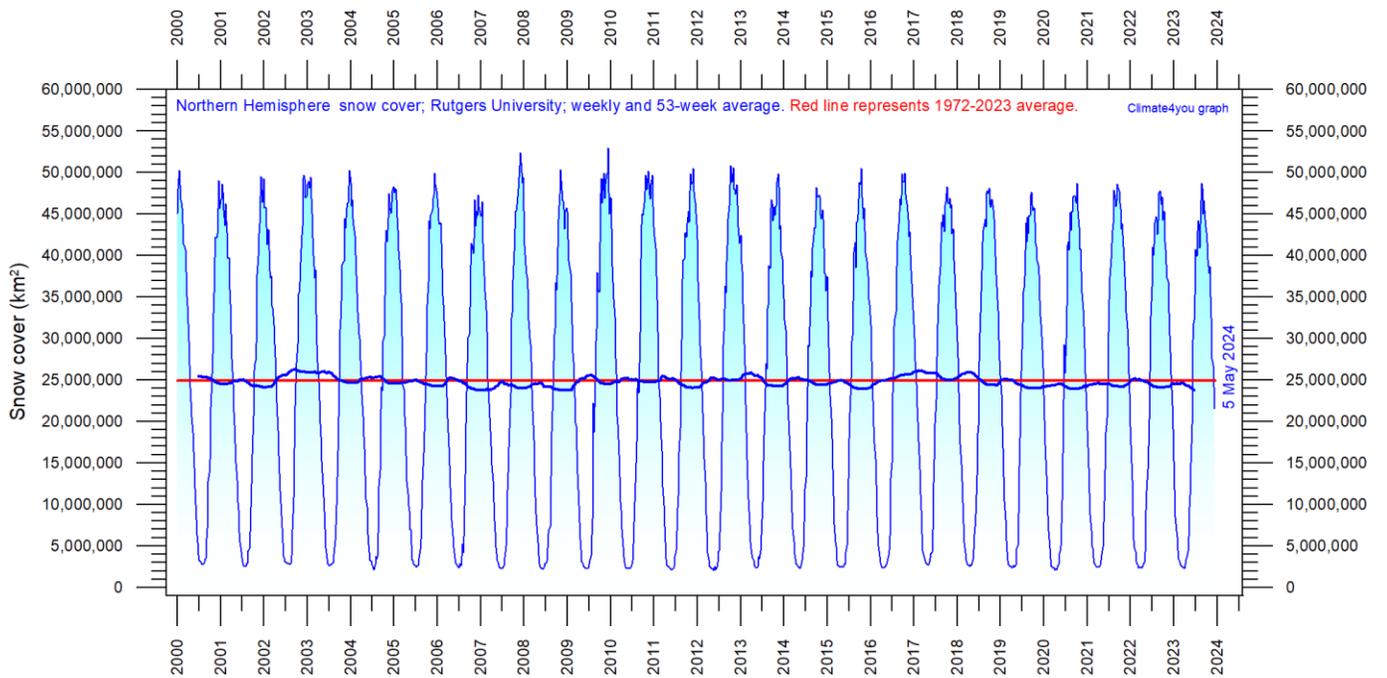
Northern hemisphere weekly snow cover since January 2000 according to Rutgers University Global Snow Laboratory. The thin blue line is the weekly data, and the thick blue line is the running 53-week average (approximately 1 year). The horizontal red line is the 1972-2023 average.
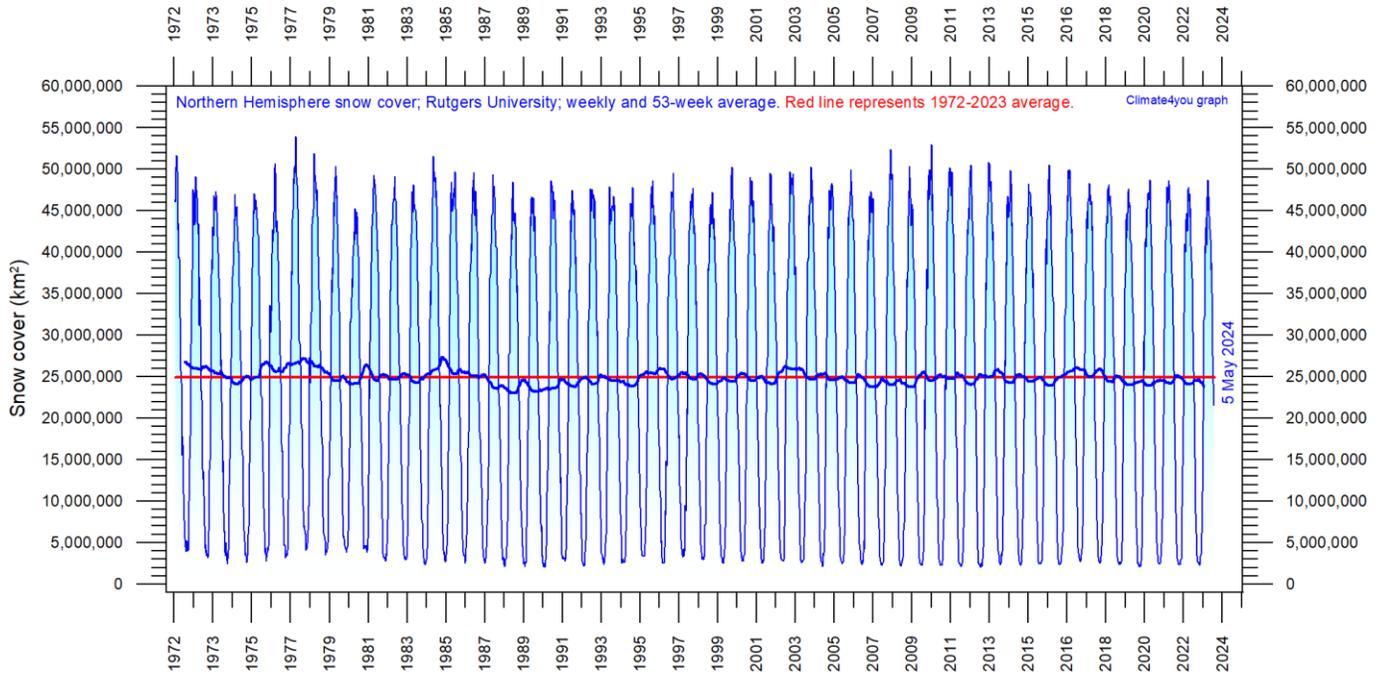
Northern hemisphere weekly snow cover since January 1972 according to Rutgers University Global Snow Laboratory. The thin blue line is the weekly data, and the thick blue line is the running 53-week average (approximately 1 year). The horizontal red line is the 1972-2023 average.
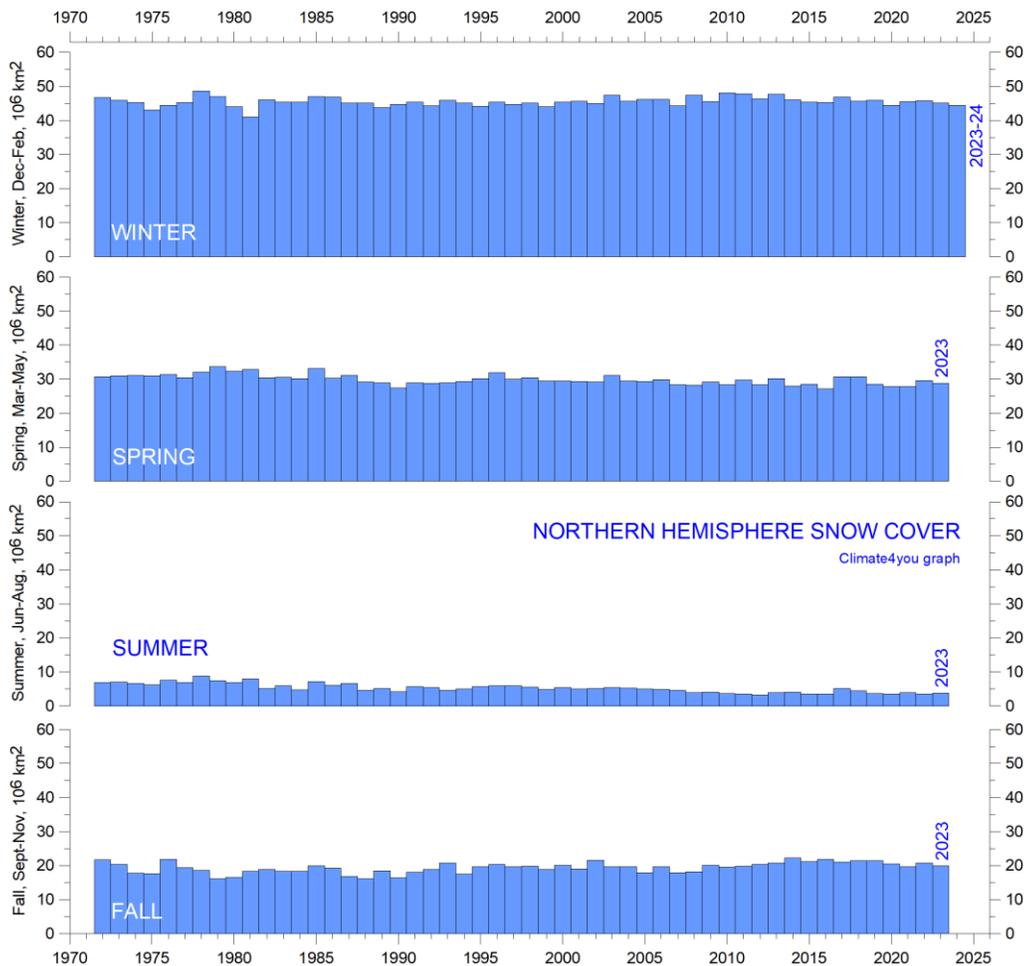
Northern hemisphere seasonal snow cover since January 1972 according to Rutgers University Global Snow Laboratory.

Greenland Ice Sheet net surface mass balance, updated to April 2024
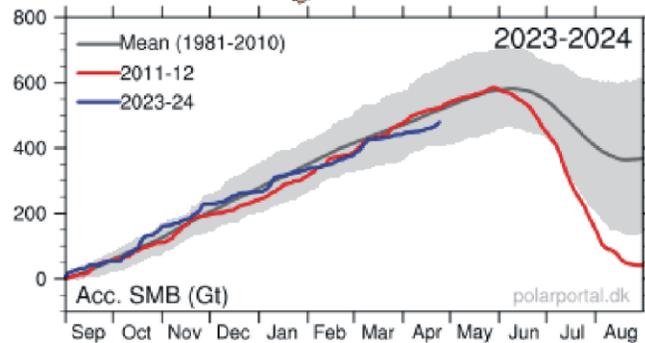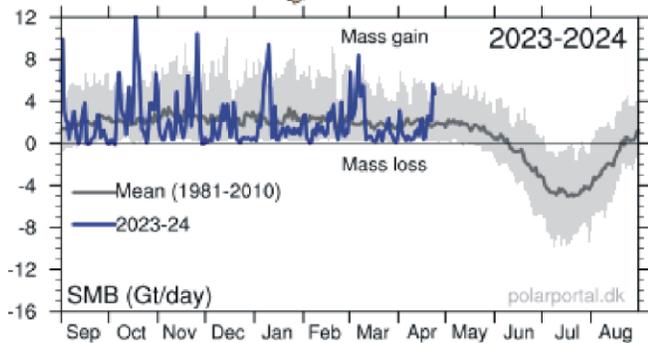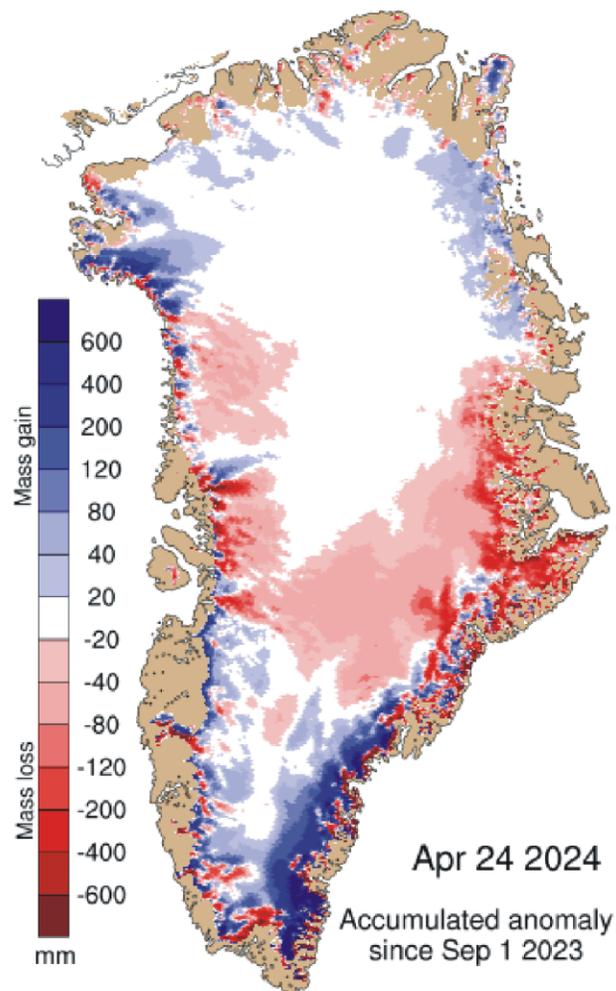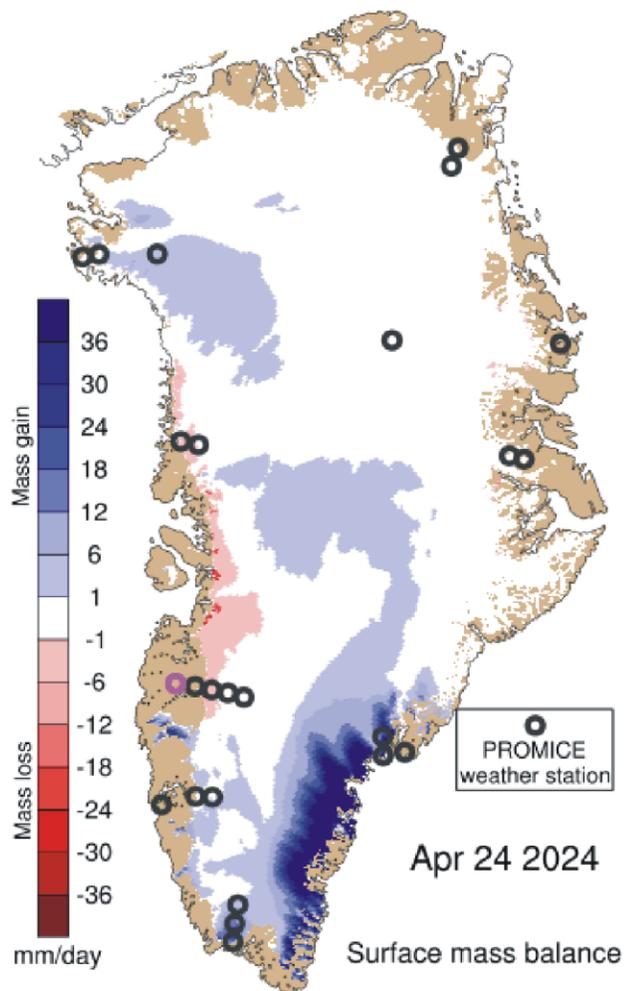
Left: Surface mass balance 24 April 2024. Right: Net surface mass balance anomaly since September 1, 2023. Courtesy of Danish Meteorological Institute (DMI).

Atmospheric relative and specific humidity, updated to April 2024
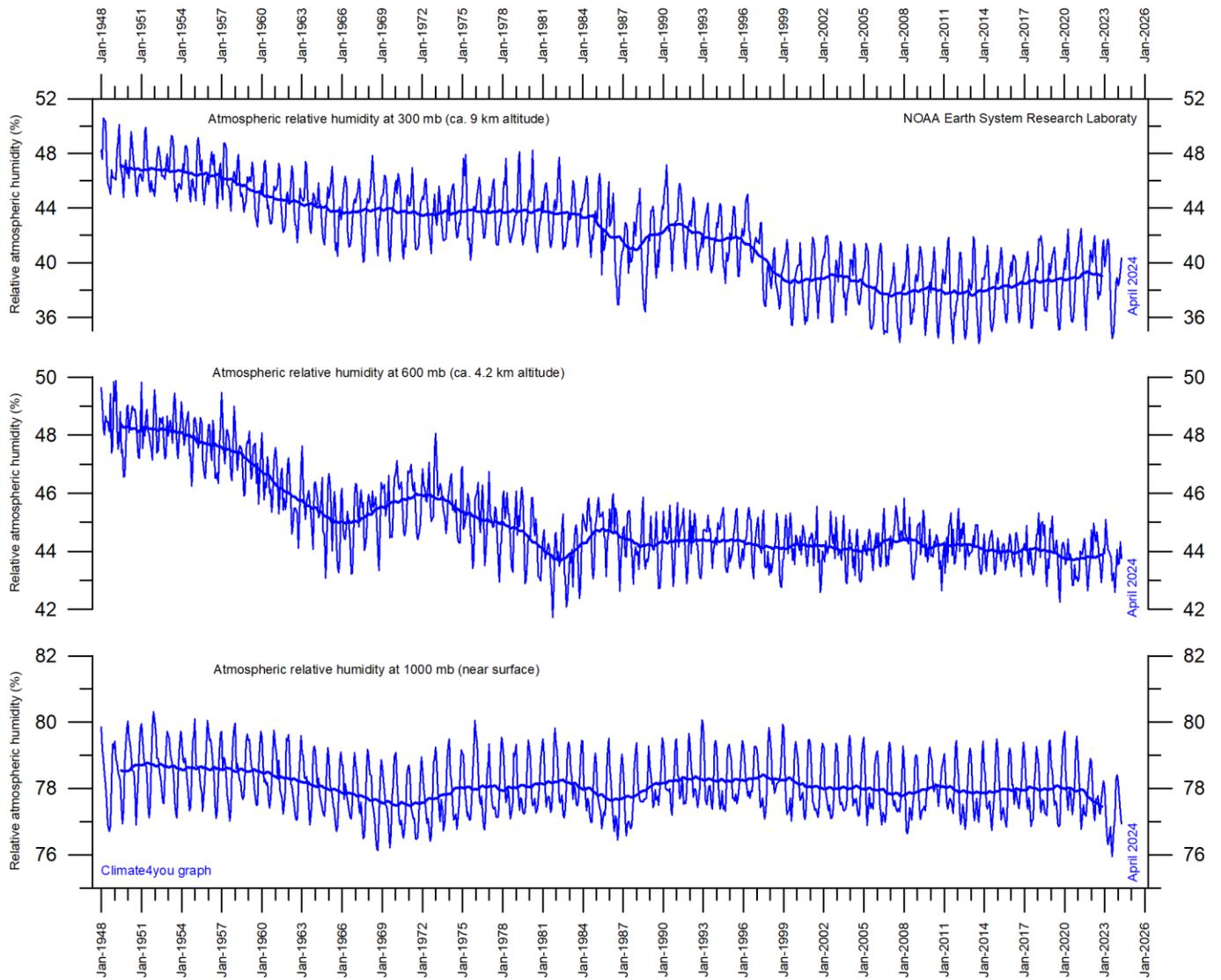
Relative atmospheric humidity (g/kg) at three different altitudes in the lower part of the atmosphere (*the Troposphere*) since January 1948 (*Kalnay et al. 1996*). The thin blue lines show monthly values, while the thick blue lines show the running 37-month average (about 3 years). Data source: *Earth System Research Laboratory (NOAA)*.
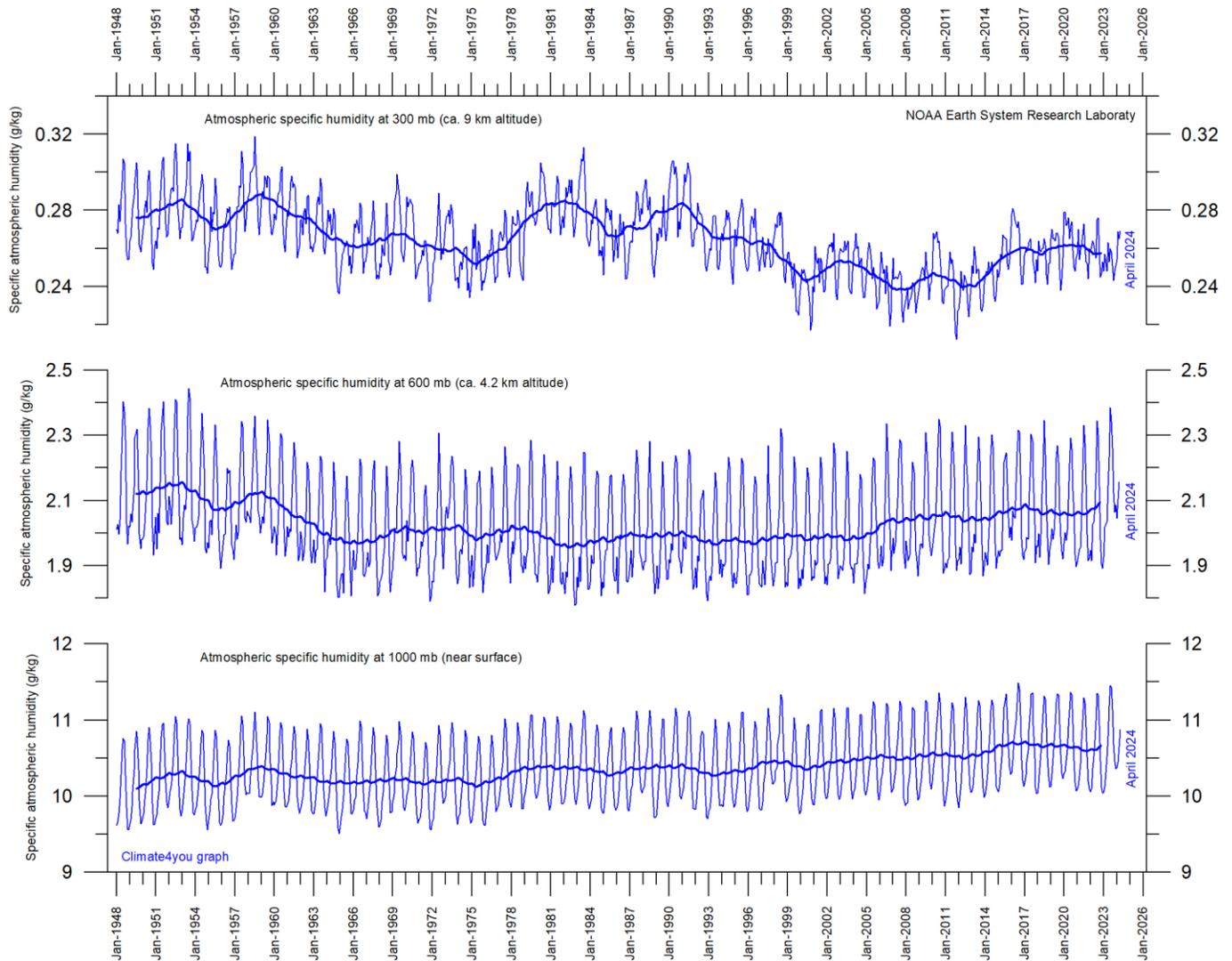
Specific atmospheric humidity (g/kg) at three different altitudes in the lower part of the atmosphere (*the Troposphere*) since January 1948 (*Kalnay et al. 1996*). The thin blue lines show monthly values, while the thick blue lines show the running 37-month average (about 3 years). Data source: *Earth System Research Laboratory (NOAA)*.

Water vapor is the most important greenhouse gas in the Troposphere. The highest concentration is found within a latitudinal range from 50°N to 60°S. The two polar regions of the Troposphere are comparatively dry.

The diagram above shows the specific atmospheric humidity to be stable or slightly increasing up to about 4-5 km altitude. At higher levels in the Troposphere (about 9 km), the specific humidity has been decreasing for the duration of the record (since 1948), but with shorter variations superimposed on the falling trend.

A Fourier frequency analysis (not shown here) suggests these changes are influenced, not only by the significant annual variation, but feasibly also by a longer variation of about 35-years' duration.

The persistent decrease in specific humidity at about 9 km altitude is particularly noteworthy, as this altitude roughly corresponds to the level where the theoretical temperature effect of increased atmospheric CO_2 is expected initially to play out.

Atmospheric CO₂, updated to April 2024
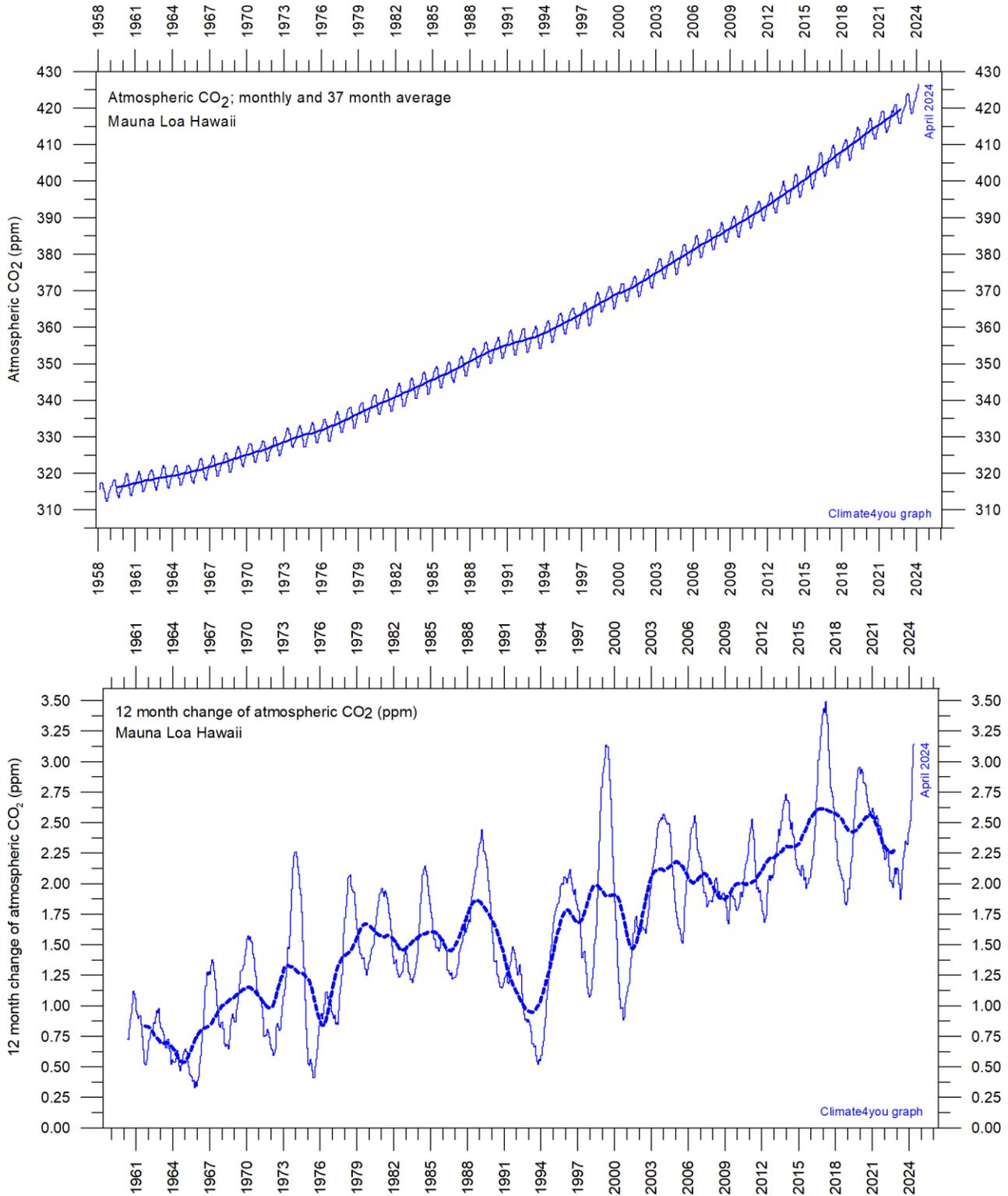
Monthly amount of atmospheric CO₂ (upper diagram) and annual growth rate (lower diagram); average last 12 months minus average preceding 12 months, thin line) of atmospheric CO₂ since 1959, according to data provided by the Mauna Loa Observatory, Hawaii, USA. The thick, stippled line is the simple running 37-observation average, nearly corresponding to a running 3-year average. A Fourier frequency analysis (not shown here) shows the 12-month change of Tropospheric CO2 to be influenced especially by periodic variations of 2.5- and 3.8-years' duration.

The relation between annual change of atmospheric CO_2 and La Niña and El Niño episodes, updated to April 2024
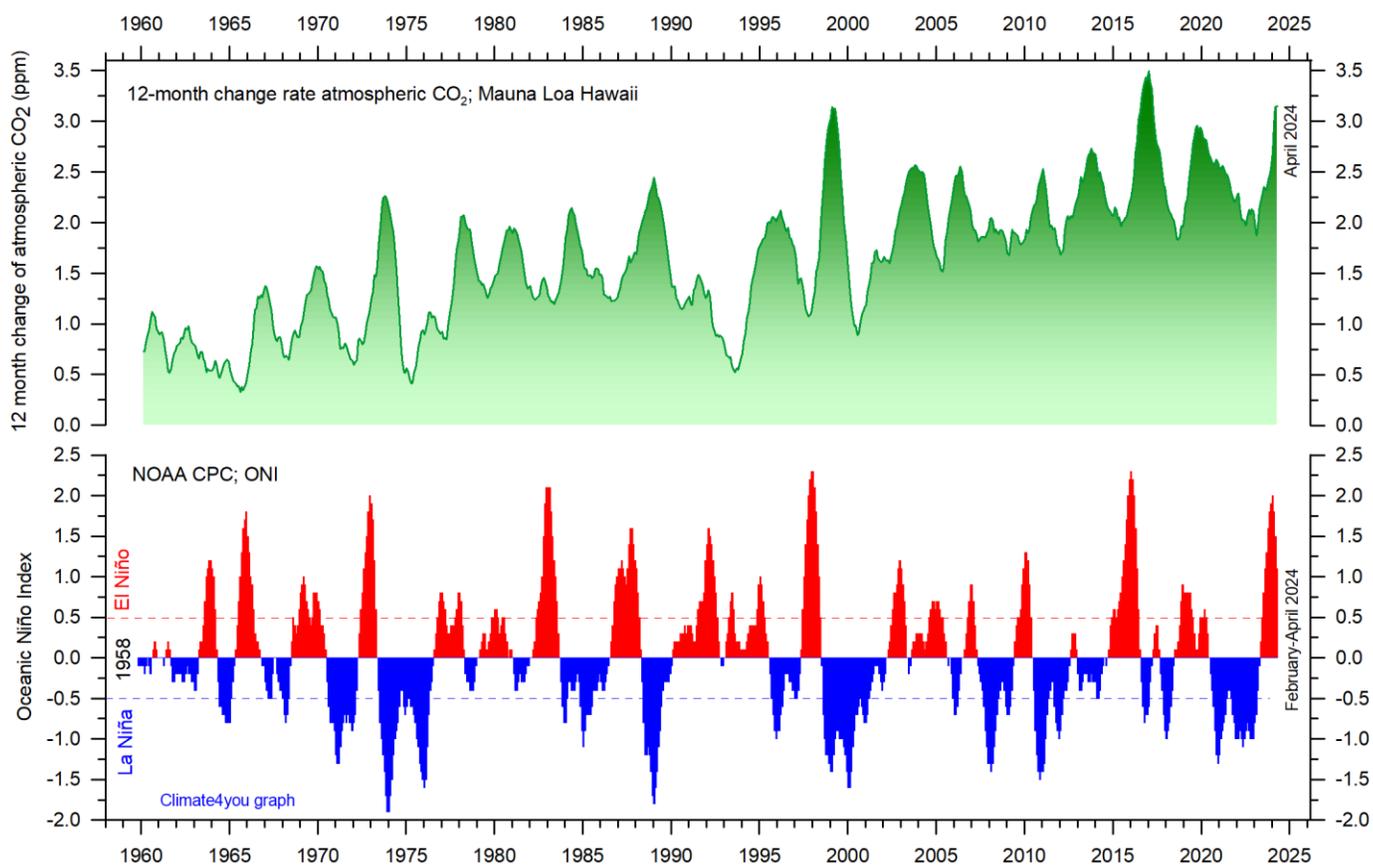
Visual association between annual growth rate of atmospheric CO_2 (upper panel) and Oceanic Niño Index (lower panel). See also diagrams on page 47 and 25, respectively.

Changes in the global atmospheric CO_2 is seen to vary roughly in concert with changes in the Oceanic Niño Index. The typical sequence of events is that changes in the global atmospheric CO_2 to a certain degree follows changes in the Oceanic Niño Index, but clearly not in all details. Many processes, natural as well as anthropogenic, controls the amount of atmospheric CO_2, but oceanographic processes are clearly particularly important (see also diagram on next page).

Atmospheric CO_2 and the recent coronavirus pandemic

Modern political initiatives usually assume the human influence (mainly the burning of fossil fuels) to represent the core reason for the observed increase in atmospheric CO_2 since 1958 (diagrams on page 47).

The coronavirus pandemic since January 2020 resulted in a marked reduction in the global consumption of fossil fuels. It is therefore enlightening to follow the effect of this reduction on the amount of atmospheric CO_2.

However, there is still no clear effect to be seen of the above reduction in release of CO_2 from fossil fuels. Presumably, the main explanation for this is that the human contribution is too small compared to the numerous natural sources and sinks for atmospheric CO_2 to appear in diagrams showing the amount of atmospheric CO_2.

The phase relation between atmospheric CO_2 and global temperature, updated to March 2024
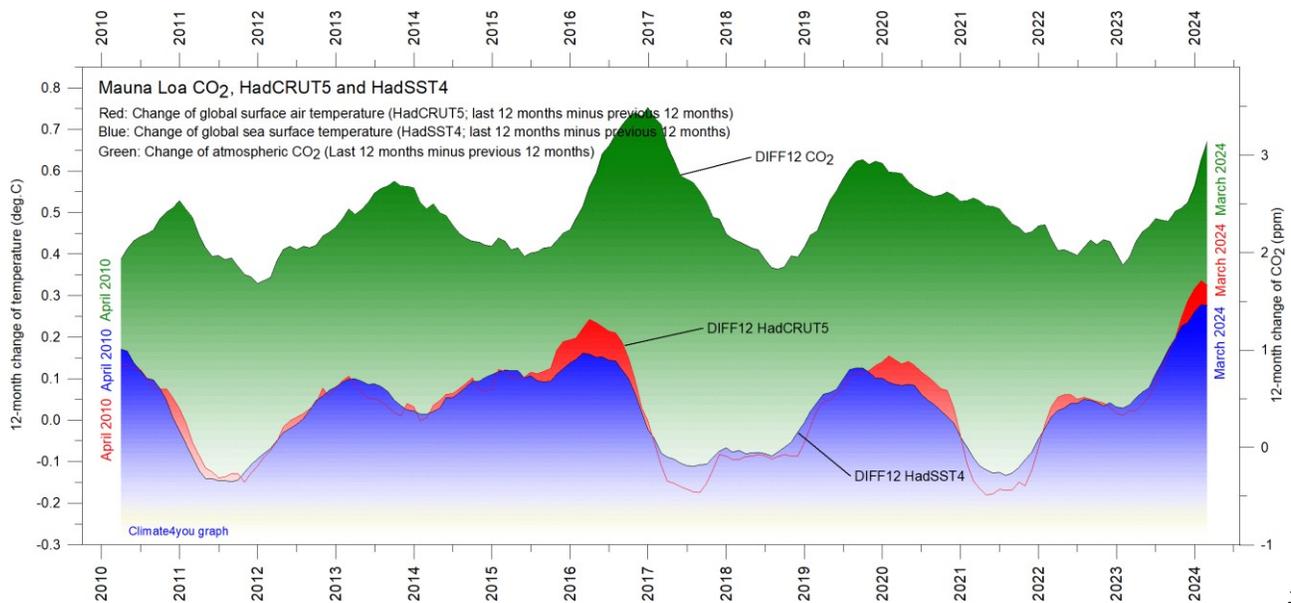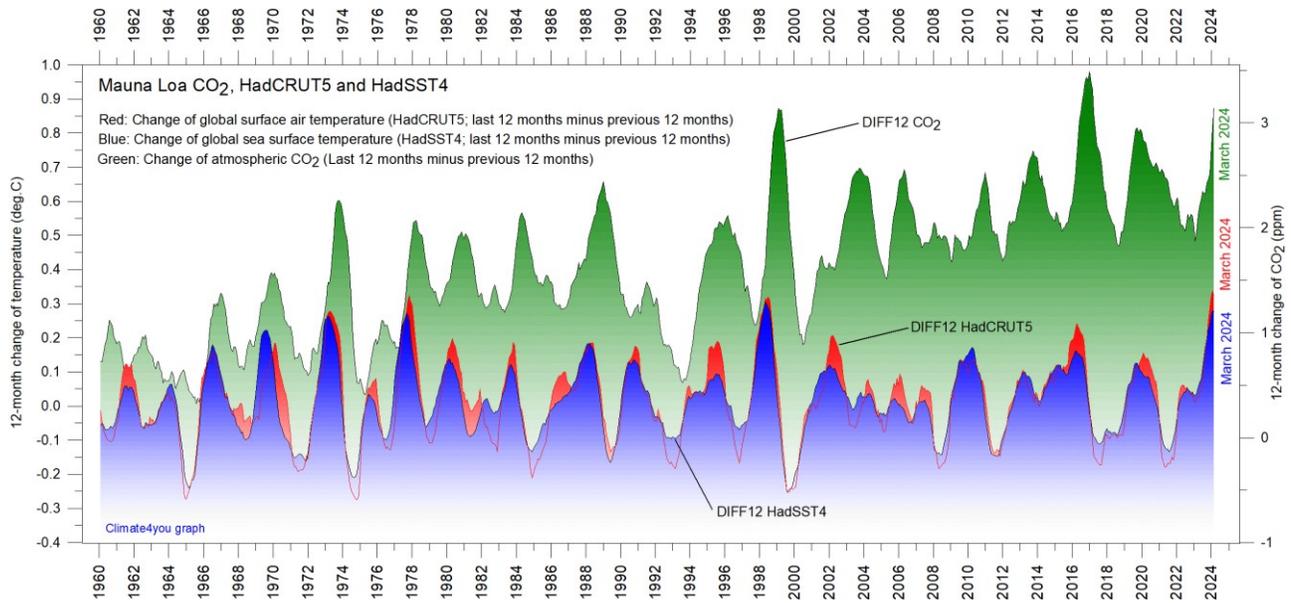
12-month change of global atmospheric CO_2 concentration (Mauna Loa; green), global sea surface temperature (HadSST4; blue) and global surface air temperature (HadCRUT5; red dotted). Entire data series since 1958 in upper figure, and last 15 years in lower figure, to enhance modern dynamics. All graphs are showing monthly values of DIFF12, the difference between the average of the last 12 month and the average for the previous 12 months for each data series.

The typical sequence of events is seen to be that changes in the global atmospheric CO_2 follow changes in global surface air temperature, which again follow changes in global ocean surface temperatures. Thus, changes in global atmospheric CO_2 usually are lagging 9.5–10 months behind changes in global air surface temperature, and 11–12 months behind changes in global sea surface temperature.

Reference: Humlum, O., Stordahl, K. and Solheim, J-E. 2012. The phase relation between atmospheric carbon dioxide and global temperature. Global and Planetary Change, August 30, 2012.
http://www.sciencedirect.com/science/article/pii/S0921818112001658?v=s5

Global air temperature and atmospheric CO₂, updated to April 2024

Top graph:

Measured global temperature anomaly (HadCRUT5 non-infilled), and running 37-month average
Theoretical temperature change derived from atmospheric CO_2
Atmospheric CO_2 (Mauna Loa)

HADCRUT temperature average 1961-1990

March 2024

March 2024

Climate4you graph

Temperature anomaly (deg. C)

Atmospheric CO_2 (ppm)

Bottom graph:

Measured global temperature anomaly (NCDC), and running 37-month average
Theoretical temperature change derived from atmospheric CO_2
Atmospheric CO_2 (Mauna Loa)

NCDC average 1901-2000

April 2024

April 2024

Climate4you graph

Temperature anomaly (deg. C)

Atmospheric CO_2 (ppm)

Diagrams showing UAH, RSS, HadCRUT5, NCDC and GISS monthly global air temperature estimates (blue) and the monthly atmospheric CO_2 content (red) according to the [Mauna Loa Observatory](), Hawaii. Purple line (running along red CO_2 curve) shows theoretical temperature change due to changing atmospheric CO2. The Mauna Loa data series begins in March 1958, and 1958 was therefore chosen as starting year for all diagrams above. Reconstructions of past atmospheric CO_2 concentrations (before 1958) are not incorporated in this diagram, as such past CO_2 values are derived by other means (ice cores, stomata, or older measurements using different methodology), and therefore are not directly comparable with direct atmospheric measurements.

From a theoretical point of view, it is generally agreed that the atmospheric temperature effect ΔT of increasing atmospheric CO_2 may be expressed as (see, e.g. Myhre et al. 1998 and IPCC Third Assessment Report, section 6.1):

$$\Delta T = \Delta F * \lambda$$

where $\Delta F = 5,35\ln(C1/Co)$ W/m^2, and where Co and C1 indicates the concentration of atmospheric CO_2 at the beginning and end of the time interval considered. The factor λ is a so-called climate sensitivity parameter (expressing the global mean surface temperature response to the imposed radiative CO_2 forcing). This factor has been determined to about 0,26°CW^{-1}m^2. The relation shows that as the concentration of atmospheric CO_2 increases, its

theoretical greenhouse effect increases in a logarithmic fashion, not linear. Therefore, for each increase in CO_2 concentration, the effect on temperature is smaller and smaller.

If all other effects in the real world are ignored, the above relation shows that any doubling of atmospheric CO_2 concentration produces a temperature increase of nearly 1°C (0.96°C), no matter how high the initial concentration of CO_2.

The purple line in the above diagrams (p.50-52) is calculated using the observed concentration of atmospheric CO_2 since March 1958. The axis for CO_2 is adjusted to show overlap between CO_2 (red) and the

calculated accumulated temperature effect (purple). In all graphs, the temperature anomaly axis has been adjusted to position the initial calculated effect of CO_2 roughly at the average for the beginning of the observed temperature graph (blue). This is done to make it possible to compare the theoretical CO_2 temperature development (purple) with the observed development (blue).

All these diagrams show the observed temperature development to be much more complicated than the theoretical development from atmospheric CO_2 alone. With exception of the UAH diagram, the overall observed temperature increases since 1958 is much larger than calculated from CO_2 alone. In addition, the observed temperature development is characterised by recurrent intervals characterised by increasing and decreasing temperatures, respectively, a development extremely different from the calculated temperature (purple graph). Clearly many other factors than only CO_2 is in control of the real-world atmospheric temperature.

In contrast to this real-world observation, climate models are programmed to give the greenhouse gas carbon dioxide CO_2 a leading role on control on the global air temperature.

The fact that the observed real-world temperature has been changing much more than expected just from CO_2, is usually ascribed to an added greenhouse effect of atmospheric water vapour in the upper Troposphere, the concentration of which by the models is expected to increase along with CO_2 (see, e.g. Schneider et. al. 1999).

However, measurements of water vapour in the upper Troposphere apparently show this assumption to be mistaken (see, e.g., diagram on p.46). Therefore, the quite substantial difference between modelled and observed atmospheric temperature must be caused by other factors (see, e.g., Koutsoyiannis and Vournas 2023). In addition, the very dynamic change pattern displayed by the observed temperature also needs to be explained before a sound understanding of global climate dynamics can be claimed.

All temperature-CO_2 diagrams (p.50-52) shows both atmospheric temperature and atmospheric CO_2 to be increasing since 1959. However, this fact does not demonstrate that temperature is controlled by CO_2. In fact, it might just as well demonstrate the opposite relation (temperature controlling CO_2), or, that both temperature and CO_2 is controlled by a third factor.

Litterature:

Demetris Koutsoyiannis & Christos Vournas 2023. *Revisiting the greenhouse effect – a hydrological perspective*. Hydrological Sciences Journal, doi: 10.1080/02626667.2023.2287047

Myhre, G., E. Highwood, K. Shine, and F. Stordal 1998. *New estimates of radiative forcing due to well mixed greenhouse gases*, Geophys. Res. Lett., 25(14), 2715–2718, doi:10.1029/98GL0190

Schneider, E.K., Kirtman, B.P., and Lindzen, R.S. 1999. *Tropospheric Water Vapor and Climate Sensitivity.* Journal of the Atmospheric Sciences, 56, 1649-1658.

Latest 20-year QC1 global monthly air temperature changes, updated to February 2024
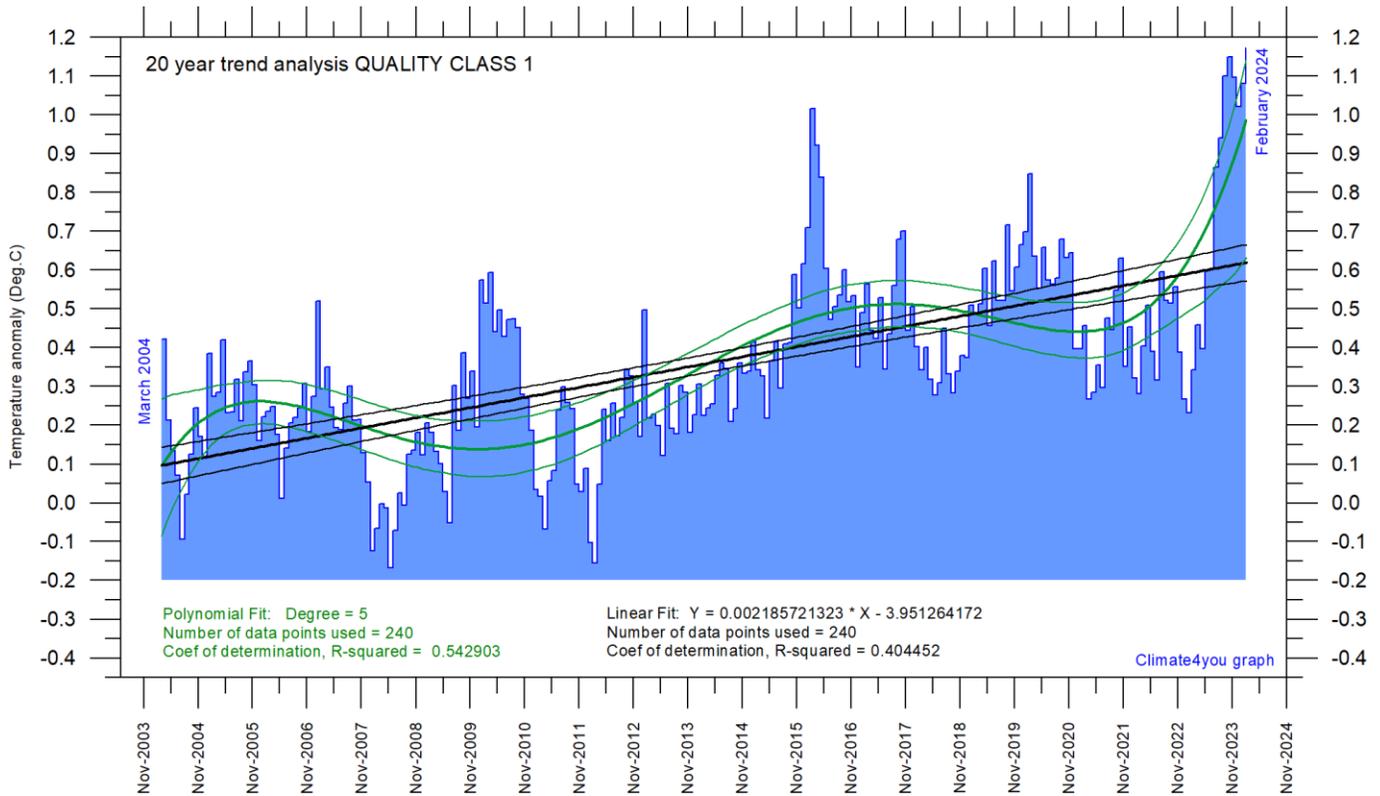
Last 20 years' global monthly average air temperature according to Quality Class 1 (UAH and RSS; see p.6 and 9) global monthly temperature estimates. The thin blue line represents the monthly values. The thick black line is the linear fit, with 95% confidence intervals indicated by the two thin black lines. The thick green line represents a 5-degree polynomial fit, with 95% confidence intervals indicated by the two thin green lines. A few key statistics are given in the lower part of the diagram (please note that the linear trend is the monthly trend).

In the enduring scientific climate debate, the following question is often put forward: Is the surface air temperature still increasing or has it basically remained without significant changes during the last 15-16 years?

The diagram above may be useful in this context and demonstrates the differences between two often used statistical approaches to determine recent temperature trends. Please also note that such fits only attempt to describe the past, and usually have small, if any, predictive power.

In addition, before using any linear trend (or other) analysis of time series a proper statistical model should be chosen, based on statistical justification.

For global temperature time series, there is no *a priori* physical reason why the long-term trend should be linear in time. In fact, climatic time series often have trends for which a straight line is not a good approximation, as is clearly demonstrated by several of the diagrams shown in the present report.

For an commendable description of problems often encountered by analyses of temperature time series analyses, please see Keenan, D.J. 2014: Statistical Analyses of Surface Temperatures in the IPCC Fifth Assessment Report.

Sunspot activity (SIDC) and QC1 average satellite global air temperature, updated to February 2024
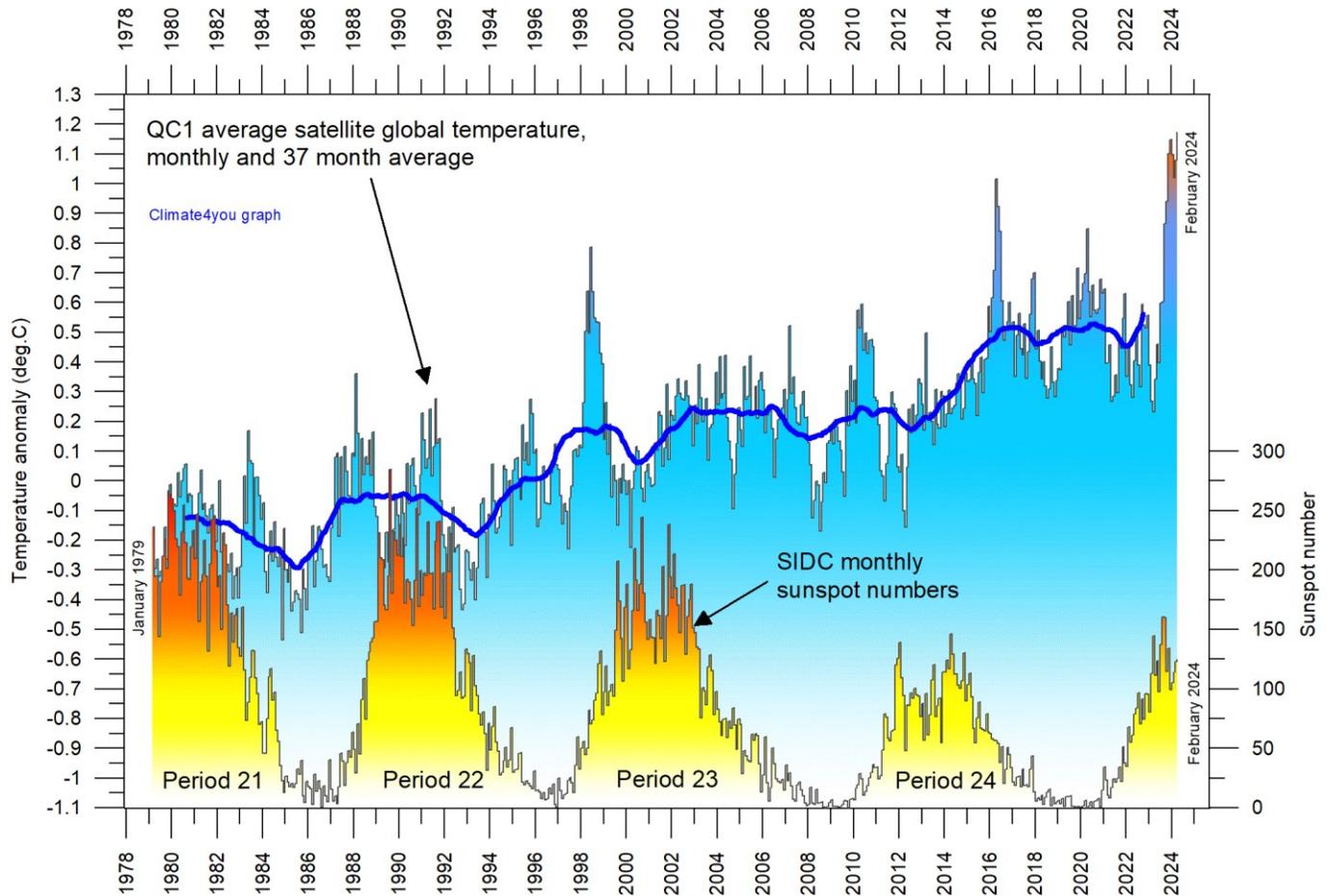
Variation of global monthly air temperature according to Quality Class 1 (UAH and RSS; see p.4) and observed sunspot number as provided by the Solar Influences Data Analysis Center (SIDC), since 1979. The thin lines represent the monthly values, while the thick line is the simple running 37-month average, nearly corresponding to a running 3-year average. The asymmetrical temperature 'bump' around 1998 is influenced by the oceanographic El Niño phenomenon in 1998, as is the case also for 2015-16. Temperatures in year 2019-20 was influenced by a moderate El Niño. In summer 2023 a new El Niño episode has begun (see diagram on p.25).

Monthly sunspot activity (SIDC) and average neutron counts (Oulu, Finland), updated to April 2024
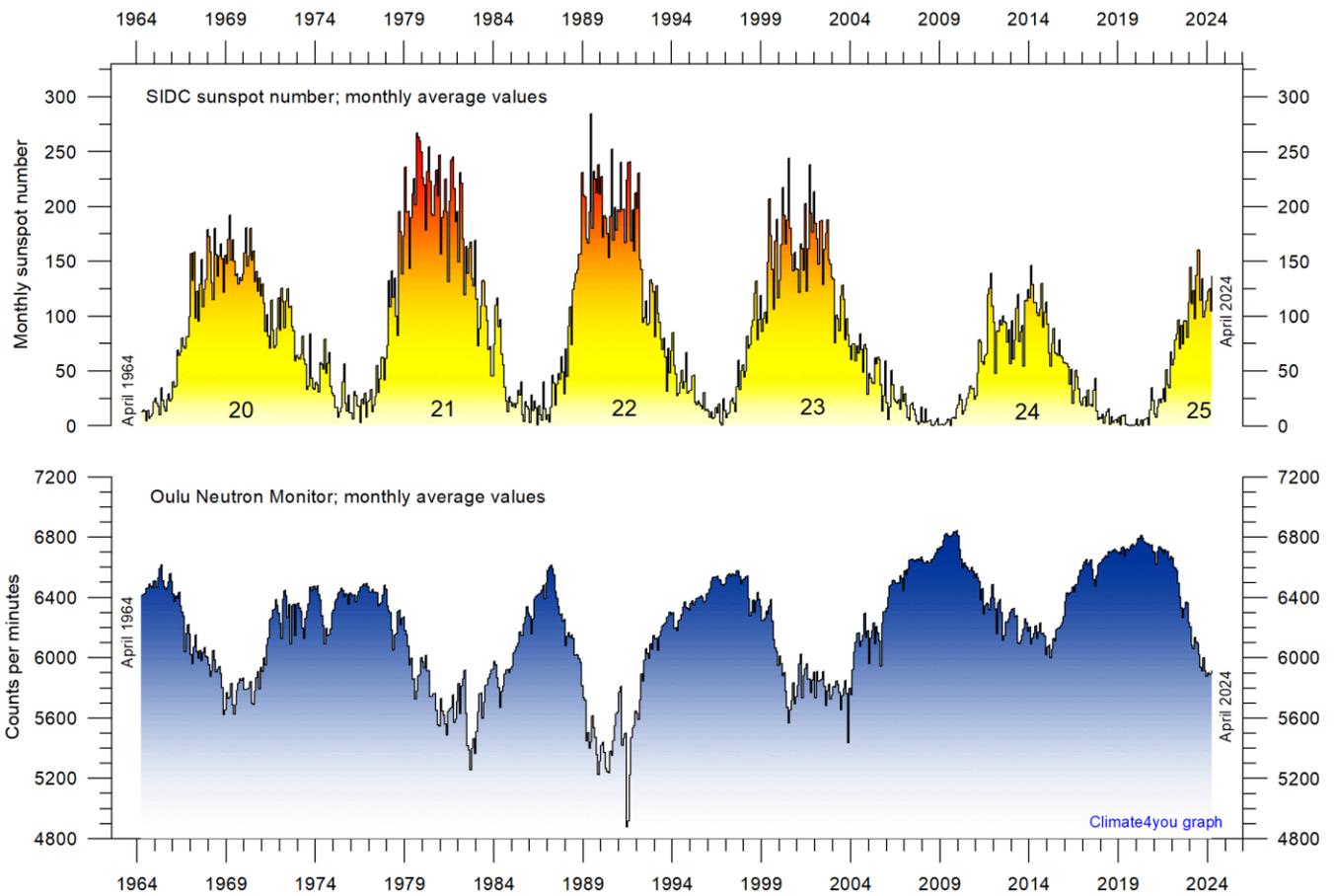
Observed monthly sunspot number (Solar Influences Data Analysis Center (SIDC) since April 1964, and (lower panel) monthly average counts of the Oulu (Finland) neutron monitor, adjusted for barometric pressure and efficiency.

Monthly sunspot activity (SIDC), Oceanic Niño Index (ONI), and change rates of atmospheric CO2 and specific humidity, updated to April 2024
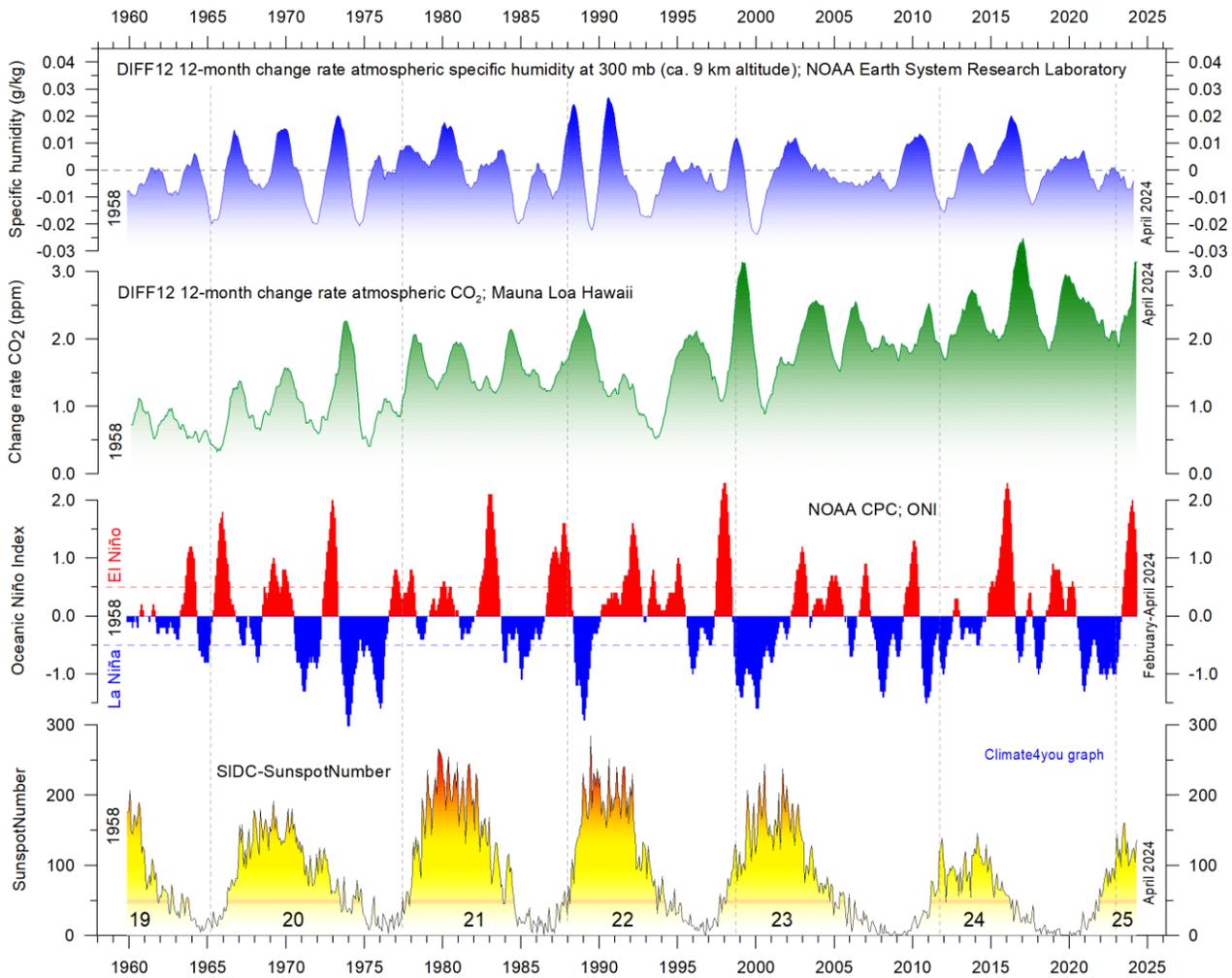
Visual association since 1958 between (from bottom to top) Sunspot Number, Oceanic Niño Index (ONI) and annual change rate of atmospheric CO2. and specific humidity at 300 mb (ca. 9 km altitude). Upper two panels: Annual (12 month) change rate of atmospheric CO2 and specific humidity at 300 mb since 1959, calculated as the average amount of atmospheric CO2/humidity during the last 12 months, minus the average for the preceding 12 months (see also diagrams on page 43+44). Niño index panel: Warm (>+0.5°C) and cold (<0.5°C) episodes for the Oceanic Niño Index (ONI), defined as 3 month running mean of ERSSTv4 SST anomalies in the Niño 3.4 region (5°N-5°S, 120°-170°W)]. For historical purposes cold and warm episodes are defined when the threshold is met for a minimum of 5 consecutive over-lapping seasons. Anomalies are centred on 30-yr base periods updated every 5 years. Thin vertical stippled lines indicate the visually estimated timing of sunspot minima. The typically sequence following a sunspot minimum appears to be a warm El Niño episode followed by a cold La Niña episode. Effects on change rates of atmospheric CO_2 and atmospheric specific humidity are visually apparent, with ONI variations being followed by changes in first humidity, and then (last) by CO_2.

The above diagram is inspired by the Leamon et al. 2021 publication: *Robert J. Leamon, Scott W. McIntosh, Daniel R. Marsh. Termination of Solar Cycles and Correlated Tropospheric Variability. Earth and Space Science, 2021; 8 (4) DOI: 10.1029/2020EA001223*

Monthly lower troposphere temperature (UAH) and global cloud cover, updated to April 2021
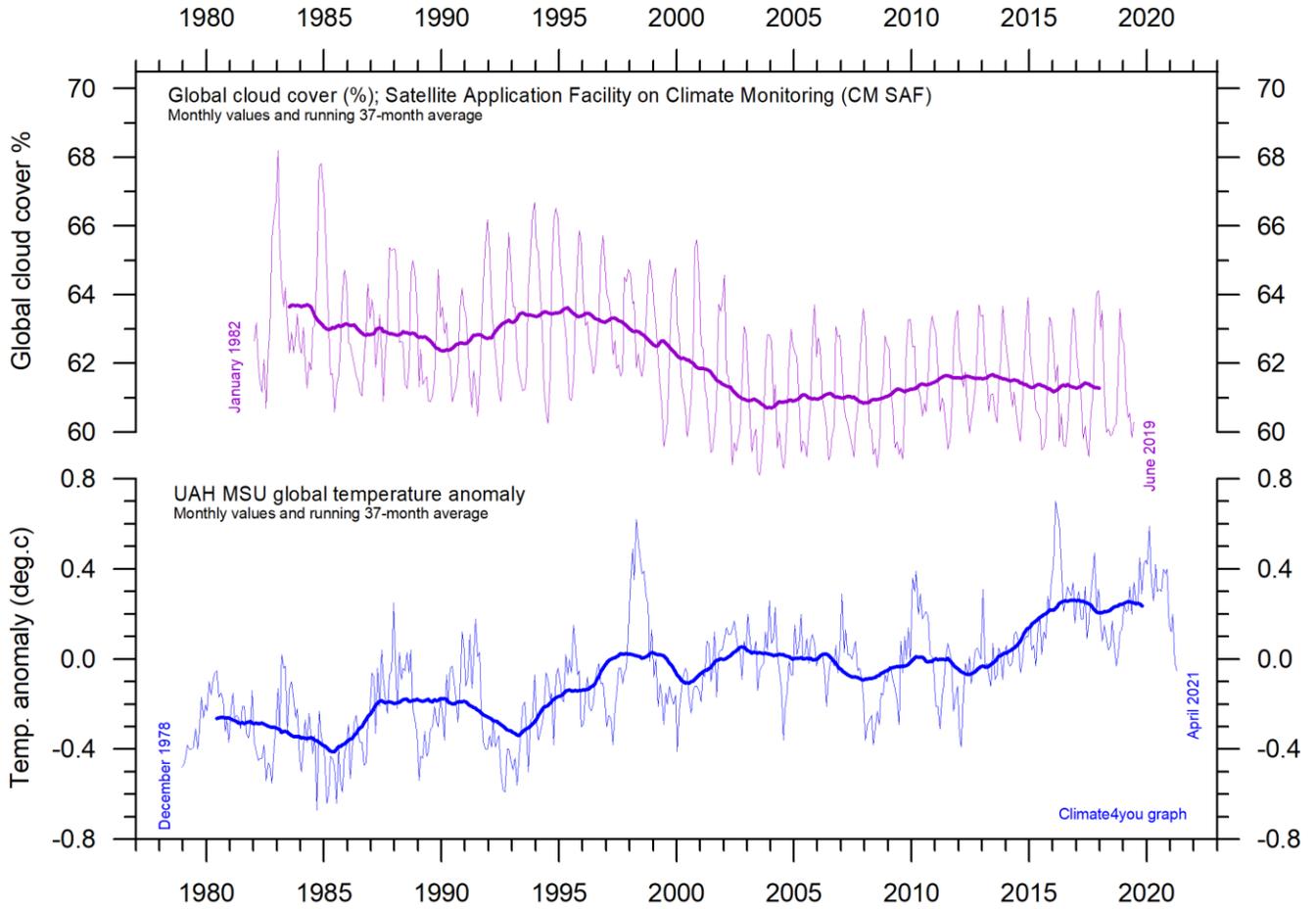
*Lower tropospheric air temperature and global cloud cover. Upper panel: Global cloud cover according to Satellite Application Facility on Climate Monitoring. Lower panel: Global monthly average lower troposphere temperature (thin line) since 1979 according to University of Alabama at Huntsville, USA. The thick lines represent the simple running 37-month average. Reference period for UAH is 1991-2020.*

60

Climate and history; one example among many

620-540 BC: Ionian nature philosophers Thales and Anaximander
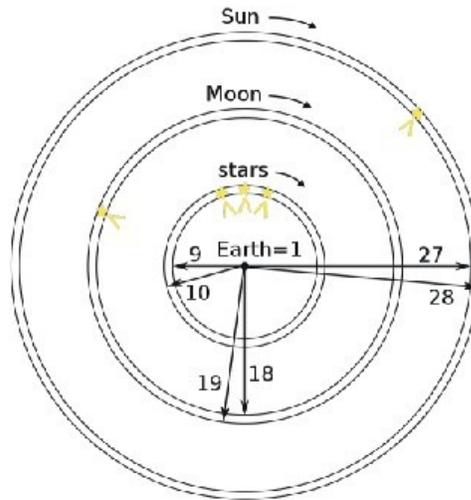
Thales of Miletus (left). Map of Anaximander's universe (centre). Detail of Raphael's painting The School of Athens (right). Presumably this is a representation of Anaximander leaning towards Pythagoras on his left.

Ionia is an ancient region of central coastal Anatolia in the western part of present-day Turkey. Never a unified state, it was named after the Ionian tribe who in the Archaic Period (800-480 BC) occupied mainly the shores and islands of the Aegean Sea. Ionia comprised a narrow coastal strip from near the mouth of the river Hermus in the north to the mouth of the river Meander in the south and included the islands of Chiros and Samos. Much of the summary below is adopted from Rasmussen (2010) and Wikepedia.

Ionia was settled by the Greeks probably during the 11th century BC. Ionia was always a maritime power founded by a people who made their living by trade in peaceful times and marauding in unsettled times. The coast was rocky and the arable land limited. The coastal cities were placed in defensible positions on islands or headlands. The populations of the cities were multi-cultural and received cultural stimuli from many civilizations in the eastern Mediterranean, which resulted in a brilliant society able to make contributions of worldwide and millennial significance.

The philosopher Tales (c.620-c.540 BC) was born in the city of Miletus (Milet in modern Turkey), one of the biggest Ionian cities. Many, most notably Aristotle, regard him as the first philosopher in the Greek tradition. According to

Bertrand Russell, "Western philosophy begins with Thales."

By tradition, the Greeks often invoked explanations of natural phenomena by reference to the will of gods and heroes. Thales, however, aimed to explain natural phenomena by a rational explanation that referred to natural processes themselves. For example, he attempted to explain earthquakes by hypothesizing that the Earth floats on water, and that earthquakes occur when the Earth is rocked by waves, rather than assuming that earthquakes were the result of supernatural processes.

In mathematics, Thales used geometry to solve problems such as calculating the height of pyramids and the distance of ships from the shore. He is credited with the first use of deductive reasoning applied to geometry, by deriving four corollaries to Thales' Theorem. As a result, he has been hailed as the first true mathematician and is the first known individual to whom a mathematical discovery has been attributed. Also, Thales was the first person known to have studied electricity. In addition, it appears that Thales also successfully predicted a solar eclipse.

Thales had a profound influence on other Greek thinkers and therefore on Western history. Many philosophers followed Thales' lead in searching for explanations in nature rather than in the supernatural. Eventually Thales' rejection of mythological explanations became an essential idea for the scientific revolution. He was also the first to define general principles and set forth hypotheses, and as a result he has been dubbed the "Father of Science", though it may

be argued that Democritus more correctly deserve this title.

One of Thales students was Anaximander (c. 610 BC – c. 546 BC). He became famous by explaining how the four elements of ancient physics (air, earth, water and fire) are formed, and how Earth and terrestrial beings are formed through their interactions. His knowledge of geometry allowed him to introduce the gnomon (the part of a sundial that casts the shadow) in Greece. Early sources report that one of Anaximander's more famous pupils was Pythagoras. Anaximander also created a map of the world that contributed greatly to the advancement of geography.

Like many thinkers of his time, Anaximander's contributions to philosophy relate to many disciplines. In astronomy, he attempted a description of the mechanics of celestial bodies in relation to the Earth. In Anaximander's model, the Earth floats very still in the centre of the infinite, not supported by anything.

Anaximander was the first astronomer to consider the Sun as a huge mass, and consequently, to realize how far from Earth it might be. He constructed a celestial sphere and thereby was the first to present a system where the celestial bodies turned at different distances. This presumably this made him the first to realize the obliquity of the Zodiac. His knowledge and work on astronomy also suggest that he must have observed the inclination of the celestial sphere in relation to the plane of the Earth to explain the meteorological changes associated with the annual seasons.

Anaximander saw the oceans as a remnant of the mass of humidity that once surrounded Earth. A part of that mass evaporated under the sun's action, thus causing the winds and even the rotation of the celestial bodies, which he believed were attracted to places where water is more abundant. He explained rain as a product of the humidity pumped up from Earth by the sun. For him, the Earth was slowly drying up and water only remained in the deepest regions, which eventually would dry up as well.

Anaximander was the first to describe wind as the movement of air (Rasmussen 2010), a notion which later was strongly opposed by Aristotele. Anaximander attributed other meteorological phenomena, such as thunder and lightning, to the intervention of elements, rather than to divine causes. In his system, thunder results from the shock of clouds hitting each other; the loudness of the sound is proportionate with that of the shock. Thunder without lightning is the result of the wind being too weak to emit any flame, but strong enough to produce a sound. A flash of lightning without thunder is a jolt of the air that disperses and falls, allowing a less active fire to break free. Thunderbolts are the result of a thicker and more violent air flow.

References:

Rasmussen, E.A. 2010. *Vejret gennem 5000 år* (Weather through 5000 years). Meteorologiens historie. Aarhus Universitetsforlag, Århus, Denmark, 367 pp, ISBN 978 87 7934 300 9.

63

*****

All diagrams in this report, along with any supplementary information, including links to data sources and previous issues of this newsletter, are freely available for download on www.climate4you.com

Yours sincerely,

Ole Humlum (Ole.Humlum@gmail.com)

Arctic Historical Evaluation and Research Organisation, Longyearbyen, Svalbard

25 May 2024.

Planned publication of next newsletter: around 24 June 2024.